Citric Acid Assisted 58S Bioactive Glass with Hydrogen Peroxide for Invitro Bioactivity and Invitro Biodegradability

Tsion Chuni Aklilu

A Thesis Submitted to

The Department of Materials Science and Engineering

School of Mechanical, Chemical and Materials Engineering

Presented in Partial Fulfillment of the Requirement for the Degree of Masters in Materials Science and Engineering

Office of Graduate studies

Adama Science and Technology University

June, 2023

Adama, Ethiopia

Citric Acid Assisted 58S Bioactive Glass with Hydrogen Peroxide for Invitro Bioactivity and Invitro Biodegradability

Tsion Chuni Aklilu

Advisor: Fetene Fufa Bakare (PhD)

Co advisor: Tadele Hunde Wondimu (PhD)

A Thesis Submitted to

The Department of Materials Science and Engineering

School of Mechanical, Chemical and Materials Engineering

Presented in Partial Fulfillment of the Requirement for the Degree of Masters in Materials Science and Engineering

Office of Graduate Studies

Adama Science and Technology University

June, 2023

Adama, Ethiopia

Declaration

I hereby declare that this Master Thesis entitled “Citric acid assisted 58S bioactive glass with hydrogen peroxide for invitro bioactivity and invitro biodegradability” is my original work. That is, it has not been submitted for the award of any academic degree, diploma or certificate in any other university. All sources of materials that are used for this thesis have been duly acknowledged through citation.

_____	_____	_____
Name of the student	Signature	Date

Recommendation

I/We, the advisor(s) of this thesis, hereby certify that I/We have read the revised version of the thesis entitled “Citric acid assisted 58S bioactive glass with hydrogen peroxide for invitro bioactivity and invitro biodegradability” prepared under my/our guidance by Tsion Chuni Aklilu submitted in partial fulfillment of the requirements for the degree of Masters of Science in materials science and engineering. Therefore, I/We recommended the submission of revised version of the thesis to the department following the applicable procedures.

Major Advisor	Signature	Date
Co-advisor	Signature	Date

Approval Board Reviewers

We, the undersigned, members of the Board of Examiners of the thesis by Tsion Chuni Aklilu have read and evaluated the thesis entitled “Citric acid assisted 58S bioactive glass with hydrogen peroxide for invitro bioactivity and invitro biodegradability” and examined the candidate during open defense. This is, therefore, to certify that the thesis is accepted for partial fulfillment of the requirement of the degree of Master of Science in Materials science and engineering.

Chairperson	Signature	Date
Internal Examiner	Signature	Date
External Examiner	Signature	Date

Finally, approval and acceptance of the thesis is contingent upon submission of its final copy to the Office of Postgraduate Studies (OPGS) through the Department Graduate Council (DGC) and School Graduate Committee (SGC).

Department Head	Signature	Date
School Dean	Signature	Date
Office of Postgraduate Studies, Dean	Signature	Date

ACKNOWLEDGEMENT

I want to thank God most of all for the strength and grace given to me during the difficult parts of finishing this task. I would like to express my gratitude to Adama Science and Technology University (ASTU) for providing me with the MSc opportunity and research funding to carry out this study. My advisor, Dr. Fetene Fufa, has been a great asset to me during my study, and I am very appreciative of his essential counsel, ongoing encouragement, and patience. Throughout of my academic research and daily life, his vast knowledge and wealth of experience have inspired me. I also want to extend sincere thanks to my co-advisor, Dr. Tadele Hunde, for his unwavering assistance and support. For his assistance during the sample characterization, I would especially want to thank Mr. Demeke Tesfaye. Thanks to Dr. Gebisa Bekele head of our department and all staff members of the Materials Science and Engineering department. Words cannot adequately explain how grateful I am to my family for their love, prayers, support, patience, advice, and help with my education and future preparation. I also thank Mr. Fasil Tegenu for all his help, kindness, and patience. Last but not least, I want to thank my classmates and everyone else who offered support in any way that they could.

TABLE OF CONTENTS

LIST OF TABLES

LIST OF FIGURES

LIST OF ACRONYMS

ABG	Acetic acid derived Bioactive Glass
BET	Brauner-Emmet-Teller
BG	Bioactive Glass
BO	Bridging Oxygen
CTAB	Cetyltrimethyl ammonium bromide
Ca/P	Calcium phosphate ratio
CBG	Citric acid derived Bioactive Glass
DTA	Differential Thermal Analysis
EDS	Energy Dispersive X-ray Spectroscopy
FTIR	Fourier Transforms Infrared Spectroscopy
HAp	Hydroxy Apatite
HMBG	Hollow Mesoporous Bioactive Glass
H_2O_2	Hydrogen Peroxide
LBG	Lactic acid derived Bioactive Glass
MBG	Mesoporous Bioactive Glass
NBO	Non-Bridging Oxygen
NMBG	Non-Mesoporous Bioactive Glass
SEM	Scanning Electron Microscope
TEOS	Tetraethyl orthosilicate
TGA	Thermogravimetric analysis

XRD	X-ray Diffraction
PBG	Porous Bioactive Glass
MBG	Mesoporous Bioactive Glass
PEG	Polyethylene Glycon
DDA	Dodecyleamine
PVP	Polyvinyl Propylene
P123, F127	Triblock copolymers
SSA	Specific Surface Area

ABSTRACT

Bioactive glass (BG) is a material that adheres to tissues when implemented in the human body because of its surface reactive properties. The development of hydroxyapatite (HAp) layer on its surface is basic characteristic of bioactive glass, which is primarily determined by its chemical composition and morphology. In order to develop porous BGs with large specific surface areas (SSA), surfactants have been usually utilized. However, such compounds induce micell aggregation and carbon contamination. On the other hand, acid catalysts have been utilised to alter the morphology of particles as well as for hydrolysis and condensation of alkoxides in sol-gel method. Most inorganic acid catalysts employed at high concentrations (0.5-2 M) leave behind numerous residual ions that can affect BG particles HAp development as well as subsequent cell proliferation and differentiation. In this study, hydrogen peroxide (H_2O_2), a carbon-free and highly soluble compound was used as a poreforming agent instead of conventional surfactants for the synthesis of BG. The hydrolysis and condensation reaction also executed lower concentrations (0.5 mM) of citric acid, an organic acid catalyst. The H_2O_2 untreated BG (BG0),1M H_2O_2 treated BG (BG1),2M H_2O_2 treated BG (BG2), and 3M H_2O_2 treated BG (BG3) were all made using the sol-gel method. Thermal stability, phase, surface morphology, chemical composition, constituent composition, pore volume, pore size, and specific surface area were analyzed using Thermogravimeteric analysis (TGA), X-ray diffraction (XRD), Scanning electron microscopy (SEM), Fourier transform infraredspectroscopy (FTIR), Energy dispersive x-ray spectroscopy (EDS), and Brunauer-Emmett-Teller (BET) respectively. Invitro bioactivity test was performed by immersing BG powders in simulated body fluid (SBF) solution and HAp formation was analyzed. Also invitro biodegradability test was performed by immersing BG pellets in SBF solution and weight loss was analyzed for 30 days. Finally, invitro bioactivity and biodegradability of the BGs were correlated with H_2O_2 concentration and SSA. According to the results, BG particles treated with 2 M H_2O_2 obtained a larger SSA which is 189.55 cc/g and exhibits better invitro bioactivity and biodegradability.

Key words: *Bioactive glas; Citric acid; Hydrogen peroxide; Bioactivity; Biodegradability; Specific surface area.*

CHAPTER ONE

1. INTRODUCTION

1.1 Background

The body's musculoskeletal system is a crucial part of the human body that is always vulnerable to damage or injury due to diseases, trauma, infections, physiological resorption, and ageing *(Collins et al., 2021; Xiang Wang, Zhang, Lin, & Zhong, 2017)*. Bioinert materials like metal, polymer, and ceramic were used to address these issues *(Khalid, Zafar, Farooq, Khan, & Najmi, 2017)*. However, they don't regenerate new tissues; instead, they just provide temporary structural support for the defects *(Gautam, Kumar, & Kumar, 2022)*. Common conventional ways to regenerate tissue for such incidences are allograft and autograft, which have been used as bone substituent methods *(Mosaad, Shoueir, Saied, & Dewidar, 2021)*. Allograft technique increase the risk of disease transmission, while autograft needs a second surgical site on the host, extra therapies, time, and a higher price *(Fiume, Barberi, Verné, & Baino, 2018; Wisanuyotin, Paholpak, Sirichativapee, & Kosuwon, 2022)*. Due to the stated drawbacks of these techniques, alloplastic materials have been developed that included various calcium and phosphate combinations, frequently in the form of Hydroxyapatite (HAp), as well as various bioceramics, such as bioactive glasses *(Anil, Sadasivan, & Koshi, 2020)*.

A bioactive glass, when implemented in human body, exhibits a specific biological response at the interface that allows it to adhere to both soft and hard tissues *(Shearer, Montazerian, & Mauro, 2023)*. It has been extensively used for dental and bone reconstruction due to its cell proliferation, osteogenesis, and osteoproductive properties *(Leite & Mano, 2017; Zheng, Sui, Ilyas, & Boccaccini, 2021)*. It is well recognized that bioactive glass is a biocompatible, biodegradable, and bioactive material that is very crucial for promoting bone regeneration *(AlHarbi et al., 2021)*. Studies illustrated that when implemented in the human body, the surfaces of BGs generate HAp layers *(Ferraris et al., 2020)*. This layer is the primary inorganic component in bone and they are found to chemically adhere with human bones which indicates the bioactive property of the material *(Fiume, Magnaterra, Rahdar, Verné, & Baino, 2021; B. Lei, Chen, Wang, & Zhao, 2009)*. The mechanism of glass dissolution or

biodegradability also has a vital role in the expressing bioactivity whereby ions are released under physiological conditions and form a strong bond through the creation of calcium phosphate layers with the host bone tissue *(Mehrabi, Mesgar, & Mohammadi, 2020)*.

45S5 Bioglass®, the initially developed and most thoroughly researched bioactive glass, is regarded as a standard for the sector because it can chemically adhere to living bone tissue *(Bellucci & Cannillo, 2018; Hench, 2006)*. However, the lack of an internal microporous network has an impact on the bioactivity of the BG since it was synthesized at a relatively high melting temperature (1300–1500°C) using melt derived method *(Huang et al., 2021)*. Subsequently, BGs prepared by the sol-gel method have more porosity and a higher surface area than melt-derived ones, allowing for a wider range of applications *(Kaya, Cresswell, & Boccaccini, 2018)*. The rates of bone bonding were rather high, and their resorption degradation properties were improved *(Q. Lei et al., 2020)*. A sol-gel process was found to obtain chemically pure, highly homogeneous, low processing temperature, and controlled parameters than the traditional glass melting methods, but mostly the particles structure was found to be solid and difficult to control the particles size and structure *(Almeida & Gonçalves, 2021; Vafa, Bazargan-Lari, & Bahrololoom, 2021)*. Thus using a sol-gel technique with a combination of different structure directing agents (SDA) and catalysts enable synthesizing of BGs with better specific surface area, pore volume, and pore size *(Deshmukh et al., 2020)*.

The morphology of BG particles determines the bioactivity and dissociation or biodegradability *(Gharbi et al., 2023; Oudadesse et al., 2021)*. Silicate BGs have been proven to attach to bone through a series of surface reactions that result in the development of a hydroxyapatite (HAp) layer on the glass surface *(Oluwatosin, El Mabrouk, & Bricha, 2023)*. Thus, bioactivity and dissolution/degradability rate of glass in biological fluids in which first depends on BGs surface morphology and are directly related to its porous structure in order to provide space for tissue regeneration and actively stimulate cells to produce new tissue *(Kargozar et al., 2022; Zheng, Niu, Lei, & Boccaccini, 2021)*. Because of large the specific surface area, a porous bioactive glass becomes preferable in terms of properties and applications *(Q. Lei et al., 2020; Zheng, Sui, et al., 2021)*.

The synthesis of glasses using the sol-gel method involves the hydrolysis and polycondensation of stoichiometric proportions of the oxide precursors in the glass: Tetraethyl orthosilicate (TEOS), Calcium nitrate tetrahydrate, and triethyl phosphate/phosphoric acid (H_3PO_4) *(D Durgalakshmi, Rakkesh, Aruna, Ganesan, & Balakumar, 2020; El-Fiqi et al., 2012).* As a type of third-generation biomaterial which is bioactive, resorbable, and osteoproductive, bioactive glass can be produced by combining the sol-gel technique with catalysts and structure-directing agents *(Schumacher, Habibovic, & van Rijt, 2021).* Catalysts for hydrolysis reaction and structure directing agents for pore formation are used in BG synthesis to obtain particles with enhanced specific surface area, bioactivity, and biodegradability of the BGs *(Anand et al., 2019; Vafa et al., 2022).*

Studies have been investigated using the sol-gel method with different catalysts in order to catalyze the hydrolysis reaction and their influence on the bioactivity and biodegradability of bioactive glass *(Issa & Luyt, 2019; Pajares-Chamorro & Chatzistavrou, 2020)*. The distinctive chemical frameworks of biological hydroxyl-carboxyl acids, such as acetic acid, malic acid, and citric acid, might affect the structure and morphology of materials made from sol-gel processes *(Kuo, Chen, Tseng, & Chou, 2021)*. Inorganic acid catalyzed sol-gel reactions involve the use of stronger acids at high concentrations, such as nitric acid and hydrochloric acid *(Chakraborty, Adhikari, & Saha, 2021)*. For instance, replacing inorganic acid with organic acid enables a significant reduction in the acid concentration required for catalyzing the hydrolysis of alkoxides of silicon and phosphorus *(Ben-Arfa, Fernandes, Salvado, Ferreira, & Pullar, 2018).* Even though both acetic and hydrochloric acid derived BGs have high specific surface areas as well as apatite-forming rates, their first stages of cell proliferation are hindered *(B. Lei et al., 2010)*. In comparison to hydrochloric acid BG and acetic acid BG, lactic acid BG and citric acid BG have adequate apatite-forming capacity, surface morphology, and demonstrate preliminary cell proliferation *(B. Lei et al., 2010; Pahlevanzadeh et al., 2020)*. Therefore, citric acid has excellent catalytic activity at lower concentrations and produces more pure BG when compared to inorganic acids like nitric and hydrochloric acids, which are employed in larger concentrations *(Chakraborty et al., 2021; B. Lei, Chen, & Koh, 2011a; Vafa et al., 2021)*.

Surfactants as a structure forming agents have been frequently employed in sol-gel processing to minimize shrinkage and protect against cracking *(Baino, Fiume, Miola, & Verné, 2018;*

Gupta & Santhiya, 2018). Surfactant molecules act as structure-directing agents (SDA), which are incorporated into the sol and essential for obtaining porous as well as well-ordered structures *(Baino & Fiume, 2020)*. The two surfactants most frequently used in the softtemplate sol-gel processing of BGs are cationic and amphiphilic surfactants *(Mehmood et al., 2019)*. The ability of BG to operate as medication and other biomolecule carriers for controlled release is improved by the enhanced porosity and surface area *(Cao, Wang, Yang, Cao, & Cao, 2021)*. Some of the templates mostly used in porous BGs synthesis include Cetyltrimethylammonium bromide (CTAB), Poly (ethylene glycol) (PEG), Polyurethane (PU), Pluronics (PEO-PPO-PEO), Dodecyleamine (DDA) etc. However, problems like micelle aggregation and carbon contamination may arise when using surfactants *(Shih, Lin, Valentino Posma Panjaitan, & Rahayu Meyla Sari, 2016)*. The final specimen's porosity and surface area decreases as a result of the micelle aggregation, which creates particles with wrinkled surfaces *(Deka, Song, & Yang, 2018; Shih et al., 2016)*. Additionally, BG particles' porosity and specific surface area decrease due to carbon contamination *(Hong, Hsiao, Bakare, Sun, & Shih, 2018)*.

High purity BG with high SSA was developed by using hydrogen peroxide (H_2O_2) as a novel pore-forming agent and BG with high SSA resulting from its decomposition behavior ($2H_2O_2 \rightarrow 2H_2O + O_2$) produces significant amounts of oxygen gas to build the pore structures *(Hong et al., 2018; Hong & Shih, 2017)*. H_2O_2 can replace conventional surfactants as a pore-forming agent because it has no carboxyl groups and is completely soluble in water, which eliminates the need for concern about the effects of carbon contamination and aggregation. In addition to this acidic catalysts used in sol-gel synthesis as catalysis of the hydrolysis reaction has a great influence on the properties of BG *(Issa & Luyt, 2019)*. Among these catalysts biological hydroxyl-carboxyl acids like citric acid have unique chemical structures that can highly influence the surface morphology and structure of the resulting materials formed from sol-gels *(Chakraborty et al., 2021; B. Lei et al., 2011a)*. Thus in this paper hydrogen peroxide as a structure directing agent and citric acid as a catalyst are used for the synthesis of BGs and the effect of hydrogen peroxide (H_2O_2) on the invitro bioactivity and invitro biodegradability of bioactive glass is studied.

1.2 Statement of problem

Human beings are increasingly experiencing bone failure for a variety of reasons. Since their discovery, BGs are receiving plenty of interest in bone tissue regeneration. These materials can bond to the bone; integrate with it and enables bone regeneration *(Mulchandani & Katiyar, 2019)*. However, synthesizing methods and parameters highly influence the bioactivity and biodegradability properties of BGs. When BGs are synthesized using the meltderived approach, a comparatively high melting temperature (1300–1500 °C) is required, and the absence of an internal porous network affects the bioactivity of bone in later phases of HAp formation *(C. Wu, Chang, & Xiao, 2011)*. The employed high processing temperature causes recrystallization of particles after they have been quenched, which lowers the nucleation of HAp crystallites from body fluid, their adhesion to the bone, and the glass' degradability *(Baino, Fiume, et al., 2018)*. It also resulted in a significant probability of the incorporation of contaminants due to multiple interactions at each stage of the process *(Schuhladen & Boccaccini, 2021)*.

A sol-gel process was found to make it possible to obtain pure, highly homogeneous, bioactive glass by using low processing temperature and controlled parameters than the traditional glass melting methods, but mostly the particles structure was found to be solid and difficult for controlling the surface morphologies of BG particles *(Baino, Hamzehlou, & Kargozar, 2018; Zheng, Sui, et al., 2021)*. Thus, using the sol-gel technique in combination with structure directing surfactants and catalysts enables synthesizing of BGs with better specific surface area and morphology than the conventional sol-gel method *(Deshmukh et al., 2020)*. Unfortunately, most surfactants consist of long chain carbon functional groups which result in carbon contamination and they are not completely soluble so aggregation will be formed which reduces bioactivity and biodegradability properties *(Kumar, Aditya, & Murugavel, 2019)*. Most commercial surfactants are difficult to dissolve at low temperatures and are not recommended *(Migneco, Fiume, Verné, & Baino, 2020)*. Also, inorganic acid catalysts result in high concentration, phase segregation and influence the structure and surface morphology of synthesized BG particles *(Faure et al., 2015)*. The use of higher concentrations of inorganic acids such as HCl, HF, HNO_3, and so on leaves much residue of

ions which influences the HAp formation, further cell proliferation, and differentiation of BG particles.

Thus, synthesizing bioactive glasses by sol-gel method using hydrogen peroxide as structure directing agent might have a promising effect on the bioactivity and biodegradability of BG particles. Hydrogen peroxide is completely soluble, cheap, and free from carboxyl group, so it would not result in micelle aggregation and carbon contamination on the synthesized particles *(Hong & Shih, 2017)*. Also using organic acid catalysts such as citric acid enables the catalysis of hydrolysis and condensation reactions in lower concentration and capable of changing the morphology and assist the bioactivity and biodegradability of BGs *(Shah et al., 2018)*.

1.3 Objectives

1.3.1 General objective

- The general objective of this study focuses on synthesis and characterization of citric acid assisted 58S bioactive glass with hydrogen peroxide for invitro bioactivity and invitro biodegradability.

1.3.2 Specific objectives

- To synthesize bioactive glass powder with sol-gel method.
- To analyze thermal stability, morphology, composition, specific surface area, pore volume, and pore size of the synthesized samples.
- To analyze invitro bioactivity and invitro biodegradability of the synthesized samples.
- To investigate the impact of H_2O_2 concentration on specific surface area, invitro bioactivity, and invitro biodegradability of prepared bioactive glass powders.
- To investigate the effect of specific surface area on invitro bioactivity and invitro biodegradability.

1.4 Significance

This study focuses on the effect of hydrogen peroxide effect on the bioactivity and biodegradability properties of bioactive glass. It enables to reduce the expensive surgical costs required for the conventional bone substitute methods like bioinert implants, autograft,

and allograft. Even developing countries like Ethiopia would have a chance to minimize the foreign currency expenditure of bone victims for treatment and enables to start the treatment in its own country by training physicians since it does not require any complex surgeries. Additionally, it minimizes the morbidity, cellular damages, disease transmission, infection formation, and other surgical related damages caused by conventional methods. On the other hand, these BGs using H_2O_2 are expected to be free from any carbon contamination and micelle aggregation in their structure, high purity bioactive glass particles would be achieved which is essential for well controlled bioactivity, biodegradability properties of bioactive glass, and enhance those essential properties in relative to other BGs. This would enhance the attachment of BGs with bone and better formation of HAp so that it provides enough space for new cell formation during bone tissue regeneration. Thus, it would develop the clinical advances in terms of tissue regeneration. Besides this study might be used as a reference for related researches and it can be starting idea for more improvements.

1.5 Scope of the study

This study focuses on the synthesis of bioactive glass with hydrogen peroxide as structure directing agent and citric acid as catalyst for analyzing invitro bioactivity and invitro biodegradability. A 58S bioactive glass (58% SiO_2, 33% CaO, and 9% P_2O_5) (mol %) was synthesized using sol-gel method in stoichiometric amount of precursors Tetraethyl orthosilicate (TEOS, $Si(OC_2H_5)_4$), Phosphoric acid (H_3PO_4), and Calcium nitrate tetra hydrate ($Ca(NO_3)_2.4H_2O$). As-prepared samples were characterized by TGA, SEM, XRD, EDS, FTIR, and BET. Thermal stability was analyzed by TGA, morphology of particles by SEM, phase analysis by XRD, constituent composition by EDS, functional groups of the samples by using FTIR, specific surface area, pore size, and pore volume by BET. Invitro bioactivity test was done by soaking prepared samples in to SBF solution and analysis of HAp layer formation on the particles were done using XRD for day 1, day 3, and day 7 bioactivity. Further HAp formation was analyzed for day 3 bioactivity using SEM, FTIR, and EDX. Biodegradability test was also done by measuring weight loss of the samples for 30 days in SBF solution. Finally correlations among invitro bioactivity, invitro biodegradability, H_2O_2 concentration, and specific surface area were done.

CHAPTER TWO

2. LITERATURE REVIEW

2.1 Bioactive glass

Bioactive glass is a material that has shown promise for bone tissue regeneration which is more suited for using as a biomaterial for its bioactivity, biocompatibility, and biodegradability *(Soni, Kumar, Chameettachal, Pati, & Rath, 2019)*. Due to illness, injury, aging, dietary inefficiency, and other factors, the loss of bone function has become a typical occurrence *(Collins et al., 2021)*. Making solutions for bone regeneration was necessary because bone loss frequently has negative both functional and aesthetic effects *(Skallevold, Rokaya, Khurshid, & Zafar, 2019)*. Implantable materials were first made available, such as polymers and metals, are bioinert and activated fibrous encapsulation after implantation, but they do not create a stable interface or bind with tissues as bioactive glass *(Sergi, Bellucci, & Cannillo, 2020)*. This scar tissue will cause tightness, pain, and difficulty to move *(Malik et al., 2021)*. Since biological tissues are not made of such materials, *Hench et al.* hypothesized that the human body rejects them through the formation of scar tissue *(Hench, 2006; Vallet-Regi & Salinas, 2021)*.

Autografts, xenografts, allografts, and alloplastic materials, each with unique benefits and drawbacks, have all been employed in the regeneration of bone *(Kumawat, BandyopadhyayGhosh, & Ghosh, 2022)*. The antigenicity and high osteogenic potential of autografts are advantages, but the need for a second surgical site increases morbidity, treatment time, and costs;Though problems with the donor site, like disease transfers, are eliminated *(Wisanuyotin et al., 2022)*. Allograft, on the other hand, has eliminates the need for a second surgical treatment which reduce a littel morbidity. This approach's possible drawbacks including infection, disease transmission, and the scarce supply of donors *(Wisanuyotin et al., 2022)*. Eventhough xenograft has an advantage in terms of affordability and usability, the genetics and histology of the tumors are often not symptomatic of human tumors, the fundamental drawback of xenograft is that it is difficult to achieve therapeutic success with this method *(Chaves et al., 2023)*.

Due to the aforementioned drawbacks, synthetic alloplastic materials including hydroxyapatite with calcium and phosphate as well as bioceramics like bioactive glass were developed *(Cheah et al., 2021)*. Bioactive glass was first discovered by professor Larry Hench at the University of Florida in 1969 *(Hench, 2006)*. Professor Hench began his research by investigating the need for implant materials that could adhere with living tissues in order to replace inert plastic and metal implants that the body failed to handle well *(Baino, Hamzehlou, et al., 2018; Todros, Todesco, & Bagno, 2021)*. For these reason the first bioactive glass, 45S5 bioglass, was developed using traditional melt method under high temperatures (1400 ℃) *(Neto & Ferreira, 2018; Vizureanu et al., 2021)*.

The 45S5 Bioglass® were produced with components 45% SiO_2 –24.5% Na_2O–24.5% CaO–6% P_2O_5 (weight %) *(Hench, 2006)*. It is a silicate based BG having a SiO_2 tetrahedron which serves as the oxide forming network. Since 45S5 bioglass, BG in various preparations has been produced for bone tissue regeneration. Because of its multifunctional features, including osteoconductivity, osteoinductivity, and angiogenesis, bioactive glass, an inorganic biomaterial, has received much interest in a number of biomedical applications *(Lalzawmliana, Anand, Roy, Kundu, & Nandi, 2020; Punj, Singh, & Singh, 2021; Zheng, Sui, et al., 2021)***.** It has been effectively applied to soft tissue repair, orthopedic/dental implant coatings, bone tissue engineering, and bone substitutes *(Ana, Satria, Dewi, & Ardhani, 2018; Shanmugam & Sahadevan, 2018)*.

Additionally, due to the biological effects of metallic ions released during the dissolution of the BGs, it has recently been used in soft tissue regeneration, cancer treatment, chronic wound healing, and so many other applications *(Fernandes et al., 2018; Mehrabi et al., 2020)*. It was also produced in different forms of sizes from a few millimeters to submicron powders and in a variety of shapes such as discs, rods, porous scaffolds, spheres, and fibers which are used in several applications including periodontal defect repair, nerve repair, implant components for bone scaffolds, bioactive coating for plastics metals and ceramics, dental applications such a toothpaste ingredient, fiber recruitment for composites, vascular regeneration, etc. *(ÖZEL, KIZIL, EMİR, & YÜCEL)*.

2.2 Bioactivity

Bioactivity refers to a material's essential capacity to form bond with living tissue *(Ferraris et al., 2020)*. The release of therapeutic ions and the partial dissolution of bioactive glass in the physiological fluid are the primary mechanisms of the development of this bonding *(Mehrabi et al., 2020)*. As stated by *Tiskaya et al.*, if a substance creates bonds with tissues, it is referred to as being "bioactive" material *(Tiskaya, Shahid, Gillam, & Hill, 2021)*. Additionally, it has been proposed that a substance is referred to as a bioactive material if it induces HAp which is the inorganic mineral of natural bone tissue *(Baino, Hamzehlou, et al., 2018)*. The HAp layer's development makes it easier for live tissues and implants to build a solid bond *(Kalpana & Nagalakshmi, 2022)*.

The most often studied bioactive glass compositions made from sol-gel are silicate glasses. The 3D network structure of bioactive silicate glasses, which are amorphous solids and are shown in figure 1, is made up of SiO_4 tetrahedron building blocks that are connected covalently to up to four neighboring SiO_4 tetrahedra by bridging oxygen (BO) atoms *(Montazerian & Zanotto, 2021)*. The modifying elements Na, Ca, and P forms an open silicate network of bioactive glasses which allows ion exchanges *(Tite et al., 2022)*. These elements are subsequently released into the surrounding physiological fluid, where the process of the HAp layer formation begins *(Deshmukh et al., 2020)*. The main components of bioactive glass, Si ions, in particular, promote angiogenesis, whereas Ca and P ions encourage osteogenic activity and cell proliferation *(Vallet-Regí, 2019)*. It is essential to understand the structure of BGs since it is important to recognize the role of each component in the bioactivity and biodegradability properties *(Mouriño, Vidotto, Cattalini, & Boccaccini, 2019)*.

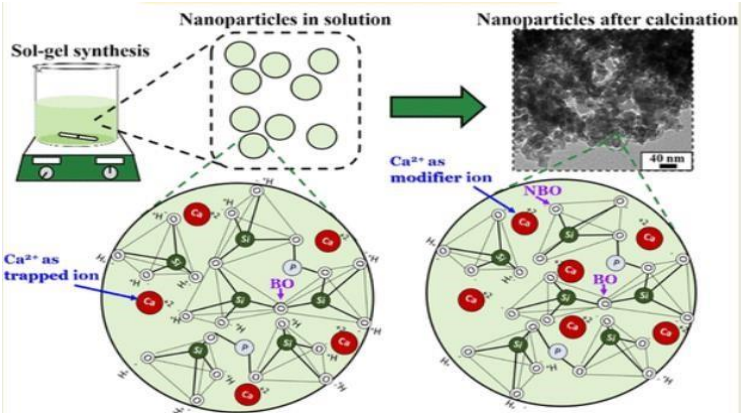

Figure 1. *Schematic representation of bioactive glass structure (Pajares-Chamorro & Chatzistavrou, 2020).*

The bioactivity process has been studied in vivo when BGs interact with bone tissues and in vitro when BGs interact with simulated body fluid (SBF) *(Cañas, Orts, Sánchez, Bellucci, & Cannillo, 2022).* It was suggested in 1991 that without using any animal testing, a material's capacity to adhere to the bone might be evaluated in vitro by studying how well apatite could develop on its surface in an acellular simulated body fluid (SBF) *(Kokubo & Yamaguchi, 2019).* Since then, SBF has been used by many researchers for evaluating bone-bonding ability of a material in vitro. The SBF solution consists of ion concentrations and pH nearly equal to those of human blood plasma as shown on table 1.

Table 1. *Ion Concentrations of SBF in Comparison with Human Blood Plasma (Kokubo & Yamaguchi, 2019).*

Ion	**Ion Concentration (mM)**	
	Blood Plasma	**SBF**
Na^+	142.0	142.0
K^+	5.0	5.0
Mg^{2+}	1.5	1.5
Ca^{2+}	2.5	2.5
Cl^-	103.0	147.8
HCO_3^-	27.0	4.2
HPO_4^{2-}	1.0	1.0
SO_4^{2-}	0.5	0.5
pH	7.2–7.4	7.4

The bioactivity or HAp forming process involves a variety of physico-chemical reactions, such as ionic exchange, diffusion, dissolution, and precipitation *(Baino, Hamzehlou, et al., 2018)*. The stages of bioactive apatite layer formation include ion release from BGs, the formation of silanol (Si-OH) groups on the glass surface, the adsorption of calcium and phosphate ions on the glass surface to stimulate the nucleation of amorphous calcium phosphate nanoclusters, and eventually growth and crystallization of the calcium phosphate (apatite) layer *(Chang & Zhou, 2018; Zambanini, Borges, Kai, & Marchi, 2019)*. Bioactive glasses which possess a suitable degradation rate, the capability to stimulate biologically beneficial responses, and the appropriate ability to promote the formation of HAp layer are desirable for bone tissue regeneration application *(Al-Harbi et al., 2021)*. However, textural properties like porosity and surface area provide the real key for enhanced bioactivity of BGs *(Kargozar et al., 2019)*.

Leaching, dissolution, and precipitation are the sources of the chemical reactions which take place on the surface of the glass as it comes into contact with body fluid *(Fernandes et al., 2018)*. Based on such interfacial interactions, the biological responses cause the bioactive glass and live tissues to chemically adhere *(Zheng, Kapp, & Boccaccini, 2019)*. Following invivo implantation or soaking into SBF, the first immediate reaction that occurs on the surface of the glass is the cation replacement of Ca^{2+}, Na^{+}, or K^{+} with H^{+} or H_3O^{+} from the SBF solution *(Park, Rezabeigi, & Nazhat, 2021)*. The breakdown of Si-O-Si bonds during the dissolution reaction, which is mainly caused by hydroxyl ions, results in an alkaline microenvironment where the solution's alkalinity is revealed *(Deshmukh et al., 2020)*. The dissolution that takes place at the glass surface leads to the formation of silanol groups (Si-OH) at the glass and solution interface *(Nommeots-Nomm, Hupa, Rohanová, & Brauer, 2020)*. A layer rich in SiO_2 (silica gel) is created on the surface as a result of the condensation and re-polymerization of hydrated silica groups with the silanol group. Such precipitations are aided by the amorphous Ca-P layer that forms on top of the SiO_2 rich layer as a result of the Ca^{2+} and PO_4^{-3} ions moving to the surface within the SiO_2 rich layer *(Hupa, 2018)*. Surface reactions at the BGs surface take place at various phases and result in the formation of Si-rich and Ca-P layers *(Deshmukh et al., 2020; Siekkinen, Karlström, & Hupa, 2022)*. The introduction of soluble

Ca-P from the supersaturated solution causes the amorphous Ca-P layer to grow *(Siekkinen et al., 2022)*. Diffusion-controlled alkali ion exchange results in an increase in the SiO_2-rich layer's thickness *(A. Salinas, Vallet-Regi, & Heikkilä, 2018)*.

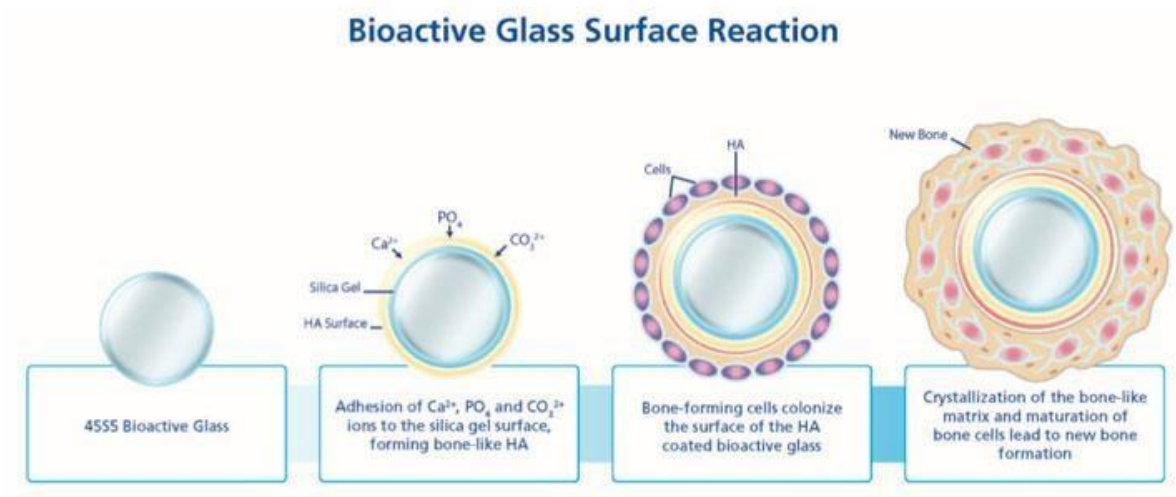

Figure 2. *Schematic diagram for HAp formation process of silicate bioactive glass (Pedanaboyina, 2019).*

As *Deshmukh et al.* stated typically, sol-gel produced BGs with high porosity and specific surface area have poorer mechanical stability but higher bioactivity and biodegradability *(Deshmukh et al., 2020)*. The BGs synthesized via the sol-gel method have been utilized in a number of applications including the encapsulation of enzymes, proteins, and biomolecules for controlled drug administration, and bone tissue regeneration because of their exceptional bioactivity, *(Catauro & Ciprioti, 2021; Deshmukh et al., 2020)*. Additionally, it was discovered that the network structure and enhanced textural properties, including porosity, which is associated with a large surface area and higher dissolution rate, are the main keys to improving the bioactivity of sol-gel glasses *(Abdullah, Lee, Idris, & Selimin, 2020)*. The in vitro bioactivity of BGs is determined by the textural properties, which include specific surface area, pore volume, and pore size *(Lalzawmliana et al., 2020)*. Narrow mesopore size distribution and high specific surface area can induce high invitro and invivo bioactivity as well as biodegradability of BGs *(Schumacher et al., 2021)*.

2.3 Biodegradability

Biodegradability is one of the most essential qualities of bioactive glasses. Increased reactivity is a characteristic of biodegradable bioactive compounds, which is closely related the HAp layer formation *(Du, Chen, Liu, Xing, & Song, 2021)*. Although biodegradation is crucial when utilizing bioactive glasses, rapid degradation rates negatively affect cell adhesion and proliferation, which hinders the formation of new bone tissues *(Koons, Diba, & Mikos, 2020; Wei, Ma, Xu, Gu, & Ma, 2020)*. For the purpose of bone tissue regeneration, it is preferable to use bioactive glass that have a reasonable degradation rate, the capacity to support the formation of HAp layer, and the capacity to stimulate biologically advantageous reactions *(Punj et al., 2021)*. Bioactive glasses' ionic dissolution products are widely known for promoting vascularization, osteogenesis, and angiogenesis *(Zheng, Niu, et al., 2021)*.

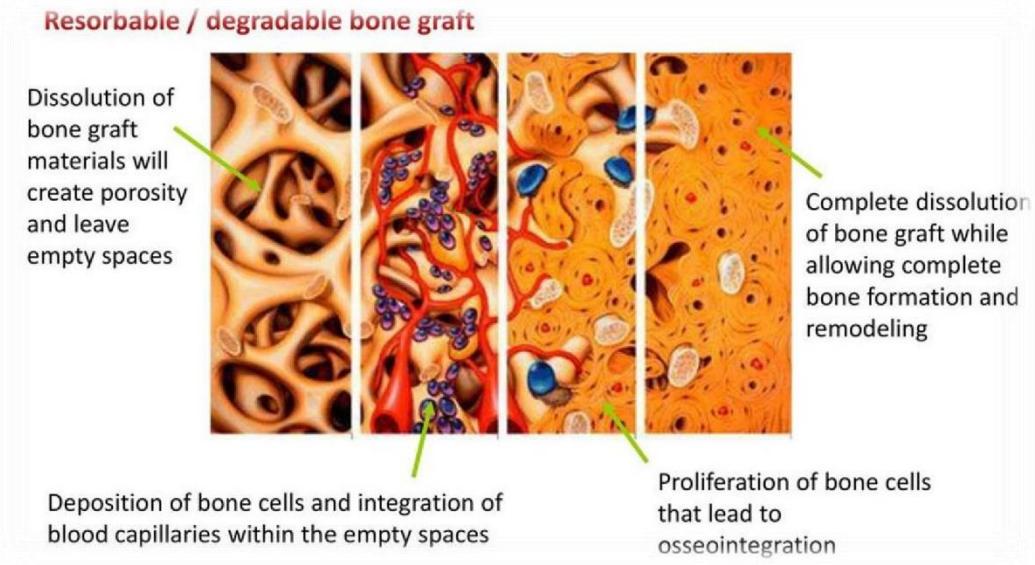

Figure 3. *Biodegradation process of degradable bone grafts (Singh, 2013).*

Degradable materials are preferable than durable implant materials for a range of applications because they can be replaced by regenerated tissues and are resorbable into the body *(Koons et al., 2020)*. Understanding the degradation mechanism and the factors that affect the rates of degradation of sol-gel-based bioactive glasses is essential since it can be challenging to control the rate of degradation *(Deshmukh et al., 2020; Ramli et al., 2023)*. Additionally, the dissolution of the glass in contact with physiological fluids and the release of Ca and P ions

are both necessary for the bio-mineralization of glasses *(Ben-Arfa, Fernandes, Miranda Salvado, Ferreira, & Pullar, 2018).* The glass network connectivity, which is often lower for BGs made from sol-gel than for glasses made from melt, determines the kinetics of this process *(Schumacher et al., 2021).* Modifier cations like Ca ion, which introduce non-bridging oxygen, further reduce network connectivity *(Brauer & Jones, 2021).* As a result, there was a tendency for glasses to degrade more quickly as the CaO content rose in which reduction in Ca/P ratio (i.e., increased phosphate content) led to a less significant dissolution for materials that contained both CaO and P_2O_5 *(Schumacher et al., 2021).*

Simulated bodily fluids (SBF), tris buffer solution, phosphate buffered saline, and culture media are typical solutions used in dissolution studies *(Deshmukh et al., 2020; Yilmaz, Pazarceviren, Tezcaner, & Evis, 2020).* Ionic dissolution products have been demonstrated to be the primary agents in gene activation, enabling a favorable gene response that is directly related to the osteogenesis process *(Baino, Fiume, et al., 2018).* Monitoring mass loss, the concentration of released dissolving products, and the pH change in the solution allow one to determine the rate at which a material degrades *(Baino, Fiume, et al., 2018; Lopes, Bueno, Mazali, & Bertran, 2019).* Studies have shown that increased surface area and pore volume in sol-gel bioactive glasses accelerate the ability to generate HAp more quickly than melt-derived ones *(Fiume et al., 2018; Xie et al., 2020).*

2.4 Synthesis of bioactive glass

Melt-quenching and sol-gel methods are used for the synthesis of bioactive glass. These techniques are utilised for developing distinct BGs with diverse features, including porosity, bioactivity, biodegradability, and others. The melt-quenching method produces glass by melting a mixture of raw ingredients, which is then solidified by quenching to form glass frits. The organic precursors are utilised in the sol-gel process to generate the amorphous glass through gelation and drying.

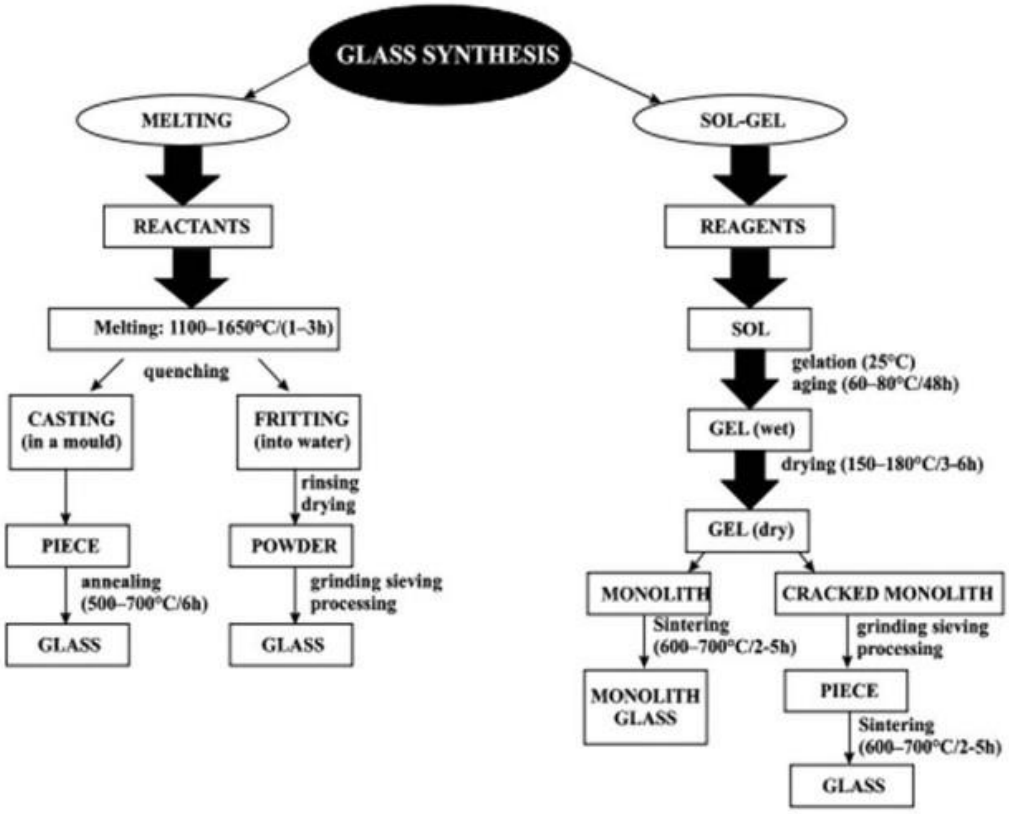

Figure 4. *Melting and sol-gel process of BG synthesis (Kaur, Pickrell, Sriranganathan, Kumar, & Homa, 2016).*

2.4.1 Melt-derived BG synthesis

Glass is most frequently produced by fusing two or more component oxides followed by quenching. It involves (a) mixing an appropriate mole/weight fraction of initial ingredients for preparing batch of glasses; (b) grinding the mixture to break up agglomerate particles and obtain uniform powder; (c) The mixture is then transferred to a ball mill to be ground into a more uniform particle size (the ball milling can be done using porcelain or agate balls in the appropriate jar); (d) the resulting mixture is dried in air; (e) the powder is then melted in recrystallized alumina crucible or platinum crucible at a high temperature furnace; (f) the molten component then quenched in a graphite mould (for rods or monoliths) or in water (frit) *(Kaur et al., 2016; ÖZEL et al.).*

In 1969, Professor Larry Hench invented the first BG 45S5 bioglass using conventional melt method at high temperatures (1400°C) *(Hench & Jones, 2015)*. SiO_2, CaO, NaO, and P_2O_5 were the four components that made up the first bioactive glass via a melt-derived process *(Fletcher, Alles, Keenan, & Wren, 2022)*. The BG produced was with components 45 % SiO_2, 24.5 % Na_2O, 24.5 % CaO, 6 % P_2O_5 (weight %) which later referred to as 45S5 bioglass *(Fiume et al., 2018; Hench, 2006; Vafa et al., 2021)*. The biological reaction at the material tissue contact forms HAp at the surface of the glass, indicating the bioactivity of this bioactive glass *(Dhinasekaran Durgalakshmi et al., 2018)*. A strong interfacial contact between the bioactive glass and the living tissues were created as a result of the bone mineral layer growing and bonding with collagen in the bone cells in response to an increase in reaction time *(Westhauser et al., 2019)*. In both in vitro and in vivo environments, the bioactivity was thoroughly proven; however, there are certain restrictions such as the reactants must be melted at a very high temperature upto 1400 °C and lack of microporous structures in this form of BG *(Monajem-Isfahani, 2018; Vallet-Regi & Salinas, 2021)*.

2.4.2 Sol-gel derived BG synthesis

Li et al. used the sol-gel method for making BGs at a lower temperature *(Kong, Steffi, Shi, & Wang, 2018)*. Due to the benefits of low temperature processing, the sol-gel synthesis approach, as compared to the traditional melt quench method, enables the manufacture of glasses with higher purity, high specific surface area, and different surface morphology than the melt derived BGs *(Deshmukh et al., 2020)*. Solution and gelation are the two separate phases that make up a conventional sol-gel synthesis. It involves (a) small molecules (precursors) that are often created by carefully controlling the hydrolysis and condensation of metal alkoxide precursors or organic/inorganic salts inside the solution are turned into colloidal solutions (sols) during the first phase; (b) the second step is the gelation and aging step takes place at a temperature of about 60 °C, which creates a three-dimensional mesh to increase the viscosity of the solution; (c) it is then subjected drying processes to remove the liquid phase, usually at a temperature between 100 °C and 140 °C; (d) after obtaining the dried gel in the last step, the material is stabilized at a high temperature of about 600-700 °C *(Chen, Zeng, Chen, Liao, & Zheng, 2018; Esposito, 2019; ÖZEL et al.)*.

When producing bioactive materials used in tissue engineering, there are various benefits of a sol-gel derived glass over a melt derived glass. These advantages include lower processing temperatures, a wider range of SiO_2 usage (up to 90 mol%), a lack of the need for sodium oxide (which is used in conventional melt-derived bioactive glasses), and a final glass product with higher purity, bioactivity and nano-scale porosity, making the bioactive glass desirable to be impregnated with biologically active substances like growth factors *(Ahmadi, Behnamghader, & Asefnejaad, 2017; Deshmukh et al., 2020)*. These sol-gel BGs shown formation of porous BGs with superior bone bonding, degradation, and resorption characteristics as a result of the enhanced surface area and porosity *(Baino, Fiume, et al., 2018; Kong et al., 2018; Migneco et al., 2020).*

Controlling the sol-gel synthesis process requires an understanding of the kinetics of the condensation and hydrolysis events *(Bueno, Herrera, Bertran, San-Miguel, & Lopes, 2021; Q. Lei et al., 2020).* In general, the gelation process requires a clear, stable solution made up of hydrolyzed monomers with low condensation rates *(Baino, Fiume, et al., 2018)*. Thus, a variety of experimental conditions, including as the pH of the solution, temperature, reactant concentration, and the presence of additives that might be regulated throughout the sol-gel synthesis, have an impact on these processes *(Baino, Fiume, et al., 2018)*. In terms of characteristics and uses, a porous bioactive glass is favored due to its high specific surface area, controlled porosity, and composition *(Chuni, Dachasa, Gochole, Hunde, & Bakare, 2023)*. The pore-volume, specific surface area, and porosity of glasses are influenced by the synthesis method employed, compositions, and additives *(Chuni et al., 2023; Lalzawmliana et al., 2020).*

Among different techniques used for developing porous BGs, surfactants as a structure directing agent were widely used *(Kong et al., 2018; Sharifi et al., 2022)*. Mesoporous bioactive glasses (MBGs), the third generation BG, were first produced in 2004 by merging the sol-gel technique and supramolecular chemistry of surfactants in order to produce BGs with more controllable textural qualities than conventional sol-gel BGs *(Xiaoxia Yan, Yu, Zhou, Tang, & Zhao, 2004)*. Besides surfactants it was also found that acid catalysts has their own effect on surface morphologies beyond their catalytic use in the hydrolysis reaction of metal alkoxides *(B. Lei et al., 2011a; Mehrabi et al., 2020)*. Organic acids such as acetic acid,

lactic acid, and citric acid and also inorganic acids such as phosphoric acid, nitric acid, and hydrochloric acid have been used in some studies for the synthesis of MBGs *(Chakraborty et al., 2021; Dang et al., 2020; Hong et al., 2018).*

2.5 Sol-gel with surfactants

In templating approach of porous BG synthesis, surfactants are usually employed as soft template to guide the formation of porous structures *(Kabtamu, Wu, & Li, 2020)*. Surfactants are substances with long-chain organic molecules having a hydrophilic head and lipophilic (hydrophobic) tail that lower the surface tension of the medium in which they are dissolved and the interfacial tension with other phases, thus they are positively adsorbed at the liquid/vapor and/or liquid/solid interface *(Chowdhury, Rakshit, Acharjee, & Saha, 2019; Ghosh, Ray, & Pramanik, 2020)*. In order to synthesize porous bioactive glass with ordered porosity, a homogenous solutions of surfactants in a solvent is required *(Deshmukh et al., 2020; Lalzawmliana et al., 2020)*. The hydrophilic components of the surfactant molecules form connections with the glass precursors (mostly hydrolyzed silica from TEOS hydrolysis) while the hydrophobic components are maintained inside the micelle inner structure in which after being calcined yields pieces of porosity with high pore interconnectivity *(Anand, Kundu, & Nandi, 2022; Kumar, Murugavel, Aditya, & Boccaccini, 2017; Pal, Lee, & Cho, 2020)*.

The porous structure of BG particles formed by surfactants provides large specific surface area and pore volume which improve the bioactivity, degradability, loading and controlled release of biomolecules *(Kong et al., 2018)*. The idea of adding surfactants as a structural template to prepare Mesoporous bioactive glass (MBGs) was introduced by *Yan et al.* in 2004 using block copolymer as a pore forming template in the sol-gel method *(Anand et al., 2019; Xiaoxia Yan et al., 2004)*. Since then utilizing the sol-gel process and the integration of structure-directing agents such cetyltrimethyl ammonium bromide (CTAB), F127 (EO_{106}-PO_{70}- EO_{106}), and P123 (EO_{20}-PO_{70}-EO_{20}) into the glass structure, the highly ordered mesoporous bioglasses were created *(Kargozar, Montazerian, Hamzehlou, Kim, & Baino, 2018)*. BGs can be prepared as three-dimensional scaffolds, spheres, particles and fibres using different preparation routes. A well-ordered mesoporous structure with high surface area and porosity is obtained when the mixture is dried and the surfactant gets removed; *(Mohamed et al., 2020).*

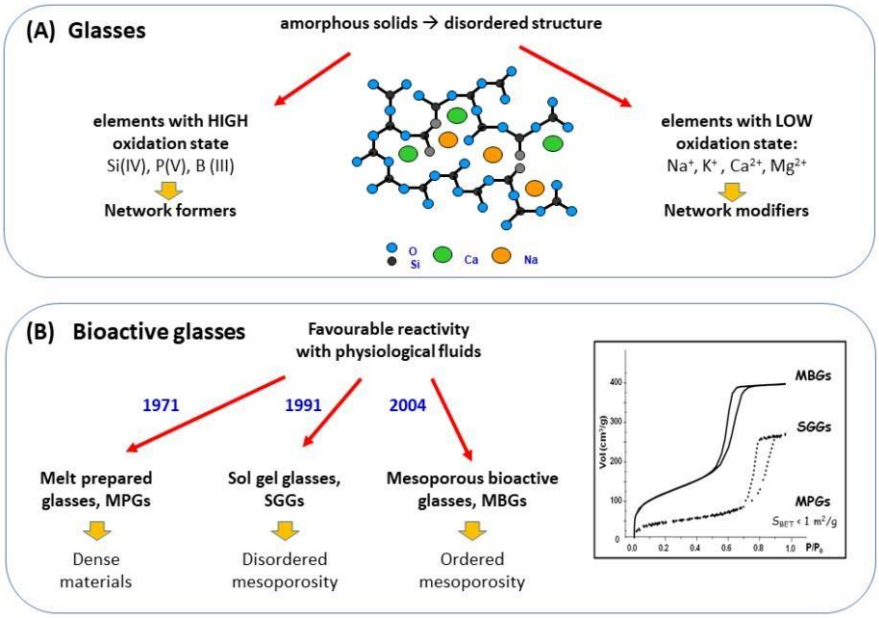

Figure 5. *Main features of: (A) glasses and (B) the three families of bioactive glasses (A. J. Salinas & Esbrit, 2022).*

Surfactants include anionic, cationic, and non-ionic types in which both basic and acidic media can use cationic surfactants because they are comparatively soluble in both media *(Migneco et al., 2020)*. However, non-ionic surfactants are non-toxic, biodegradable, readily accessible, and reasonably priced *(Koumba Ibinga, Fabre, Bikanga, & Mouloungui, 2019)*. Surfactant's propensity to produce pores may also be affected by additional features including the hydrophilic head group, counterion, and length of the hydrophobic carbon chain *(Chircov et al., 2020; Zheng, Sui, et al., 2021).* Using surfactants as a structure directing agent has been used to achieve a precise control over pore size and the formation of controlled pore structures enhanced bioactivity and biodegradability of BGs *(Zheng, Sui, et al., 2021)*.

It has been demonstrated that the choice of surfactant directly impacts on pore structure, pore size, and pore volume of porous bioactive glass (PBGs) *(Schumacher et al., 2021)*. Large specific surface area, pore size, and pore volume are provided by the porous structure of BG particles generated by surfactants, which enhances the loading and controlled release of biomolecules *(Lalzawmliana et al., 2020)*. Wherein keeping the synthesis procedure same and simply using various templates such as F127, P123, and CTAB results in cubic, hexagonal, and worm-like pore structure, respectively *(Pal et al., 2020; Sharifi et al., 2022)*. It was found

that treating MBGs with a high surfactant concentration produced a wrinkled structure, caused by the aggregated surfactant lamellae, which reduced the mesopore density and thereby lowered the specific surface area *(Chircov et al., 2020; Rastegari et al., 2021).*

In the synthesis of PBGs, cationic surfactant cetyltrimethylammonium bromide (CTAB) is the most frequently utilized and reported surfactant *(Migneco et al., 2020).* Numerous investigations on employing this surfactant for the synthesis of PBGs have been conducted since it was discovered in 2007 that CTAB may be utilized as a template for the synthesis of MBGs *(Ma et al., 2017).* According to *Lei et al.* study, a transition from a spherical to a rodlike morphology in particle shape occurs when the concentration of CTAB in solution is between 1mM and 5 mM *(Khurshid et al., 2019; Q. Lei et al., 2020).* In fact CTAB derived materials are frequently characterized by smaller pore sizes (2–3 nm) than P123 or F127-based systems (4–10 nm) *(Migneco et al., 2020).* P123 templated MBGs have greater pore volumes and specific surface areas than F127 when pore volume is taken into account which enables P123 based MBGs have a much higher drug loading efficiency than F127 based MBGs of the same composition *(Lalzawmliana et al., 2020; Migneco et al., 2020).*

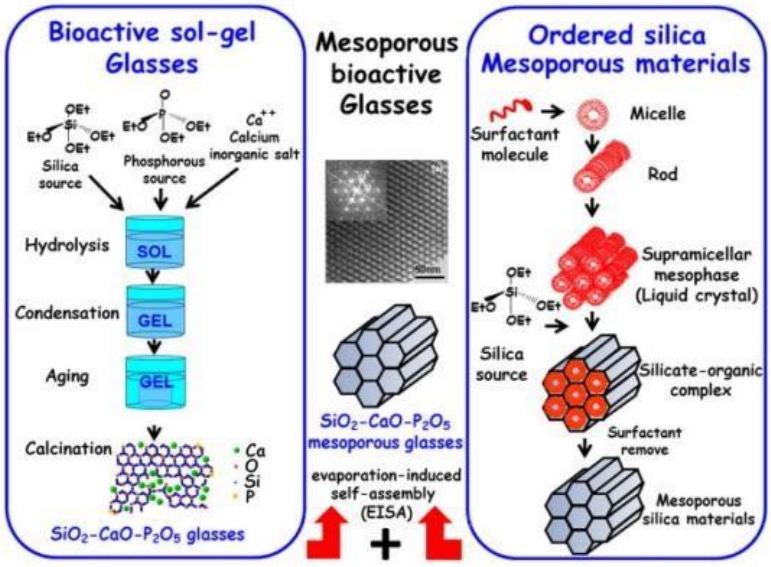

Figure 6*. Production of PBGs by sol-gel method (left side) and mesoporous silica(right side) obtained by sol–gel and supramolecular arrangement routes, respectively. MBGs are produced by combining these two routes (middle image) (Kargozar et al., 2018).*

Hu et al. reported CTAB assisted facile method for the sol-gel synthesis of hollow mesoporous bioactive glass (HMBGs) microspheres with tailorable cavity sizes *(Deshmukh et al., 2020)*. CTAB acted as a structure directing agent and favored the synthesis of HMBGs with hollow mesoporous structure, high surface area and homogeneous particle size in which the size of HMBGs particles and the cavity sizes were determined by CTAB concentration *(Liang et al., 2019)*. When the CTAB concentration was varied as 3.3, 4.6 and 5.9 mM and the average particle size for the synthesized HMBGs was reported to be 294 nm, 264 nm, and 187 nm respectively. The corresponding HMBGs the particle size of HMBGs decreased and the morphology changed from hollow spheres to solid spheres which displayed narrow particle size distribution, good dispersibility and high specific surface areas *(Y. Wang & Chen, 2017)*. A study done using tri-block copolymers (L121, P123, and F127) with various lengths of hydrophilic chains as structural templates to achieve different pore sizes shown on high resolution transmission electron microscopy (HRTEM) images in Figure 7, it appears that the L121-treated MBG powder had larger bright areas (i.e., larger pores) than did the P123- and F127-treated MBG powders. This difference implies that the L121 surfactant produced the largest pores *(Chou, Hong, Lin, Wang, & Shih, 2017)*. Although silica precursors frequently form discrete particles rather than 3D gelled structures in micelles under acidic conditions, Pluronic templates like P123 and F127 have a tendency to combine to form micelles. Thus, these surfactants never form mesophases under extremely basic conditions, which limits the capacity to produce monodispersed and homogenous spherical particles using these templates.

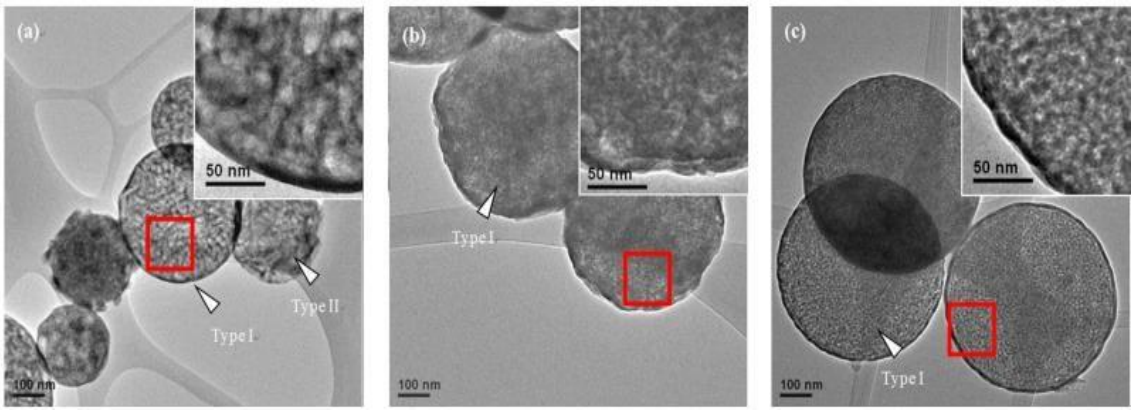

Figure 7*. TEM micrographs of (a) L121-; (b) P123-; and (c) F127- treated MBG powders (Chou et al., 2017).*

According to reports, the linear hydrophilic polymer polyethylene glycol (PEG) has been used successfully as a surfactant in the synthesis of MBG. PEG has been recognized for in vivo injection and is used in cosmetics, biotechnology, and medicine because it is an amphiphilic with the capacity to lower surface activity and has qualities such as non-toxicity, great biocompatibility, and high stability. *El-Fiqi et al.* synthesized MBGSs using PEG as the single template in a base-catalyzed sol–gel process with ultra-sound assistance *(El-Fiqi, Buitrago, Yang, & Kim, 2017)*. They studied how the morphology of the resultant particles changed depending on whether CTAB or PEG was used as the only template. Their findings showed that using CTAB as the template increased specific surface area and pore volume while decreasing pore volume and pore size when using PEG as the template.

Furthermore, neutral surfactants like Dodecyleamine (DDA) can serve as the template and catalyst *(Yao et al., 2021)*. DDA is a kind of organic weak base with amphipathy, which is usually used as template to synthetize mesoporous materials. The particle size, pore size, and pore volume of MBGSs can be adjusted by varying the amount of DDA utilized *(Hu, Chen, Zhao, & Li, 2013; Hu, Chen, Zhao, Li, & Mao, 2014)*. The use of DDA as a catalyst and template has effectively solved the existing problems such as the severe agglomeration, irregular shape and low specific surface area of the conventional sol–gel BGs particles *(Hu, Chen, et al., 2014)*. Also nonionic surfactants such as Hexadecylamine (HDA) can also be used as pore forming templates to guide the mesoporous structure in MBGs *(Xiaojian Wang & Li, 2016)*. The effects of different surfactants on specific surface area, pore volume, and pore size are summarized on table 2.

Table 2. *Textural characteristics of BGs prepared by using different structure directing agents.*

Structure directing agent	**Specific surface area (m^2/g)**	**Pore volume (cm^3/g)**	**Pore size(nm)**	**References**
	300–350	0.4–0.49	4.3–4.6	*(Xiaoxia Yan et al., 2004)*
	278-400	0.54-0.73	6.5-6.9	*(Xia & Chang, 2006)*

P123	250-350	0.4-0.5	5	*(Li et al., 2007; C. Wu, Miron, et al., 2011; Zhu et al., 2008)*
	438-466	-	3.5-3.7	*(X. Wu et al., 2010)*
	450-480	0.63-0.73	5.37-6.43	*(A García, Cicuéndez, Izquierdo-Barba, Arcos, & Vallet-Regí, 2009)*
	499	0.7	6.1	*(P. Yan et al., 2010)*
F108	516		5	*(Xiaoxia Yan et al., 2004; Yun, Kim, & Hyun, 2008)*
B50-6600	301	0.41	6.4	*(XX Yan et al., 2005)*
P85	328	0.36	3.4	*(Ana García, IzquierdoBarba, Colilla, De Laorden, & Vallet-Regí, 2011)*
F127	520	0.51	5.4	*(Yun, Kim, & Hyun, 2009)*
	228-300	0.36-0.42	5.0-7.1	*(X. Yan et al., 2010)*
	152-310	0.235-0.356	4.2-5.0	*(X. Yan et al., 2010)*
CTAB	1040	1.54	1.82-2.2	*(Yun, Kim, Lee, & Song, 2010)*
	443	0.57	2.9	*(C. Wu, Fan, & Chang, 2013)*
P123+CTAB	552-618	0.69-1.08	4.1-6.2	*(S. Zhao, Li, & Li, 2010)*
DDA	115	0.685	2.3	*(Hu, Li, Miao, Zhao, & Chen, 2014)*
Hexadecylamine	400	0.48	3	*(Xiaojian Wang & Li, 2016)*
	150	0.20	3	*(Xiaojian Wang & Li, 2016)*
	56	0.07	-	*(Xiaojian Wang & Li, 2016)*

MBG powder with various surfactant types and surfactant concentration were synthesized and characterized to examine the specific surface area and bioactivity. However, the majority of surfactants can lead to issues including carbon contamination and micelle aggregation *(Hong et al., 2018)*. The specimen's particle morphology will have wrinkled surfaces as a result of the micelle aggregation *(Shih et al., 2016)*. Carbon contamination will also prevent HAp from forming. Both occurrences will cause the bioactivity and other crucial qualities of bioactive glass to decrease. *Shih et al.* have studied surfactants incomplete decomposition causes carbon contamination which also affect bioactivity of MBGs *(Shih, Chou, & Panjaitan, 2013)*. Fourier transform-infrared spectroscopy (FT-IR) spectra of the precursors and the various temperature calcinated MBG particles were examined for potential carbon contaminations in those particles. The result reveals that residual carbonates were found in the particles at different calcination temperature which requires higher decomposition temperature which reaches up to 800 ℃.

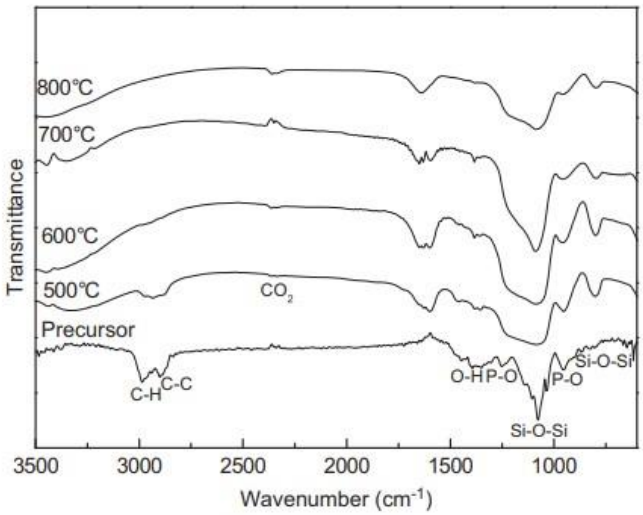

Figure 8. *FTIR spectra of the MBG particles calcinated at the temperatures of 500, 600, 700 and 800 ºC (Shih et al., 2013).*

Therefore, according to recent research, a surfactant-free method must be developed to create PBGs and enhance the bioactivity, biodegradability, and biocompatibility of BG. A novel method of BG synthesis by *Hong et al.* using hydrogen peroxide (H_2O_2) has been used as a pore-forming agent to replace the traditional surfactants *(Hong & Shih, 2017)*. The quick

oxygen generating ability, complete solubility, and absence of carboxylic group in this pore forming agent makes it possible to achieve a bioactive glass free from carbon contamination and micelle aggregation which enables effective bioactivity and biodegradability.

2.6 Sol-gel with acid catalysts

The hydrolysis and condensation reactions depend on the catalyst type and concentration employed *(Issa & Luyt, 2019)*. Several acid catalysts have been used in the synthesis of bioactive glass for catalyzing hydrolysis reaction of alkoxide precursors *(Bueno et al., 2021)*. Acid catalysts provide H^+ ions that speed up hydrolysis by removing electron density from the atom bearing the leaving group and making it more vulnerable to nucleophilic attack by H_2O *(Lopes, Magalhães, & Bertran, 2022)*. The type of catalyst used affects dramatically the surface morphology of particles and the selection of the catalyst depends on the desired properties of the final product *(Ben-Arfa, Fernandes, Salvado, et al., 2018)*.

For the hydrolysis of silicon (Tetraethyl orthosilicate, TEOS) and phosphorous (Triethyl phosphate, TEP) alkoxides, acid catalysts have been utilized in the synthesis of bioactive glass, which tends to alter the surface morphology of the particles *(Kuo et al., 2021)*. The morphology of the particles and the hydrolysis reaction are both significantly influenced by the catalyst source (often inorganic or organic acids), which is a major aspect of the sol-gel process *(Deshmukh et al., 2020; Kuo et al., 2021)*. The first ordered MBG with improved specific surface area and pore volume was created using the acetic anhydride as a catalyst *(Migneco et al., 2020)*. According to experimental findings, acetic anhydride was able to form highly structured MBG in place of inorganic strong acids *(Hong et al., 2018)*.

According to the study by *Kuo et al.* forming hydrogen bonds with the inorganic precursor, the weak organic acids lactic and citric acids, which are both hydroxyl-carboxylic acids, may promote the development of silicate particles and cause homogenous hydrolysis of the precursor *(Kuo et al., 2021)*. A study by *Li et al.* shows that without any acid catalyst, BG displays partial hydrolysis and, as a result, an irregularly structured morphology with a cracked surface was obtained. Sol–gel BG without using organic acid (BG0) exhibits the irregular shape and cracked surface. Acetic acid derived BG (ABG) displays the similar feature to BG0 (Fig. 9g, h). Comparing with BG0 and ABG, citric acid and lactic acid derived

BGs (CBG and LBG) show the regularly spherical shape and micro-rough surface (Fig. 9c, d, e, f) *(B. Lei et al., 2011a).* As a result, under the catalysis of citric and lactic acids, regularly shaped microspheres with a comparatively smooth surface were produced. Acetic acid, a relatively weak organic acid without hydroxyl in its structure compared to citric and lactic acids, causes the inhomogeneous hydrolysis of BG and produces the irregularly shaped structure *(B. Lei, Chen, & Koh, 2011b).*

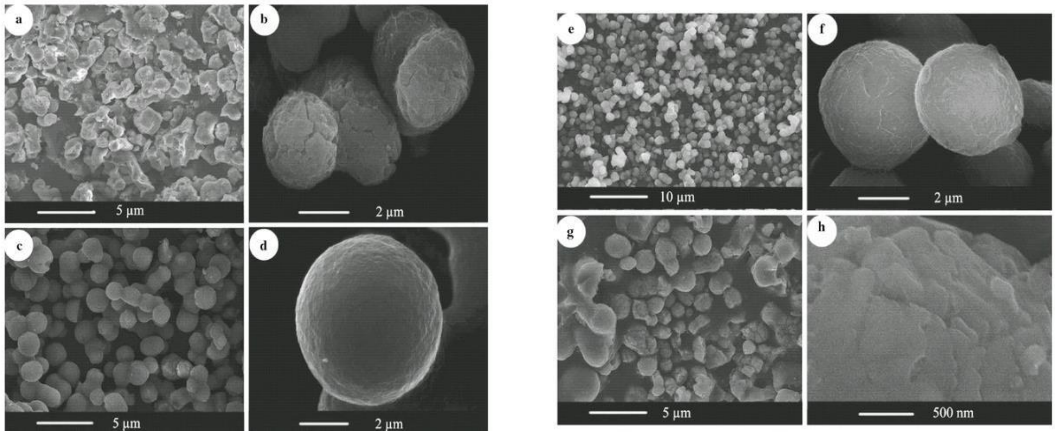

Figure 9. *FE-SEM analysis of acid catalyzed BGs: untreated BG ((a, b) BG0), citric acid treated BG ((c, d) CBG), lactic acid treated BG ((e, f) LBG), acetic acid treated BG ((g, h) ABG) at different magnification (B. Lei et al., 2011a).*

Compared with inorganic acids such as nitric and hydrochloric acids, biological hydroxyl–carboxyl acids like acetic acid, malic acid and citric acid possess particular chemical structures that can affect the structure and morphology of sol–gel-derived materials which also have a great potential for low-temperature sol–gel synthesis *(B. Lei et al., 2010).* Due to issues with the removal of their by-products, it was discovered that the main disadvantage of employing inorganic acids as catalysts is the increase in the concentration of inorganic acids in the sample *(Ben-Arfa, Palamá, Salvado, Ferreira, & Pullar, 2020). Faure et al.* effectively exploited citric acid as a catalyst for the manufacture of 45S5 bioactive glass ceramic by substituting weak organic acids (0.5-50 mM) with much lower concentrations of strong inorganic acids (0.5-2 M) *(Faure et al., 2015).*

A study by *Lei, Chen et al.* shows on Figure 10 that after soaking BG particles in SBF for 24 h, the surface morphology of particles has changed and a layer of deposit forms on their surfaces. However, the deposit morphology on the surface of BG was different from each other based on the type of catalysts used to synthesize. Irregular non-dense particles formed on untreated bioactive glass BG0 (a, b), a continuous layer of dense particles emerged on citric acid treated BG (c, d), lactic acid treated BG (e, f) and acetic acid treated BG (g, h) were obtained.

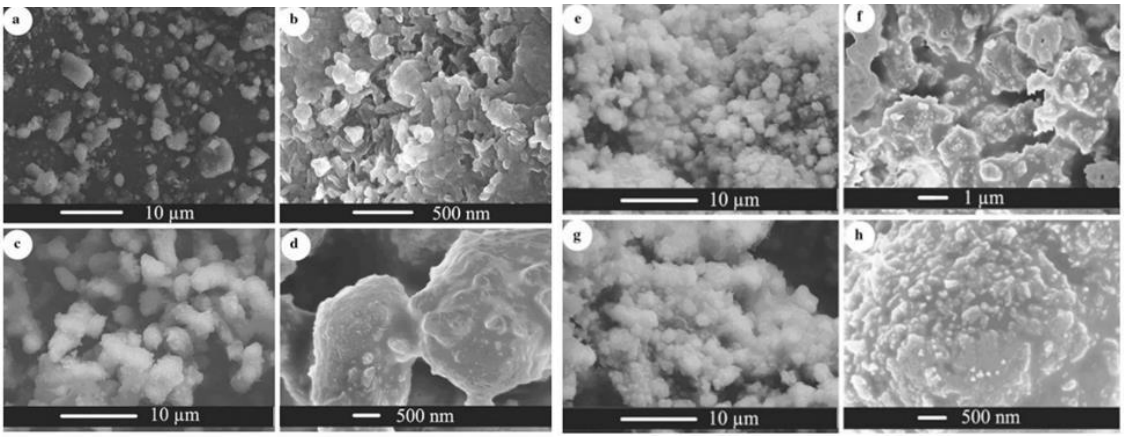

Figure 10. *Surface morphology of BG0 (a, b), CBG (c, d), LBG (e, f), and ABG (g, h) after soaking in SBF for 24 h (B. Lei et al., 2010).*

As *lei et al.* study of organic acid effect on HAp formation, bioactivity test showed that all samples induce the formation of crystalline apatite layers in 24 h *(B. Lei et al., 2011a)*. It was indicated that addition of different organic acids changed the morphology and microstructure of microspheres, but did not weaken their apatite-forming capacity. As compared to irregular shaped particles, the smooth morphology facilitates procedures of bone tissue regeneration, optimizes drug release and minimizes inflammatory reactions. In this study, the use of citric acid and lactic acid in the sol–gel process makes it possible to control spherical morphology and structure of BGs as well as their in vitro apatite-forming bioactivity.

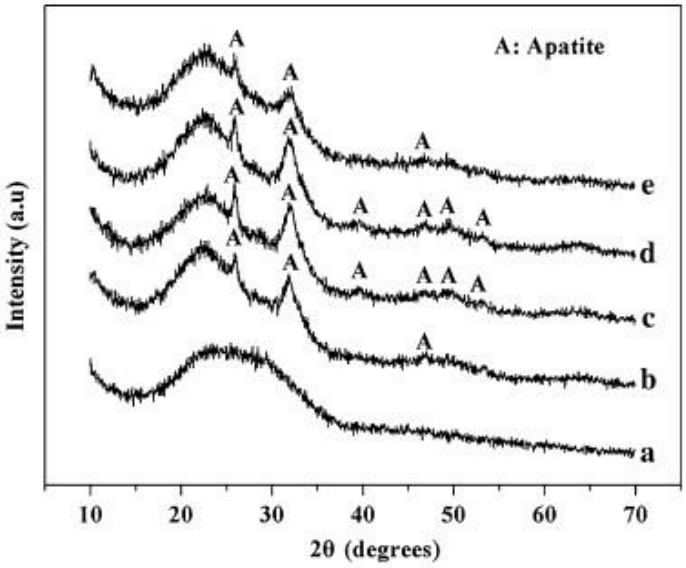

Figure 11. *XRD patterns of (a) sample before soaking in SBF, (b) BGM0soaked, (c) CBGM,(d) LBGM (e) ABGM soaked in SBF for 24 h (B. Lei et al., 2011b).*

2.7 Effects of composition and porosity on bioactive glass

It is well-recognized that the surface morphology (porosity, pore size and pore volume) and chemical composition of BGs determine their physiochemical and biological properties *(Zheng, Sui, et al., 2021)*. For BGs applications to be successful, morphology and composition of particles must be precisely controlled. The hydrolysis and condensation of silica precursors, the type and concentration of templates, interactions between precursors and templates, catalysts, temperature, and additives are just a few examples of the many variables that might impact the morphology of BGs during sol-gel processing *(Ijaz, Yagci, Ow-Yang, Demirel, & Miko, 2020; Xun et al., 2022)*. Particle morphology and pore structure of gel-derived BGs can be precisely tuned and regulated by adjusting these variables.

From 1969 to 1971, three types of glass with different compositions based on the Na_2O–CaO– SiO_2 ternary state diagram were evaluated as to create a viable biomaterial *(ÖZEL et al.)*. The hypothesis behind choosing the chemical compositions of bioactive glasses is that the bone comprised collagen fiber, bone cells and HAp crystals, the implant material should be capable of forming the HAp layer on the surface in the biological fluids *(Ingole, Sathe, & Ghule, 2018)*. Since their discovery, most of the research work being carried out on bioactive glasses is dealing with the compositions that form interfacial bonding with the tissue. The formation of the HAp layer on the surface in vitro or in vivo is considered as an indicator of glass bioactivity *(Łukowicz et al., 2020)*.

The composition of bioactive glasses can be easily adjusted thereby conferring specific properties to the materials which can be effective in fulfilling the demands of a vast variety of biomedical applications *(Y. Zhao, Zhang, Pan, & Liu, 2021)*. The sol–gel process significantly expands the range of chemical composition of bioactive glasses, including conditions and preparation protocols *(Dhinasekaran & Kumar, 2022)*. There are four BG classes; (1) 35-60 wt% SiO_2, 10-50 wt% CaO, 5-40 wt% Na_2O; BGs are bioactive and can attach to bone and soft tissues with some formulations: (2) <35wt% SiO_2: non-glass forming: (3) >50wt% SiO_2, <10wt%CaO, <35wt% Na_2O resorption in 10-30 days; resorption of BGs: (4) >65wt% SiO_2:

BGs are not bioactive, and nearly inert *(ÖZEL et al.)*.

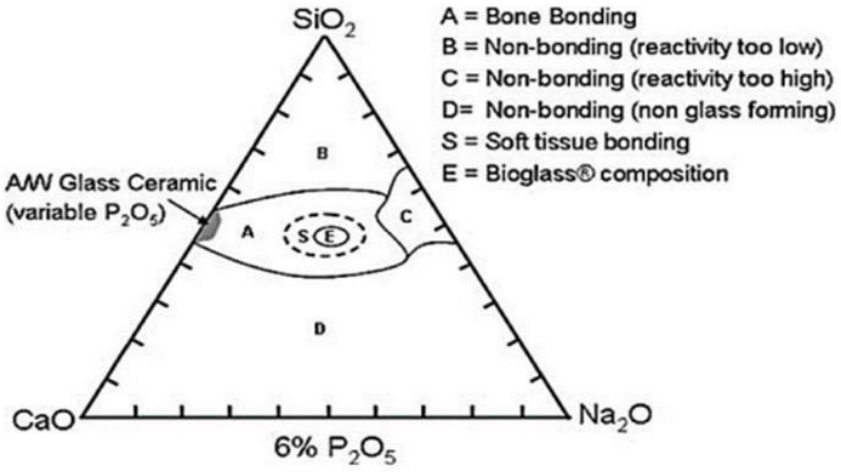

Figure 12. *Diagram for bone bonding (Fiume et al., 2018).*

There are different types of bioactive glasses which consist of SiO_2, Na_2O, CaO, P_2O_5, and other various compositions as summarized on Table 3. Compared to conventional soda-lime glass, BG has a lower amount of silica, a higher amount of CaO and Na_2O, and higher calcium to phosphorus ratio *(Ershad, 2018)*. Bioactive glasses with higher silica contents usually exhibit less bioactivity due to their dense network structure and the reduction of active elements *(Wen et al., 2021)*. It is noteworthy that bioglass with a low Si content can facilitate the formation of porous structures with large surface areas during the sol-gel process *(Schumacher et al., 2021)*. The Ca/P ratio is known to play an important role in modifying and tailoring the bioactivity of glasses. Compositions that enhance the non–bridging oxygen/bridging oxygen (NBO/BO) ratio reduce the glass network structure and connectivity *(Ben-Arfa et al., 2020)*. The high calcium/phosphate ratio in bioactive glass stimulates the formation of apatite crystals and makes the surface highly reactive under physiological conditions when silicon and calcium ions act as nuclei for crystallization *(Lopes et al., 2022)*.

Table 3. *Compositions of various types of bioactive glass (Rahaman et al., 2011).*

Composition (wt%)	**S^{5}_{45}**	**13-93**	**P53B 6**	**$S^{}_{58}$**	**S30C 70**	**$13\text{-}B^{1}_{93}$**	**$13\text{-}B^{3}_{93}$**	**P50C35 N15**
Na_2O	24..5	6.0	10.3	0	0	5.8	5.5	9.3
K_2O	0	12.0	2.8	0	0	11.7	11.1	0
MgO	0	5.0	10.2	0	0	4.9	4.6	0
CaO	24.5	20.0	18.0	32.6	28.6	19.5	18.5	19.7
SiO_2	45.0	53	52.7	58.2	71.4	34.4	0	0
P_2O_5	6.0	4.0	6.0	9.2	0	3.8	3.7	71.0
B_2O_3	0	0	0	0	0	19.9	56.6	0

Making porous structures is one of the current aims of orthopedic biomaterials for efficient tissue regeneration which is done to mimic the naturally occurring hierarchical porosity of bone *(Kong et al., 2018)*. The properties of PBGs are improved including greater surface reactivity and degradation, as well as the expansion of their potential biomedical applications (e.g., in nano medicine) *(Zheng, Sui, et al., 2021)*. By making cells more accessible and

simulating the local environment of implantation, hierarchical porosity can improve bioactivity by enabling neighboring cells to carry out their intended repair and remodeling tasks *(Koons et al., 2020)*. Based on the distribution of pore diameters, porous biomaterials can be categorized into three main groups: micro-pore, meso-pore, and macro-pores, which have pore sizes of 2 nm or less, 2–50 nm, and > 50 nm, respectively *(Deshmukh et al., 2020)*.

MBGs (2-50nm) are third-generation bioactive glasses using of the sol-gel technique and different structure directing agents *(Baino, Fiume, et al., 2018)*.

The capacity of sol-gel processing to create nanoscale PBGs, which is difficult for other techniques like melting method, is another noteworthy benefit *(Q. Lei et al., 2020)*. By utilizing the proper sol-gel techniques, the porosity of sol-gel produced PBGs can be controlled into micro-, meso-, and macro-porosity *(Q. Lei et al., 2020; Zheng & Boccaccini, 2017)*. The majority of reported PBGs possess mesopores whose size is located between 2 and 50 nm *(Zheng, Sui, et al., 2021)*. The specific surface area, pore-size, and pore-volume of a bioactive glass are determined by the procedures and conditions utilized to create it *(Z. Wu et al., 2019)*. The MBGs have superior pore volume, surface area, high cytocompatibility and the capacity to stimulate apatite mineralization in SBF compared to conventional non-mesoporous bioactive glasses (NMBGs) *(Kaya et al., 2018; Kong et al., 2018)*. Due to the large specific surface area and mesoporosity of MBGs, which both promote a greater degree of reactivity between the glass and the biological fluid, HAp was developed in relation to bioactivity kinetics along with MBG development. Figure 13 compares the HAp layer formation on traditional sol-gel glass (left) and MBG (right) surface when in contact with the biological fluid.

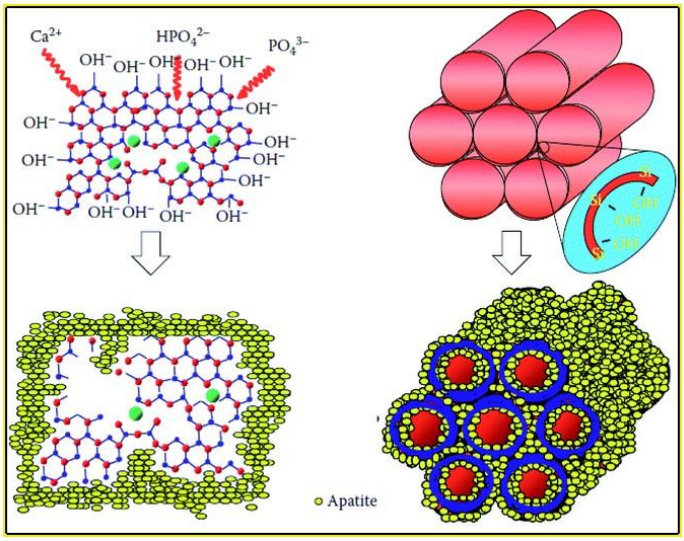

Figure 13. *HAp layer formations on the surface of traditional sol–gel glass (left) and MBG (right) after contacting the biological fluids (Kaya et al., 2018).*

2.8 Research gap

According to several studies, most of the structure directing agents used for PBGs synthesis are surfactants. Micellar aggregation as a result of their partial solubility and carbon contamination from the presence of long chain carboxylic functional groups are the main draw backs of surfactants. Due to its great solubility and absence of carboxylic group, hydrogen peroxide can be utilized in place of other structure-directing substances. It was previously found as novel pore forming agent, it was not used for studying the influence on bioactivity and biodegradability. On the other hand, majority of researches demonstrate that hydrolysis reactions primarily catalyzed by inorganic acids. But since they are used in larger concentrations these catalysts cause aggregation and leave much residual ions which can influence the HAp formation. Citric acid is one of the organic catalysts that have a major impact on catalyzing and highly soluble substance which offers superior particle morphology. This was employed as a catalyst in some research with a lower concentration and obtained to have smooth surface morphology and adequate HAp formation ability. Also in other studies, better outcomes were achieved for the catalytic effect of citric acid on the particle structure and bioactivity of bioactive glass particles. But bioactive glasses using the sol-gel synthesis process with hydrogen peroxide as a structure-directing agent and citric acid catalyst together

have not been studied. Also there effects on bioactivity and biodegradability of bioactive glass have not been investigated. Herein the bioactivity and biodegradability of citric acidassisted sol-gel-synthesized bioactive glasses with hydrogen peroxide was investigated. Additionally, the impact of hydrogen peroxide as a pore forming agent together with citric acid as a catalyst on the morphology of BG, bioactivity, as well as biodegradability effectiveness were investigated.

CHAPTER THREE

3. MATERIALS and METHODS

3.1 Chemicals and Materials

Chemicals used for the synthesis of bioactive glass are Tetraethyl orthosilicate (TEOS, $Si(OC_2H_5)_4$) (India, 98%), Phosphoric acid (H_3PO_4) (Sigma-Aldrich, 98%), Calcium nitrate tetra hydrate ($Ca(NO_3)_2.4H_2O$) (Loba chemicals ,98%), Hydrogen peroxide (H_2O_2, 30%), Citric acid ($C_6H_8O_7$) (Loba chemicals, 99.5%), and Ethanol (Loba chemicals,96%). Chemicals used for the synthesis of simulated body fluid (SBF) are Sodium chloride (NaCl) (India, 98%), Sodium bicarbonate ($NaHCO_3$) (India, 99%), Potassium chloride (KCl) (Sigma-Aldrich, 99%), Disodium hydrogen phosphate (Na_2HPO_4) (India, 99.5%), Magnesium chloride hexahydrate ($MgCl_2.6H_2O$) (India, 99%), Hydrochloric acid (HCl) (Alpha chemicals, 98%), Calcium chloride ($CaCl_2$) (Loba chemicals, 95%), Sodium sulphate (Na_2SO_4) (Loba chemicals, 99%), tris(hydroxymethyl)aminomethane (TRIS) [= $(CH_2OH)_3CNH_2$] (India, 99%). In addition, materials used for the experiment are hot plate, beaker, aluminum foil, drying oven, furnace, hydraulic press, glass bottles, water bath, and centrifuge.

3.2 Synthesis of Bioactive Glass Powders

In this study, 58S bioactive glass with glass composition of 58% SiO_2, 33% CaO, and 9% P_2O_5 (mol %) were synthesized following previously used composition procedures with some modifications *(Bui & Dang, 2019; Chen et al., 2018)*. 1.81mL Tetraethyl orthosilicate (TEOS, $Si(OC_2H_5)_4$), 1.168g Calcium nitrate tetra hydrate (CN, $Ca(NO_3)_2.4H_2O$), and 0.132mL Phosphoric acid (H_3PO_4) were used as a source of SiO_2, CaO, and P_2O_5. H_2O_2 untreated BG (BG0), 1M H_2O_2 (BG1), 2M H_2O_2 (BG2), and 3M H_2O_2 (BG3) treated powders were synthesized. 0.5 mM citric acid added in 50mL distilled water and ethanol alcohol (1:1) solvents and stirred for 15 minutes at room temperature. Then TEOS, Phosphoric acid, calcium nitrate tetrahydrate, and hydrogen peroxide were added in to the solution sequentially based on their solubility *(Deshmukh et al., 2020)*. The precursor solution was stirred with magnetic stirrer on hot plate for 2hr to obtain homogeneous solution *(Hong & Shih, 2017)*. The prepared sol was kept at 60 □C for 24hr to transform into a gel by polycondensation process and the gel was dried at 100 ℃ for 3hr to remove solvents. Then the dried specimens were calcined at 600 ℃ for 2hr to remove remaining precursor residues and solvents based on TGA result of dried gel.

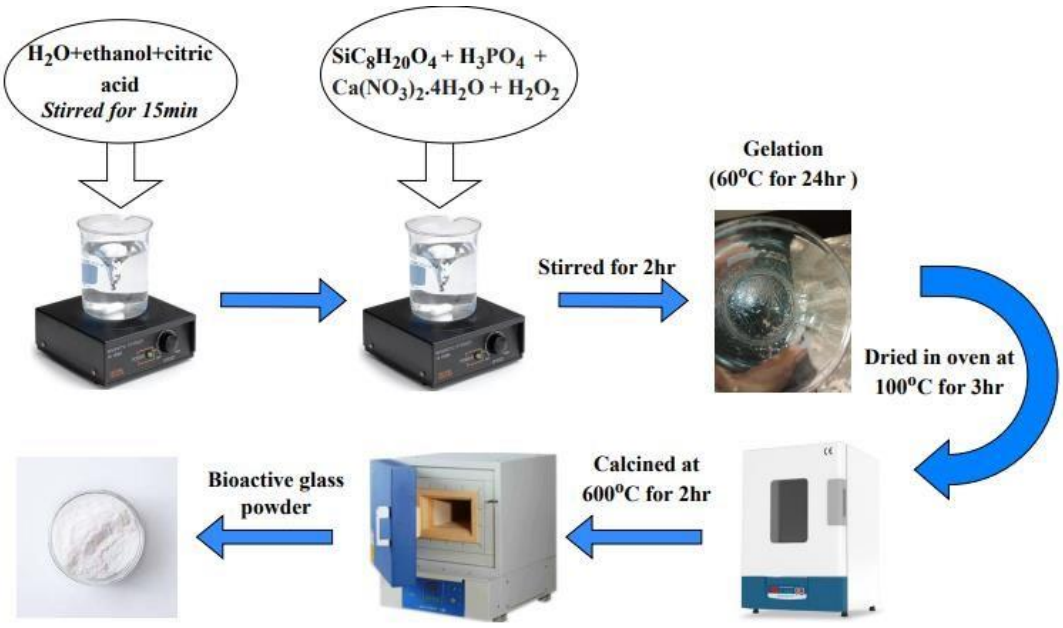

Figure 14. *Schematic diagrams for synthesis of bioactive glass powders.*

3.3 Preparation of SBF solution

SBF solution, were prepared nearly the same ionic concentration of human body plasma as studied by *Kokubo et al.* and summarized on the Table 1 *(Kokubo & Yamaguchi, 2019)*. In 1000 mL distilled water, 6.54g sodium chloride (NaCl), 2.27g Sodium bicarbonate ($NaHCO_3$), 0.37g potassium chloride (KCl), 0.14 g sodium dihydrogen phosphate (NaH_2PO_4), and 0.31 g magnesium chloride hexahydrate ($MgCl_2.6H_2O$) were added and stirred vigorously maintaining the solution temperature at 37℃. After that 1M hydrochloric acid (HCl) were slowly droped into the solution. Then 0.37 g calcium dichloride ($CaCl_2$) and 0.071 g Sodium sulphate (Na_2SO_4) were added. Finally, the solution was buffered at pH 7.4 with tris(hydroxymethyl)aminomethane (TRIS) *(Jang et al., 2018)*. The solution temperature was kept at 37℃ through the whole process and it was stirrred for 30 minutes after all components were added to obtain homogenous solution. Then the obtained transparent SBF solution were tightly capped in a clean glass media bottle of 1L capacity in a refrigerator (i.e., a regular refrigerator) to prevent precepitation of the SBF.

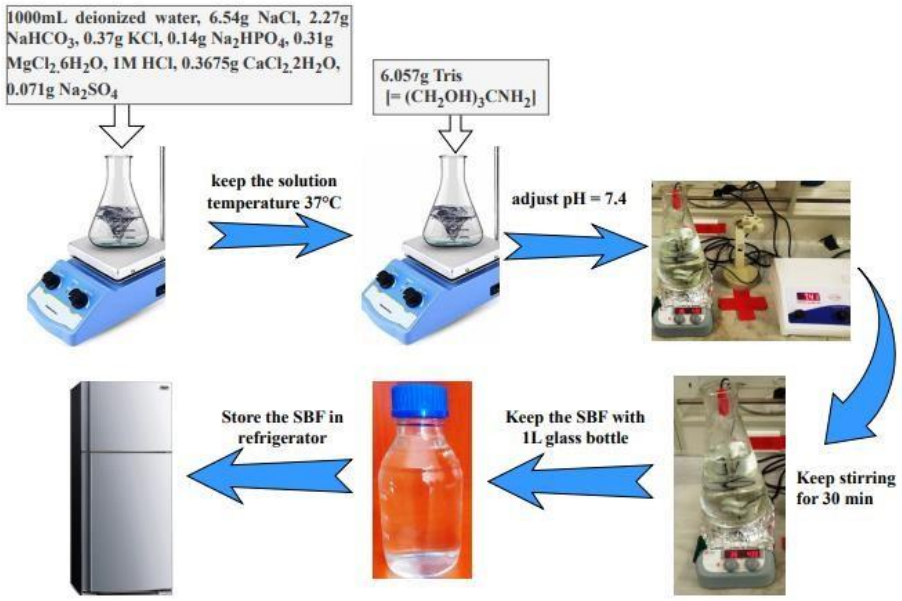

Figure 15. *Schematic diagrams for preparation of SBF solution.*

3.4 Sample characterization

Thermal stability, Phase, surface morphology, chemical composition, constituent composition, pore volume, and specific surface area analysis were done after sample

preparation. Thermo gravimetric analysis (TGA)/Differential thermal analysis (DTA) (shimadzu DTG-60H) was used for thermal analysis. X-ray diffraction (XRD) (Shimadzu XRD-7000) at copper Kα radiation (λCuKa=1.5418 Å) was used to obtain details of phase analysis. Surface morphologies of the specimens were analyzed with Scanning electron microscope (SEM) (JSM 6500F JEOL). Furiour transform infrared (FTIR) spectroscopy (Perkin Elmer spectrum 65 FT-IR) was used for chemical identification. Energy dispersive x-ray spectroscopy (EDS) (JEOL Japan) was also used to identify the constituent composition of each specimen. The pore size, pore volume, and specific surface area of the BG powders were examined using Brunauer-Emmett-Teller (BET) (Novatouch 2LX).

3.4.1 In vitro bioactivity test

In vitro bioactivity studies of H_2O_2 un-treated, 1M, 2M and 3M H_2O_2 treated BG powders were done using Kokubo's simulated bodily fluid (SBF) solution *(Kokubo & Yamaguchi, 2019)*. All BG specimens were soaked into SBF having an ionic content comparable with typical human plasma, to test in vitro bioactivity. Each of the specimens was then submerged in SBF with 1g BG powder in 10ml of SBF and kept in water bath that was maintained at 37°C for 1 day, 3 days, and 7 days. The soaked samples were rinsed with distilled water and ethanol three times and dried at 80ºC for 24hr. HAp layer formation on soaked samples was characterized by XRD for day 1, day 3, and, day 7. Bioactivity test was further investigated for day 3 bioactivity by FTIR, SEM, and EDS for HAp chemical composition, surface morphology, and constituent composition analysis. The Debye-Scherer equation (equation 1) was also used to calculate each of the specimen's crystallite size to estimate the bioactivity from XRD after using the peak area analysis of HAp.

$$\mathbf{D = \frac{k\lambda}{\beta\cos(\theta)}} \quad \textbf{…….. (1)}$$

Where D is the Crystalline size, K is the Scherer's constant (k=0.94), λ is the X-ray wavelength (1.54178Å), β is full width at half maximum (FWHM) of the diffraction peak, and θ is the angle of diffraction.

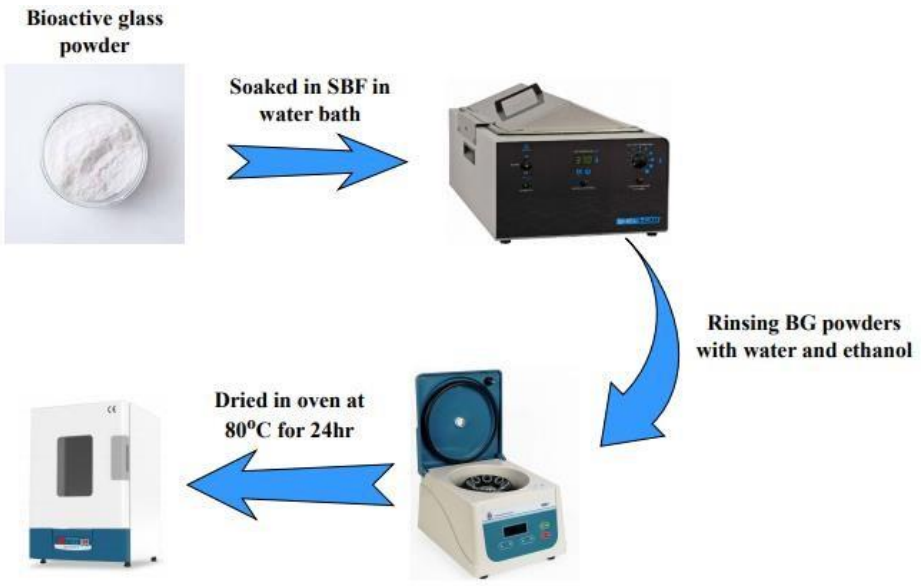

Figure 16. *Schematic diagram of invitro bioactivity test.*

3.4.2 In vitro biodegradability test

In vitro biodegradability test of H_2O_2 un-treated, 1M, 2M and 3M H_2O_2 treated BG specimens in a pellet form were tested in SBF solution. Three BG pellets for each specimen were used to obtain the average and standard deviation of weight loss. The pellets were used for the ease of holding and proper weight loss analysis throughout the biodegradability test. Grinded 58S bioactive glass powder was put into pelleting mould, the load pressure and dwell time of tablet machine was set as 15 MPa, 60 s respectively, finally the diameter of 6 mm and thick of 3.5 mm bioactive glass tablets were successfully prepared by hydraulic press. The prepared pellets were immersed in 12 mL of SBF solution. Mineralization experiment adopts international standards (ISO/FDIS 23317), the volume of the SBF solution was determined according to the following formula *(Chen et al., 2018)*:

$$Vs = \frac{Sa}{10} \quad \text{..... (2)}$$

Where Vs-the volume of SBF solution (mL) and Sa-the surface of pellets (mm^2)

The soaked pellets were kept in water bath maintained at 37°C. They were rinsed with distilled water and ethanol three times and dried at 80ºC for 24hr then weight of the pellets were measured. The assessment was repeated for 30 days, refreshing the SBF in which the solution was discarded each day while the pellets were dried and weighed again.

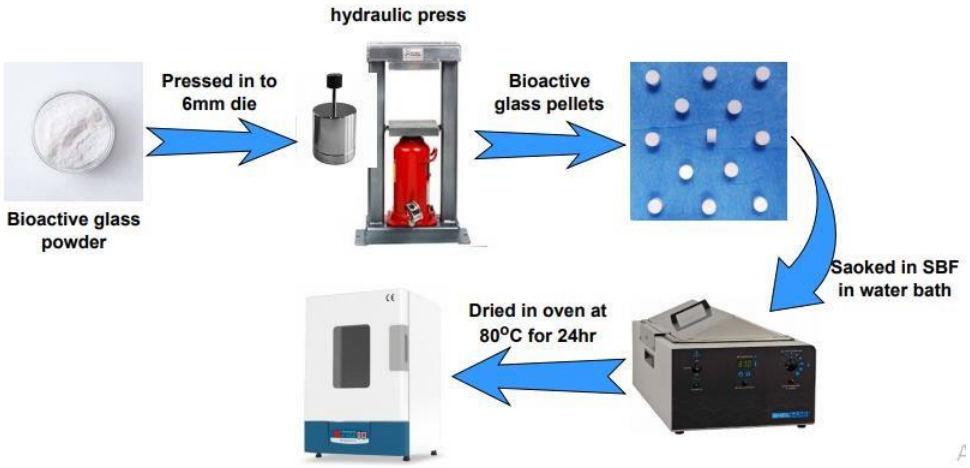

Figure 17*. Schematic diagrams for invitro Biodegradability test.*

CHAPTER FOUR

4. RESULTS and DISCUSSION

4.1 Thermo-Gravimetric Analysis (TGA)

Thermal stability analysis of H_2O_2 untreated as well as H_2O_2 treated (1M, 2M, and 3M) dried BG powders were done by TGA/DTA which determines stabilization temperature as shown on Figure 18. The samples were heated at a rate of 10 °C/min from 0 to 800 °C. The DTA and TGA curves reveal that the heat breakdown of the precursor occurs in three major stages. The endothermic peak from 50-250 °C reveals the major weight loss of H_2O_2 untreated BG, 1M H_2O_2 treated BG, 2M H_2O_2 treated BG, and 3M H_2O_2 treated BG are 45.584%, 43.240%, 45.353%, and 45.665% respectively**.** Figure 18 (a) for H_2O_2 untreated BG the weight loss corresponds mainly separation of volatile components such as physically adsorbed water, ethanol, and pore liquor from the structure which are not removed during the drying process *(Chuni et al., 2023; Lopes et al., 2019)*. In addition to this for 1M, 2M, and 3M H_2O_2 treated BG specimens, H_2O_2 decomposion at 180 °C takes place ($H_2O_2 \rightarrow 2H_2O + O_2$) *(Hong & Shih, 2017)*. The residues water and oxygen molecules from the decomposition of H_2O_2 also removed. All these mentioned residues of the specimens were released as the exothermic peak at from 250 °C shows.

The second weight loss observed from 250-340 °C was -6.544%, -6.155%,-5.457%, -5.76% for H_2O_2 untreated BG, 1M H_2O_2 treated BG, 2M H_2O_2 treated BG, and 3M H_2O_2 treated BG respectively as revealed by the exothermic peak at 275°C. It is mainly due to the condensation of silanol groups and removal of organic residues i.e alkoxyl groups as well as other residues incorporated during polycondensation reaction *(Shah et al., 2018)*. The final weight loss was obtained from 340-500 °C was -13.420%, -13.161%, -12.143%, -11.06% for H_2O_2 untreated BG, 1M H_2O_2 treated BG, 2M H_2O_2 treated BG, and 3M H_2O_2 treated BG specimens respectively. The weight loss was incorporated with the decomposition of calcium nitrate in to nitrogen oxide, oxygen, water, and CaO ($2Ca(NO_3)_2.4H_2O \rightarrow 2CaO + NO_2 + 4H_2O + O_2$) and removal of the residues *(Moghanian, Firoozi, & Tahriri, 2017)*. Calcium nitrates are most likely completely soluble in the sol and remain in solution until the first

amorphous silicate and phosphate phase formed which mostly decomposes above 400 °C *(Santos, Barreto, & dos Santos, 2016)*. These Ca ions will start to segregate in the silica network and disrupt the structure. Since all residues in the specimens were removed below 600 °C, it was used as a calcination temperature. Since all residues are removed below the thermal stability temperature, pure BGs can be obtained after calcination.

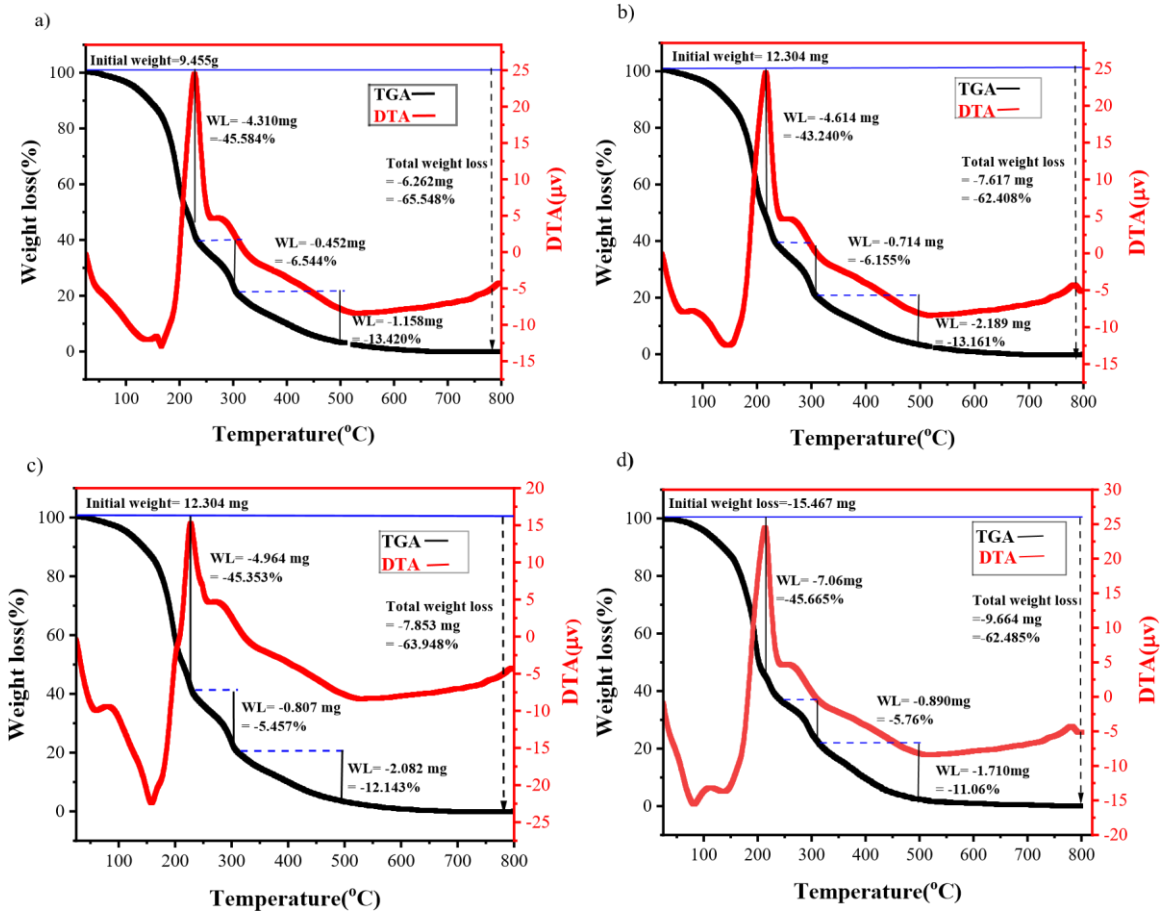

Figure 18*. TGA-DTA curve of (a) H_2O_2 untreated BG, (b) 1M H_2O_2 treated BG, (c) 2M H_2O_2 treated BG, and (d) 3M H_2O_2 treated BG.*

4.2 X-ray Diffraction analysis (XRD)

Figure 19 depicts XRD patterns of H_2O_2 untreated (BG0), 1M H_2O_2 treated BG (BG1), 2M H_2O_2 treated BG (BG2), and 3M H_2O_2 treated BG (BG3). The broad peak observed from 20º30º for all BG specimens suggests silica based glasses with amorphous nature and have no

long range order. This results much with previous studies in which BG specimens were effectively synthesized with the absence of a distinct diffraction peak that is an amorphous phase *(Bakare et al., 2019; Chuni et al., 2023)*. The broad peak obtained is indicative of a glass that is amorphous nature. Additionally, the Ca element break up the natural tetrahedral structure of typical silica glasses and increase overall reactivity and dissolution *(Sanders, 2018)*. This is consistent with the higher quantity of Ca^{2+} ions incorporated in the particles as network modifiers: the thermal treatment induces a disruption of the glass network due to the Si-O-Si bonds breaking by Ca^{2+} ions incorporation as indicated on the TGA/DTA result. Hence, non-bridging oxygens (NBOs) are created in the glass structure, resulting in the formation of (Si-O-NBO) bonds which is compensated by Ca^{2+} ions. The higher the Ca/Si ratio is, the lower the network connectivity of the glass *(Kesse, Vichery, Jacobs, Descamps, & Nedelec, 2020)*. Thus all samples have amorphous nature which implies effective synthesis of glass material.

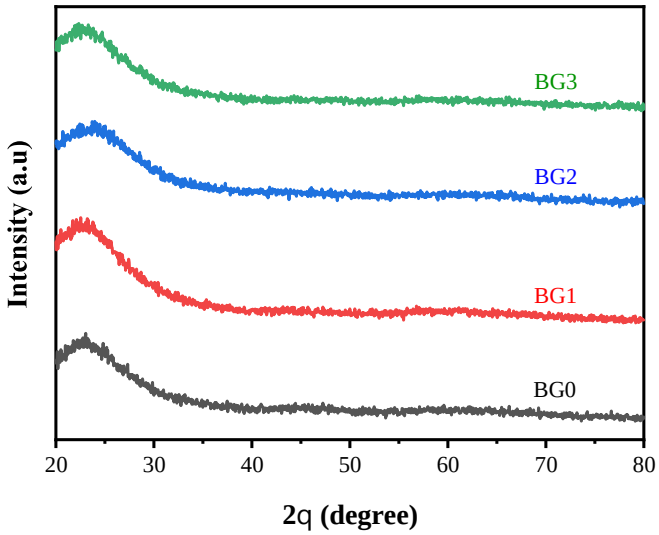

Figure 19*. XRD pattern of (BG0) H_2O_2 untreated BG, (BG1) 1M H_2O_2 treated BG, (BG2) 2M H_2O_2 treated BG, and (BG3) 3M H_2O_2 treated BG before bioactivity.*

4.3 Fourier Transform Infrared Spectroscopy (FTIR)

FTIR spectra are shown in Figure 20, for H_2O_2 untreated (BG0), 1M H_2O_2 treated BG (BG1), 2M H_2O_2 treated BG (BG2), and 3M H_2O_2 treated BG (BG3). It illustrates that the spectra for the as prepared samples exhibit Si-O-Si stretching vibrations at 1090 cm^{-1}, 800 cm^{-1}, and bending vibrations at 482 cm^{-1} *(Bakare et al., 2019)*. Si-O-Si bonds are related to the network

forming groups in the glass structure. On the other hand, Ca^{2+} ion incorporation in the Si-O-Si structure and form NBO. Many literatures distinguish different frequencies for the presence of Si-O-NBO groups with dissimilar hypotheses, but mostly found in the range of 940-1040 cm^{-1} *(Balamurugan et al., 2006)*. The Si-O-NBO obtained at 953 cm^{-1} reveals the presence of nonbridging oxygen in which the glass network is modified with glass modifier *(Spirandeli, Campos, Ribas, Thim, & de Sousa Trichês, 2020).* The network modifier provoke the disruption of the continuity of the glassy network due to the breaking of some of the Si–O–Si bonds leading to the formation of non-bridging oxygen groups (Si–O–NBO). The Si–O–NBO group is typical in amorphous structure and control the dissolution of the silica through the formation of silanol in SBF *(Barrioni et al., 2018).* In addition to this, any carbon containing functional groups were not obtained from the FTIR spectra. This reveals the BG particles are purely synthesized and residual ions that can interrupt HAp formation are well eliminated.

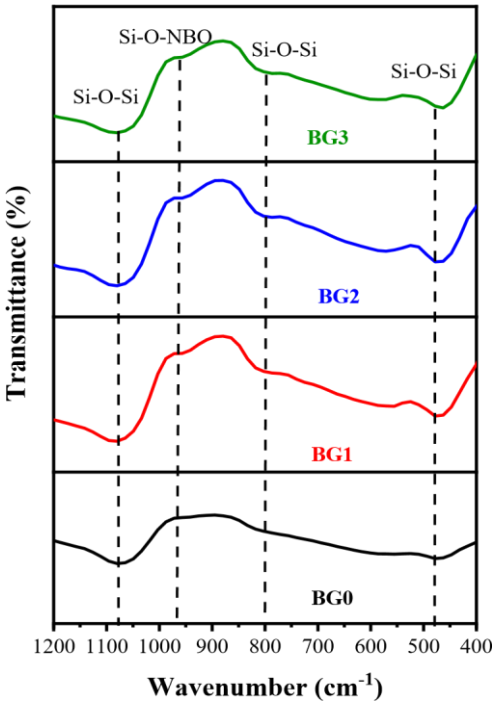

Figure 20. *FTIR spectra of (BG0) H_2O_2 untreated BG, (BG1) 1M H_2O_2 treated BG, (BG2) 2M H_2O_2 treated BG, and (BG3) 3M H_2O_2 treated BG before bioactivity.*

4.4 Scanning Electron Microscope (SEM)

Surface morphologies of H_2O_2 untreated, 1M H_2O_2 treated BG, 2M H_2O_2 treated BG, and 3M H_2O_2 treated BG before bioactivity was displayed on figure 21. In figure (21a) the H_2O_2 untreated BG particles were obtained to have solid morphology without forming any pores due to the absence of H_2O_2. It also shows a smooth and micro-rough surface in which the citric acid synthesized BG particles are obtained with smooth morphologies and micro-roughness *(B. Lei et al., 2011a)*. In the H_2O_2-derived BG particles, the precursor droplets of water and oxygen formed during the heating stage and oxygen was released from the droplets, resulting in the formation of the pores *(Hong & Shih, 2017)*. Porous morphologies were seen in all 1M H_2O_2 treated BG (BG1), 2M H_2O_2 treated BG (BG2), and 3M H_2O_2 treated BG (BG3) with different morphologies and distributions. For figure (21b) very few pores were observed in BG treated with 1M H_2O_2 compared with 2M and 3M H_2O_2 treated specimens. This is mostly caused by the lower concentration of H_2O_2 decreasing the generation of oxygen, resulting in fewer holes being formed by the released oxygen.

More narrow and homogeneous pore distributions were seen for the BG specimen treated with 2M H_2O_2 as shown on Figure (21c). The homogenous porous structure distribution is mainly due to the controlled formation and release of oxygen gas. There were very large pores with non-uniform distributions were observed on the 3M H_2O_2 illustrated on figure (21d). This is mainly due to the aggregation of H_2O_2 into larger clusters which form broader pores. The high concentration of H_2O_2 leads to the formation of high oxygen molecules while decomposion of H_2O_2 which might lead to the formation of larger pores. Additionally, because the H_2O_2 concentration was significantly higher than that of the other BG powders, it is possible that the H_2O_2 molecules gathered into larger clusters, which led to the development of wider holes in which the particles would have larger pore size *(Hong & Shih, 2017)*. From the SEM result it was generally obtained that H_2O_2 concentration influences the surface morphologies of BG particles. 2M H_2O_2 was optimum concentration to obtain homogenous, interconnected pores, and even porosity distributions. But for 3M H_2O_2 treated BG larger pores with nonhomogeneous and disrupted pore distribution were observed.

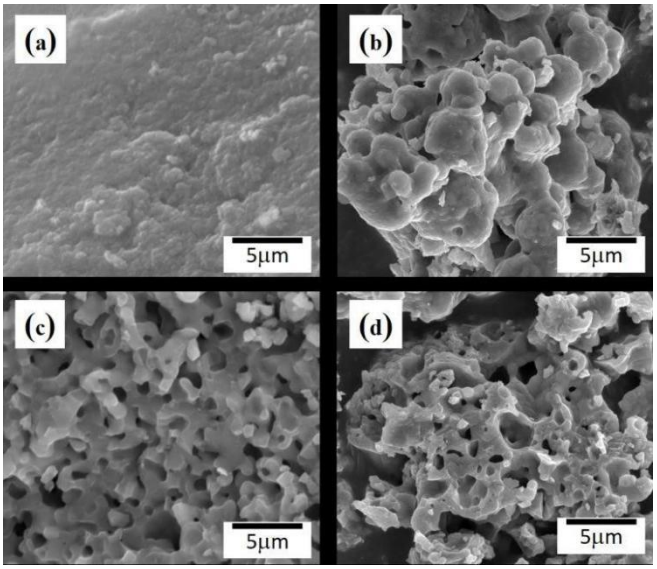

Figure 21. *SEM images of (a) H_2O_2 untreated BG, (b) 1M H_2O_2 treated BG, (c) 2M H_2O_2 treated BG, and (d) 3M H_2O_2 treated BG before bioactivity.*

4.5 Energy Dispersive X-ray Spectroscopy (EDS)

EDS spectra on Figure 22 illustrates that H_2O_2 untreated BG, 1M H_2O_2 treated BG, 2M H_2O_2 treated BG, and 3M H_2O_2 treated BG before bioactivity. All BG specimens exhibited silicon, calcium, and phosphorous peaks, which are representative of silicate bioactive glasses *(Chuni et al., 2023)*. Additionally, it shows absence of any residual organic component which implies the residues was successfully removed throughout the heating process. Since H_2O_2 induces the formation of oxygen for pore formation, its full elimination shows the successful pore formation process which enhances specific surface area of the H_2O_2 treated BG particles than that of H_2O_2 untreated one. As a result, the purity of all synthesized samples was validated that demonstrate the successful synthesis of the BG specimens. The result also reveals neither the chemical composition nor the phase compositions of the sol-gel derived BG specimens were affected. The purity of obtained BG specimens enables for good formation of HAp layer on their surface, besides the effect of porosity.

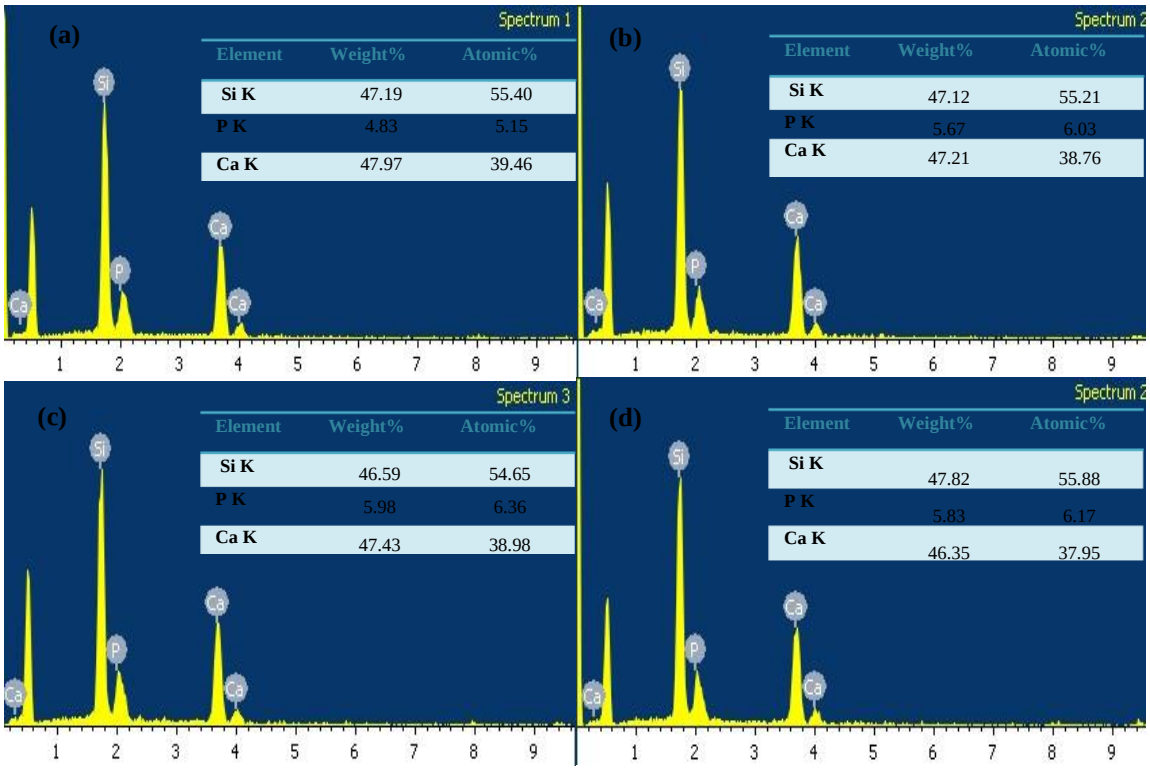

Figure 22. *EDS analysis of (a) H_2O_2 untreated BG, (b) 1M H_2O_2 treated BG, (c) 2M H_2O_2 treated BG, and (d) 3M H_2O_2 treated BG before bioactivity.*

Table 4 summarizes the theoretical and experimental atomic% of Si, Ca, and P for H_2O_2 untreated BG (BG0), 1M H_2O_2 treated BG (BG1), 2M H_2O_2 treated BG (BG2), and 3M H_2O_2 treated BG (BG3) depending on the EDS analysis on figure 22. From the obtained data, the constituent elements in both theoretical and experimental results are close to each other which reveal the desired BGs were well synthesized.

Table 4. Theoretical and experimental at% of Si, Ca, and P for H_2O_2 untreated BG (BG0), 1M H_2O_2 treated BG (BG1), 2M H_2O_2 treated BG (BG2), and 3M H_2O_2 treated BG (BG3).

Sample name	**Theoretical Atomic %**			**Experimental atomic%**		
	Si	Ca	P	Si	Ca	P
BG0	58	33	9	55.40	39.46	5.15
BG1	58	33	9	55.21	38.78	6.03
BG2	58	33	9	54.65	38.98	6.36
BG3	58	33	9	55.88	37.95	6.17

4.6 Brauner-Emmet-Teller analysis (BET)

Brunauer-Emmett-Teller (BET) method was used to analyze the specific surface areas, pore volumes, and the pore sizes of the H_2O_2 untreated BG (BG0), 1M H_2O_2 treated BG (BG1), 2M H_2O_2 treated BG (BG2), and 3M H_2O_2 treated BG (BG3) powders. Table 5 provides an overview of all the specific surface areas, pore volumes, and pore size of the H_2O_2 untreated BG, 1M H_2O_2 treated BG, 2M H_2O_2 treated BG, and 3M H_2O_2 BG specimens. The data were presented as an average standard deviation (SD) of n = 3 for all samples in which every sample reveals $p<0.05$ *(Chuni et al., 2023; Moghanian, Tajer, Zohourfazeli, Miri, & Yazdi, 2021)*. The variance in the p-value shows there is an important distinction between the BG specimens.

Table 5. *Specific surface area of H_2O_2 untreated, 1M, 2M, and 3M H_2O_2 treated BG.*

Samples	Specific surface area (m^2/g)	P-value	Pore volume (cc/g)	P-value	Pore size (nm)	P-value
BG0	77.02±1.02	0.022	0.10± 0.003	0.017	1.52±0.053	0.011
BG1	97.87±0.95	0.016	0.15±0.002	0.009	1.65±0.071	0.009
BG2	189.55±1.73	0.033	0.28±0.013	0.049	1.654± 0.05	0.024
BG3	126.56±1.66	0.017	0.17± 0.004	0.018	2.507±0.046	0.007

4.6.1 Specific surface area and pore volume

Specific surface area and pore volume of (BG0) H_2O_2 untreated BG, (BG1) 1M H_2O_2 treated BG, (BG2) 2M H_2O_2 treated BG, and (BG3) 3M H_2O_2 treated BG specimens were done using BET measurements as displayed on figure 23. The specific surface areas obtained from the BET measurements for BG0, BG1, BG2, and BG3 were 77.02±1.02, 97.87±0.95, 189.55±1.73, and 126.56±1.66 m^2/g respectively. The pore volume for BG0, BG1, BG2, and BG3 specimens were obtained to be 0.10± 0.003, 0.15±0.002, 0.28±0.013, and 0.17± 0.004 cc/g respectively. It illustrates that BG powder treated with H_2O_2 has the highest SSA when compared to BG powder untreated one. The decomposition property of H_2O_2 ($2H_2O_2 \rightarrow 2H_2O + O_2$) leads to the formation of porous structures during heat treatment *(Hong & Shih, 2017)*.

The formation of porosity in BG particles plays essential role for the specific surface area and pore volume.

According to the BET study, raising the H_2O_2 concentration from 0 to 2M increased the SSA from 77.02 to 189.55m^2/g. However, the SSA decreased to 126.56m^2/g as the H_2O_2 concentration was further increased to 3M. As it was discussed on the SEM analysis (Figure 21), solid morphologies were obtained for H_2O_2 untreated BG (BG0) which lowers the SSA of the particles due to absence of porous structure. For 1M H_2O_2 treated BG, few pores were obtained that enhances the SSA compared with H_2O_2 untreated specimen. It was highly ordered, interconnected, and homogenous pore distribution obtained for the 2M H_2O_2 treated BG specimen that leads to high specific surface area than the rest samples. Further for 3M H_2O_2 treated BG larger pores with small SSA were obtained. Since 3M H_2O_2 BG powder had a substantially higher concentration of H_2O_2 than the other BG powders, it is likely that the H_2O_2 molecules accumulated into larger clusters, leading to larger pores *(Hong & Shih, 2017)*. Generally from the SSA analysis, very low porosity and very large porous particles will have low exposed surface that is low SSA. But interconnected and homogenous porosity in the BG particles lead to have more exposed surfaces and high SSA in which allows several active locations to perform dissolution with physiological fluids and growth of HAp layer *(Fiume et al., 2018)*.

On the other hand, pore volume also increase from 0.1 to 0.28cc/g as H_2O_2 concentration increase from 0 to 2M. However, the pore volume decreased to 0.17cc/g as the H_2O_2 concentration was further increased to 3M. Pore volumes are mostly related with the number of pores induced in the particles. For small number of pores the pore volume will be lower while for higher number of pores the pore volume will be larger *(Liu, Rahaman, & Fu, 2011)*. For H_2O_2 untreated BG there was no porosity observed which leads to the pore volume of the particles to be lower than the other specimens. The little porosity obtained in 1M H_2O_2 treated BG powders increases the pore volume compared with the former one. Interconnected and homogenous porosity in the 2M H_2O_2 BG particles enhances the pore volume due to higher number of pores present in the particles. For the 3M H_2O_2 BG specimens larger pores were formed which implies as larger pores formed few number of porosity with larger pore size is formed that reduces the pore volume.

Generally high SSA and pore volume is beneficial for tissue engineering applications because it can accelerate surface crystallization of HAp, promote the degradation rate, and aid attachment and migration of cells of the BG particles *(Huang et al., 2021)*. 2M H_2O_2 BG specimens were obtained to have optimum porosity which have high SSA and pore volume.

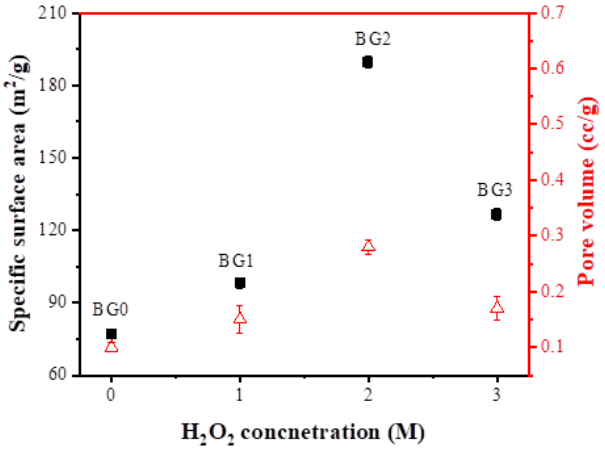

Figure 23. *Specific surface area and pore volume of (BG0) H_2O_2 untreated BG, (BG1) 1M H_2O_2 treated BG, (BG2) 2M H_2O_2 treated BG, and (BG3) 3M H_2O_2 treated BG.*

4.6.2 Pore size

The pore size of (BG0) H_2O_2 untreated BG, (BG1) 1M H_2O_2 treated BG, (BG2) 2M H_2O_2 treated BG, and (BG3) 3M H_2O_2 treated BG powders were 1.52$\pm$0.053, 1.65$\pm$0.071, 1.65$\pm$0.05, and 2.51$\pm$0.046 respectively as shown on figure 24. As the H_2O_2 concentration in the BG particles increases, the pore size also increases 1.52 to 2.51nm. 3M H_2O_2 (BG3) shows highest pore size due to the highest concentration of the H_2O_2 molecules may have aggregated into larger clusters that created larger pores *(Hong & Shih, 2017)*. A smaller size of pores allows a larger number of pores fitting within a set total volume of material which will have high SSA and pore volume; while larger size pores reduce number of pores with in the total volume of material which tends to reduce the SSA and pore volume. As a result, the 3M H_2O_2treated BG particles had large pores of 2.51 nm, which conferred a smaller surface area than did the 1.52 nm pores.

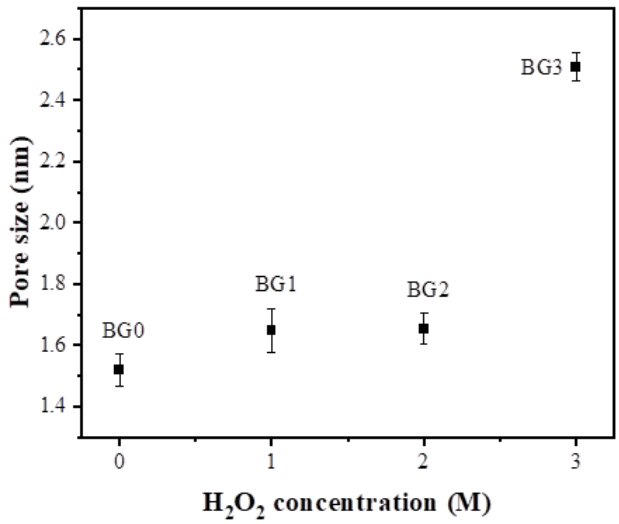

Figure 24. *Pore size of (BG0) H_2O_2 untreated BG, (BG1) 1M H_2O_2 treated BG, (BG2) 2M H_2O_2 treated BG, and (BG3) 3M H_2O_2 treated BG.*

4.7 Invitro bioactivity tests

4.7.1 X-ray Diffraction analysis (XRD)

The XRD pattern of H_2O_2 untreated BG (BG0), 1M H_2O_2 treated BG (BG1), 2M H_2O_2 treated BG (BG2), and 3M H_2O_2 treated BG (BG3) after soaking in SBF for 1 day, 3 days, and 7 days. Diffraction peaks were observed at 29.46º, 31.38º, and weak peaks at 47.68º and 48.86º which corresponds to (022), (211), (312), and (213) planes for the development of hydroxyapatite layer (JCPDF No. 00-009-0432) *(Sathiskumar et al., 2019).* HAp layer formation was observed in all BG specimens for all day 1, day 3, and day 7 tests. Ion exchange, dissolution and re-polymerization of surface silica, precipitation of amorphous calcium phosphate, nucleation and crystallization of calcium phosphate to HAp are the processes for HAp layer formation on BG particles *(Chang & Zhou, 2018; Zambanini et al., 2019).* The amorphous nature of BG particles, as confirmed by XRD analysis before bioactivity (Figure 19), has great role in the ion exchange dissolution process when the BG particles are soaked in SBF.

It was observed that HAp on the XRD patterns was increasing with the immersion time. The broadness of the XRD diffraction reflects crystal size of HAp layer and the broader the peak, the crystal will be smaller or less perfect. The low intensity and broadness seen on the XRD pattern can be understood since the XRD signal comes from a small deposited HAp layer *(Rezaei, Moztarzadeh, Shahabi, & Tahriri, 2014)*. As the soaking time increases H_2O_2 untreated BG (BG0), 1M H_2O_2 treated BG (BG1) specimens show increasing intensities on the (022) and (211). 2M H_2O_2 treated BG (BG2) also shows increasing intensities in all of its peaks with the soaking time due to the high specific surface area nature of the particles HAp formations were highly enhanced. It was little intensities observed for the 3M H_2O_2 treated BG (BG3) on day 1 and day 3 but enhanced for the day 7 bioactivity test. The lower specific surface areas of the BG0, BG1, and BG3 particles delayed the dissolution process and formation of HAp than BG2 particles *(Lalzawmliana et al., 2020)*.

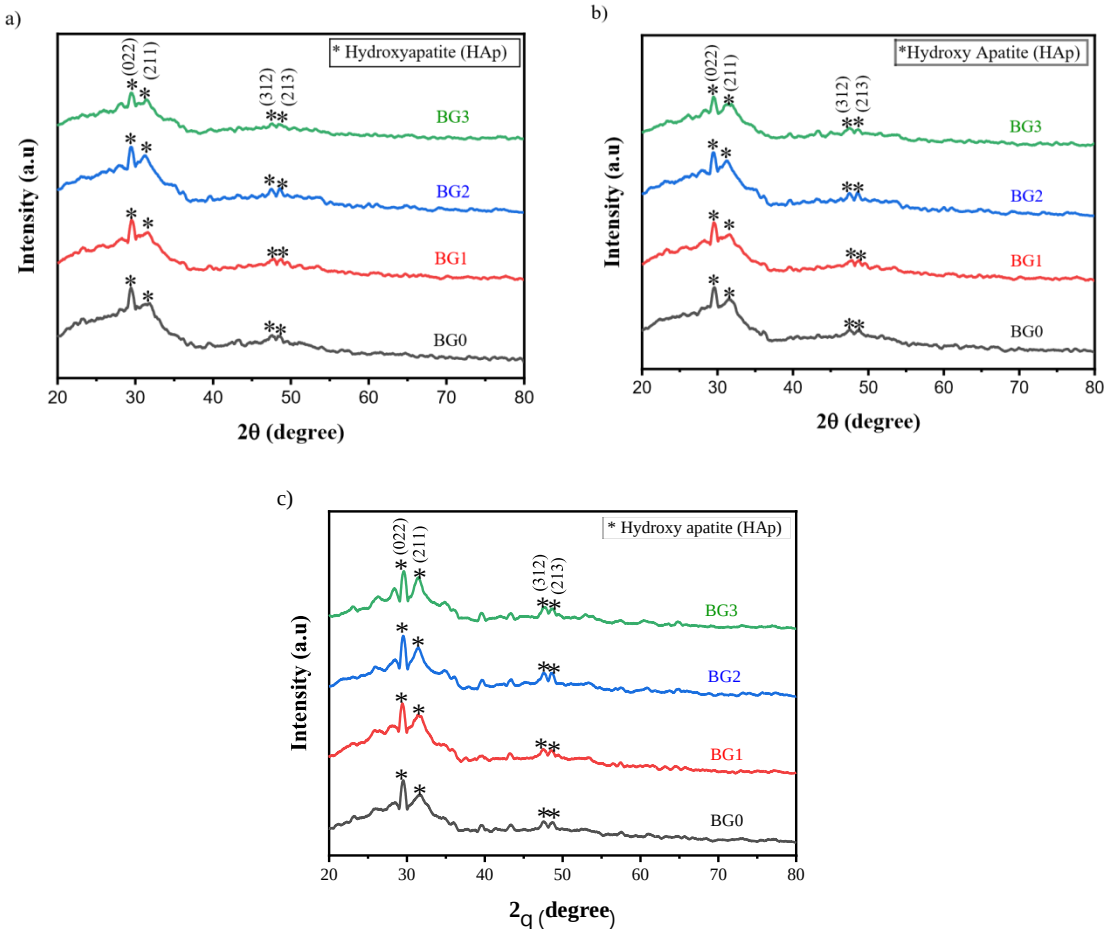

Figure 25. *XRD patterns of (BG0) H_2O_2 untreated BG, (BG1) 1M H_2O_2 treated BG, (BG2) 2M H_2O_2 treated BG, and (BG3) 3M H_2O_2 treated BG after soaking in SBF for 1 day (a), 3 days (b), 7 days (c).*

4.7.2 Bioactivity

Bioactivity as a function of H_2O_2 concentration and specific surface area for H_2O_2 untreated BG (BG0), 1M H_2O_2 treated BG (BG1), 2M H_2O_2 treated BG (BG2) , and 3M H_2O_2 treated BG (BG3) soaking in SBF for 1 day, 3 days, and 7 days shown on figure 26**.** The crystalline size was calculated from XRD pattern using Scherer formula (equation1) in order to determine the bioactivity of each specimen through HAp formation. As crystallite size for HAp formation increase bioactivity is said to increase. For the day 1 bioactivity test 11.06, 11.27, 15.51, and 12.06nm was the crystallite size obtained for BG0, BG1, BG2, and BG3 respectively. On the day 3 bioactivity 13.26, 14.03, 18.99, and 14.36nm for BG0, BG1, BG2, and BG3 respectively were obtained. Also for the day 7 bioactivity 19.59, 20.35, 23.43, 19.67nm was the crystalline size obtained for BG0, BG1, BG2, and BG3 respectively.

The crystallite size was increased with the soaking day for 0 to 2M H_2O_2 treated BG. It was decreased for the 3M H_2O_2 treated BG. The formation of HAp is the initial step in the formation of bond between BG and host tissue on the surface of the BG particles. Dissolution and ion exchange processes are the most essential steps to start the development of HAp layer. This process is highly influenced by the SSA of BG particle. As it was discussed on the SEM (figure 21) and SSA analysis (Figure 23), H_2O_2 with different concentrations has great influence on changing the morphologies as well as SSA of BG particles. H_2O_2 untreated BG (BG0) and 1M H_2O_2 treated BG (BG1) shows solid morphology and fewer pores respectively. Due to their lower SSA, the ion dissolution and exchange with the SBF will be hindered. As a result the HAp formation was lower, i.e bioactivity. The HAp formation of 2M H_2O_2 treated BG was higher than the rest specimens. The highly interconnected pores provide the BG particles to have high SSA. This enhanced high dissolution of BG particles in SBF solution and development of HAp layer. On the other hand, 3M H_2O_2 treated BG particles have larger pores with disrupted interconnections and reduced SSA. It also hinders the proper dissolution of ions and HAp formation.

Thus, BG powders HAp formation is highly influenced by the H_2O_2 concentration and SSA. The crystallite size increases with immersion time of BG particles in SBF. BG particles treated with 2M H_2O_2 obtained to have high SSA produces larger crystallite sizes than the other BG specimens, which suggests superior formation of HAp and higher bioactivity.

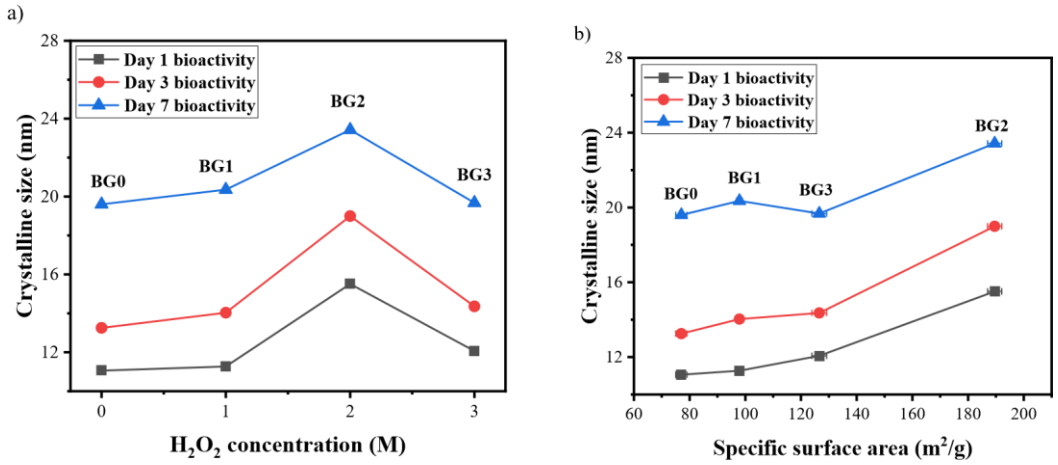

Figure 26. *Bioactivity as a function of H_2O_2 concentration (a) and specific surface area (b) for (BG0) H_2O_2 untreated BG, (BG1) 1M H_2O_2 treated BG, (BG2) 2M H_2O_2 treated BG, and (BG3) 3M H_2O_2 treated BG soaking in SBF for day 1, day 3, and day 7.*

4.7.3 Fourier Transform Infrared Spectroscopy (FTIR)

FTIR spectra are shown in Figure 27 for the (BG0) H_2O_2 untreated BG, (BG1) 1M H_2O_2 treated BG, (BG2) 2M H_2O_2 treated BG, and (BG3) 3M H_2O_2 treated BG after soaking in SBF for 3 days. It illustrates that the spectra for the samples at 1090 cm^{-1}, 800 cm^{-1}, and 482 cm^{-1} exhibit Si-O-Si bands after BG powders were submerged in SBF for 3 days. Also all specimens showed additional new peak that occurred at 566 cm^{-1} and 603 cm^{-1} were assigned to the P-O bond *(Ghorbanzade Zaferani, Nabian, Delavar, & Rabiee, 2021; Neščáková et al., 2019)*. Most of the time, these two peaks are detectable after 3 days of immersion and become more intense with increasing immersion time *(Neščáková et al., 2019)*. P–O bonds which represent HAp crystallization become evident through the new peaks. The peaks intensity increases when the H_2O_2 concentration increases from 0 to 2M. The intensity also decreases as the concentration of H_2O_2 increase to 3M.

The interruption of Ca molecule in the silicate network breaks the bonding among silicon (Si) and oxygen (O) by creating non-bridging oxygen (NBO) group which impact on the network connectivity. The NBO promotes dissolution and ionic exchange in the SBF solution to form HAp layer on BG particles. The H_2O_2 concentration also enhances the SSA of BG particles that have influenced the formation of HAp formation as discussed on bioactivity analysis (figure 26). Therefore, BG treated with 2M H_2O_2 was obtained to develop HAp with higher intensity due to its high SSA.

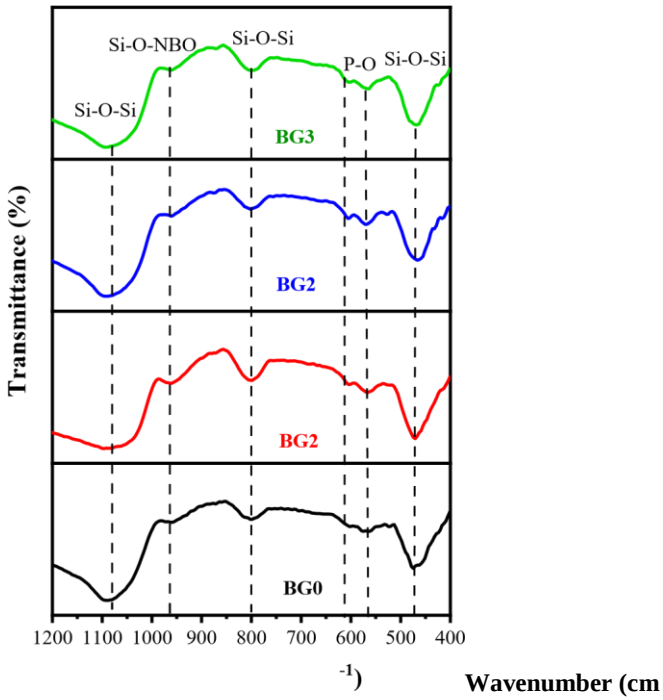

Figure 27. *FTIR spectra of (BG0) H_2O_2 untreated BG, (BG1) 1M H_2O_2 treated BG, (BG2) 2M H_2O_2 treated BG, and (BG3) 3M H_2O_2 treated BG after soaking in SBF for 3 days.*

4.7.3 Scanning Electron Microscope (SEM)

As shown on figure 28 invitro bioactivity analysis for H_2O_2 untreated BG, (b) 1M H_2O_2 treated BG, (c) 2M H_2O_2 treated BG, and (d) 3M H_2O_2 treated BG specimens were obtained from SEM image after soaking in SBF for 3 days. It illustrates that smaller needle like crystallites were formed and distributed on the surface of the BG particles which demonstrating the formation of HAp layers on BG particles. The presence of HAp crystallite by XRD and FTIR were confirmed by the SEM micrograph.

As shown on figure 28a, H_2O_2 untreated BG specimen shows little development of SBF on its surface. The solid morphology (figure 21a before bioactivity) influences dissolution of the specimen which hinders to develop adequate amount of HAp on its surface. Thus only little HAp nucleates on its surface. The little porous morphology that was appeared on 1M H_2O_2 treated BG enables better HAp formation than H_2O_2 untreated one. But still some particles were seen without the development of HAp. This is mainly the presence of little porosity and non-uniform distributions. Uniform and narrow pore distribution is obtained for the samples prepared with 2M H_2O_2. This BG specimen also leads to development of HAp layer in its whole surfaces as shown on figure 28 c. The uniform and narrow pore distribution enables the specimen to have high bioactivity than the rest samples. Thus enables expose the surface highly in SBF solution to promote dissolution and formation of evenly distributed HAp. For the 3M H_2O_2 treated BG HAp layer developments with some aggregations and uneven distribution were observed. Not all particles surface were covered with the HAp layer due to lower SSA than the 2M H_2O_2 treated BG.

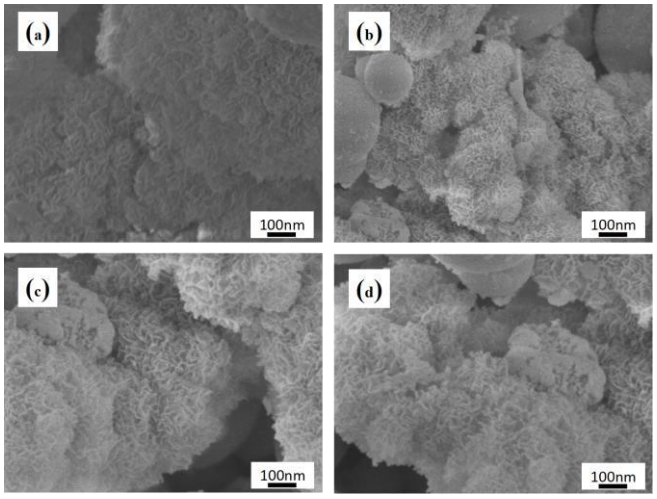

Figure 28*. SEM images of (a) H_2O_2 untreated BG, (b) 1M H_2O_2 treated BG, (c) 2M H_2O_2 treated BG, and (d) 3M H_2O_2 treated BG after soaking in SBF for 3 days.*

4.7.4. Energy Dispersive X-ray Spectroscopy (EDS)

The EDS analysis of H_2O_2 untreated BG, 1M H_2O_2 treated BG, 2M H_2O_2 treated BG, and 3M H_2O_2 treated BG after soaking in SBF for 3 days were shown on figure 29. All the BG

specimens exhibited silicon, calcium, and phosphorous peaks with different experimental percentage compared with the values of BG particles exhibited before bioactivity (Figure 22). After soaking BG specimens in SBF, the Si atomic % decreases. This is mainly due to the break down or dissolution of silica network when BGs are in contact with body fluid in order to form silanol for further development of Ca and P ions on the BG surface. Ca and P are the main component to determine bioactivity property by HAp formation on BGs in which the EDS data confirmed the formation of this mineral deposits on the surfaces of the specimens *(Al-Bakhsh et al., 2019)*. As the EDS result reveals, all BG specimens exhibit bioactivity since atomic % of P increases as summarized on table 6. The concentration of P increases as H_2O_2 increases 0-2M and decreases for 3M H_2O_2. This indicates that BG2 has high capability of developing HAp which is bioactivity due to its high SSA, well ordered and homogeneously distributed porous structures. Thus its high SSA enhances the development of HAp than the rest specimens.

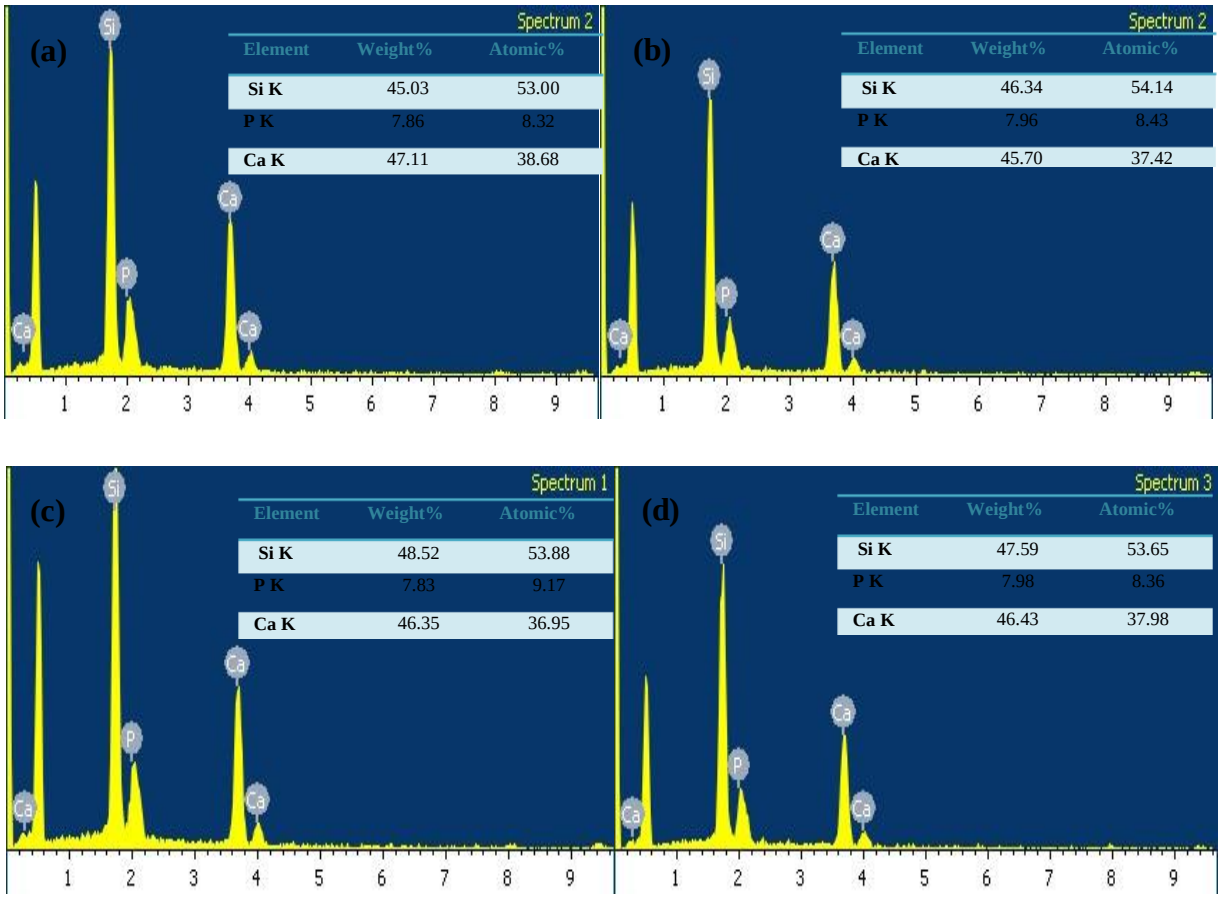

Figure 29. *EDS analysis of (a) H_2O_2 untreated BG, (b) 1M H_2O_2 treated BG, (c) 2M H_2O_2 treated BG, and (d) 3M H_2O_2 treated BG after soaking in SBF for 3 days.*

Table 6. *Si, Ca, and P concentrations of (BG0) H_2O_2 untreated BG, (BG1) 1M H_2O_2 treated BG, (BG2) 2M H_2O_2 treated BG, and (BG3) 3M H_2O_2 treated BG before and after soaking in SBF.*

Sample name	**Before bioactivity (atomic %)**			**After soaking 3 days in SBF (atomic %)**		
	Si	Ca	P	Si	Ca	P
BG0	55.40	39.46	5.15	53.00	38.68	8.32
BG1	55.21	38.78	6.03	54.14	37.42	8.43
BG2	54.65	38.98	6.36	53.88	36.95	9.17
BG3	55.88	37.95	6.17	53.65	37.98	8.36

4.8 Biodegradation test

Biodegradation property of H_2O_2 untreated BG (BG0), 1M H_2O_2 treated BG (BG1), 2M H_2O_2 treated BG (BG2), and 3M H_2O_2 treated BG (BG3) pellets after soaking in SBF were studied in SBF solution for 30 days as illustrated on Figure 30. The graph shows that after being soaked for 30 days in SBF solution, the weight loss of H_2O_2 untreated BG (BG0), 1M H_2O_2 treated BG (BG1), 2M H_2O_2 treated BG (BG2), and 3M H_2O_2 treated BG (BG3) pellets was 6.37$\pm$0.39%, 8.43$\pm$0.27%, 16.04$\pm$0.32%, and 9.93$\pm$0.54% respectively. Biodegradability in BG particles exhibit increased reactivity, which is an essential step and closely related to the development of the HAp layer. The lowest biodegradation were seen on H_2O_2 untreated BG (BG0) which has a solid surface morphology that hinders dissolution in SBF solution as discussed previously in the invitro bioactivity tests. The little porous morphology appeared on 1M H_2O_2 treated BG provides somewhat higher SSA and better degradation than H_2O_2 untreated specimen. The uniform and narrow pore distribution is obtained for the sample prepared with 2M H_2O_2 shows better biodegradation. Since the SSA of this specimens were higher, ion dissolution and interaction with SBF solution enables to form better degradation which also leads for better bioactivity *(Bakare et al., 2019).* The 3M H_2O_2 treated BG (BG3)

specimen has SSA higher than H_2O_2 untreated BG (BG0) and 1M H_2O_2 treated (BG1) but lower than 2M H_2O_2 treated (BG2). The biodegradability of the specimen was less due to lower SSA than 2M H_2O_2 treated (BG2).

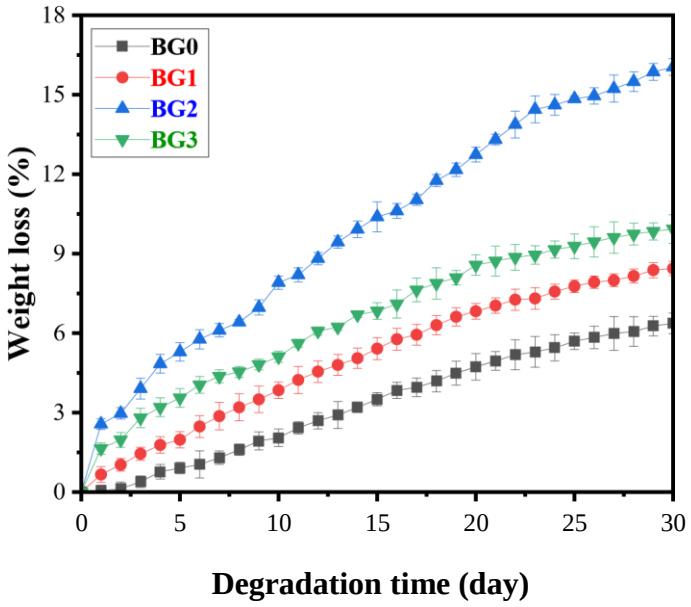

Figure 30. *Weight loss of (BG0) H_2O_2 untreated BG, (BG1) 1M H_2O_2 treated BG, (BG2) 2M H_2O_2 treated BG, and (BG3) 3M H_2O_2 treated BG after soaking in SBF for 30 days.*

4.8.1 Degradation rate Vs H_2O_2 concentration and specific surface area

Figure 31 shows degradation rate of H_2O_2 untreated BG (BG0), 1M H_2O_2 treated BG (BG1), 2M H_2O_2 treated BG (BG2), and 3M H_2O_2 treated BG (BG3) with H_2O_2 concentration and specific surface area. The degradation rate for BG0, BG1, BG2, and BG3 was 0.21$\pm$0.01%, 0.28$\pm$0.01%, 0.53$\pm$0.01%, and 0.33$\pm$0.012% respectively. Degradation rate is highly influenced by the H_2O_2 concentration as well as the SSA of BG particles. As illustrated on figure 31a, it was obtained that high weight loss and degradation rate for 2M H_2O_2 treated BG (BG2) and lowest for H_2O_2 untreated BG (BG0). The different surface morphologies formed on due to the H_2O_2 concentration leads to have BG particles with different SSA. Thus degradation rate increased with increasing SSA *(Bakare et al., 2019).*

It is preferable for a bioactive glass to have a reasonable degradation rate, the capacity to support the formation of HAp layer, and the capacity to stimulate biologically advantageous reactions *(Punj et al., 2021)*. In terms of BG particles structure, lower network connectivity will lead to a greater degradation rate (or higher solubility) and better bioactivity. It was generally observed slower degradation for all BG specimens which is essential for supporting the formation of HAp layer and biologically advantageous reactions.

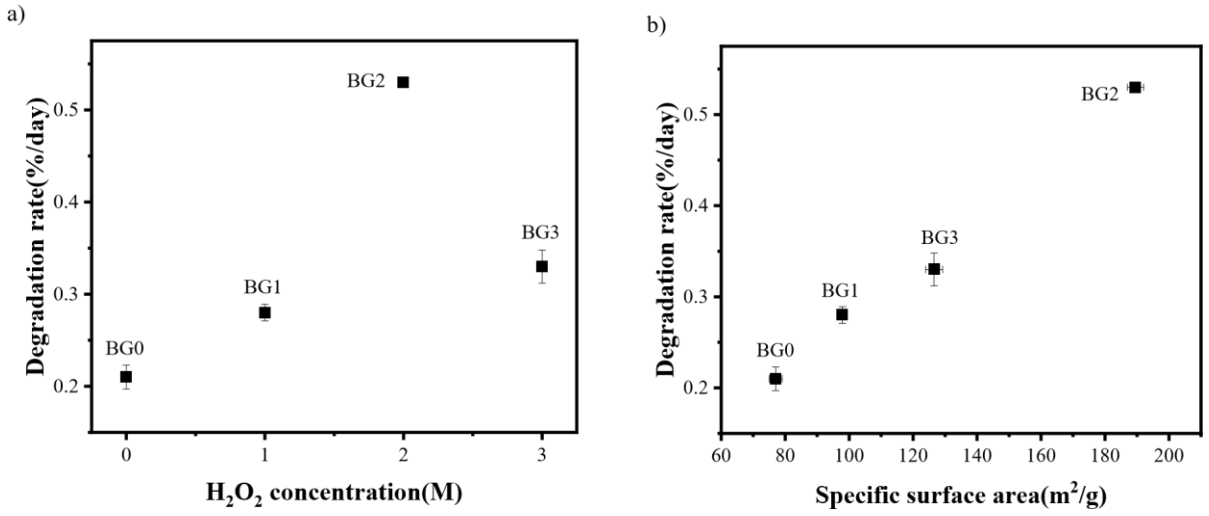

Figure 31. *Degradation rate of (BG0) H_2O_2 untreated BG, (BG1) 1M H_2O_2 treated BG, (BG2) 2M H_2O_2 treated BG, and (BG3) 3M H_2O_2 treated BG as a function of H_2O_2 concentration (a) and specific surface area (b).*

4.9. Bioactivity and biodegradation correlation

Because of its rapid ability to produce oxygen through its $2H_2O_2 \rightarrow 2H_2O + O_2$ decomposition characteristic, BG treated with H_2O_2 has a higher specific surface area. Therefore, an enormous amount of oxygen gas would be produced to form the pore structures. However, bioactivity and biodegradability decreases for higher concentrations of H_2O_2. This is mainly due to H_2O_2 molecules may have aggregated into larger clusters which will hinder the formation of HAp as well as the degradation of the BG specimens. Figure 32 shows bioactivity and biodegradation rate as a function of H_2O_2 concentration. It demonstrates that H_2O_2 treated BG specimens show better bioactivity and biodegradability

than the untreated one. As the H_2O_2 concentration increases up to 2M bioactivity and biodegradability also increases, but it decreases while raising the concentration to 3M.

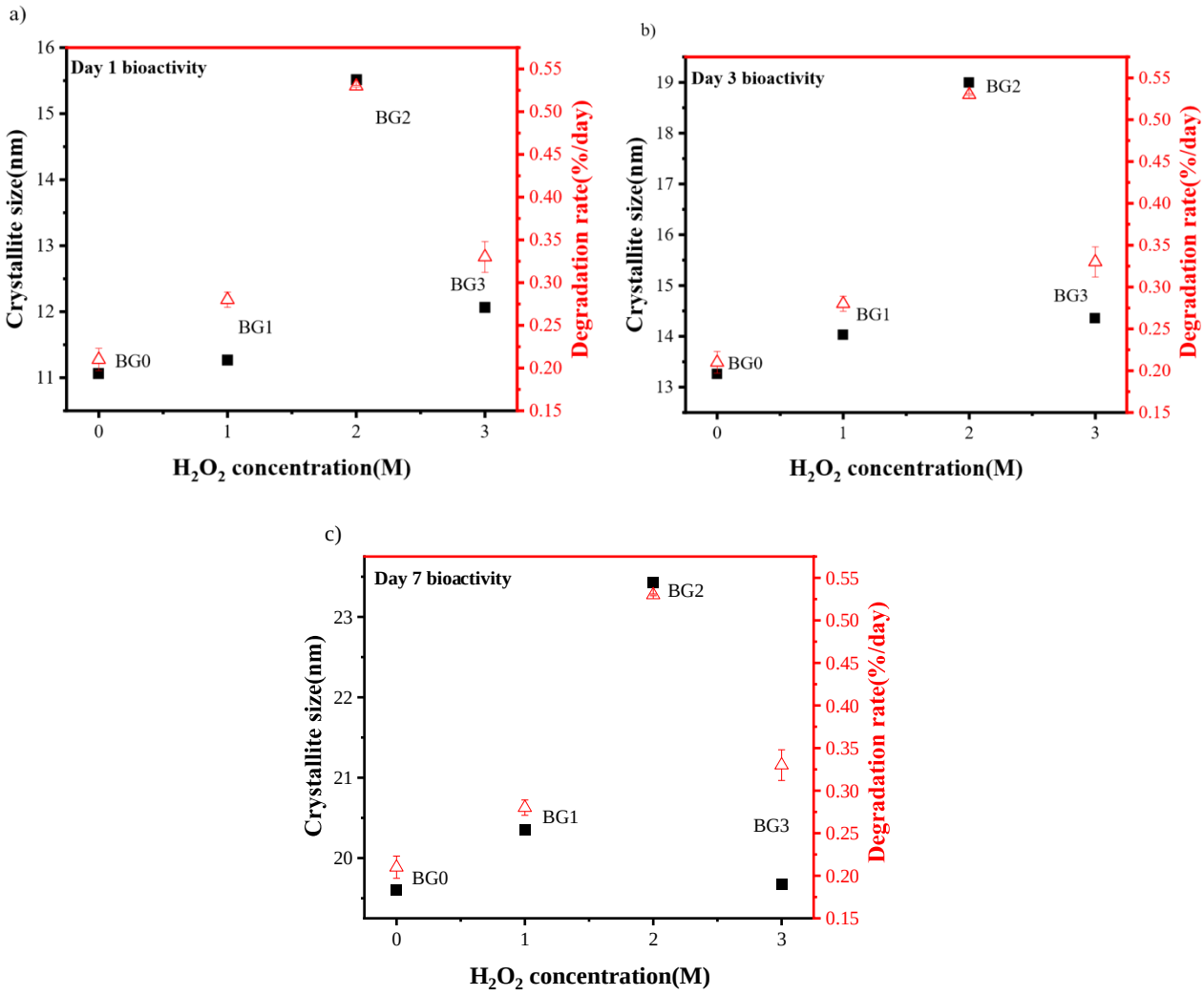

Figure 32. *Correlations between bioactivity (day 1 bioactivity (a), day 3 bioactivity (b), day 7 bioactivity(c)) and biodegradability with H_2O_2 concentration.*

According to Figure 33, bioactivity and biodegradability were correlated with specific surface area. It illustrates 2M treated BG exhibits better bioactivity and biodegradability based on its

high SSA. Thus, the BG's better bioactivity and biodegradability are dependent to the powders higher specific surface area *(Bakare et al., 2019)*. SSA enhances with H_2O_2 concentration from which determines the bioactivity and biodegradation of BGs. However for 3M H_2O_2 treated BG, SSA decreases. Thus it leads to reduce the bioactivity as well as biodegradability of the specimens. As a result both figure 32 and figure 33 illustrates bioactivity and biodegradability has a direct relation and they are highly influenced by the H_2O_2 concentration and SSA of BG particles.

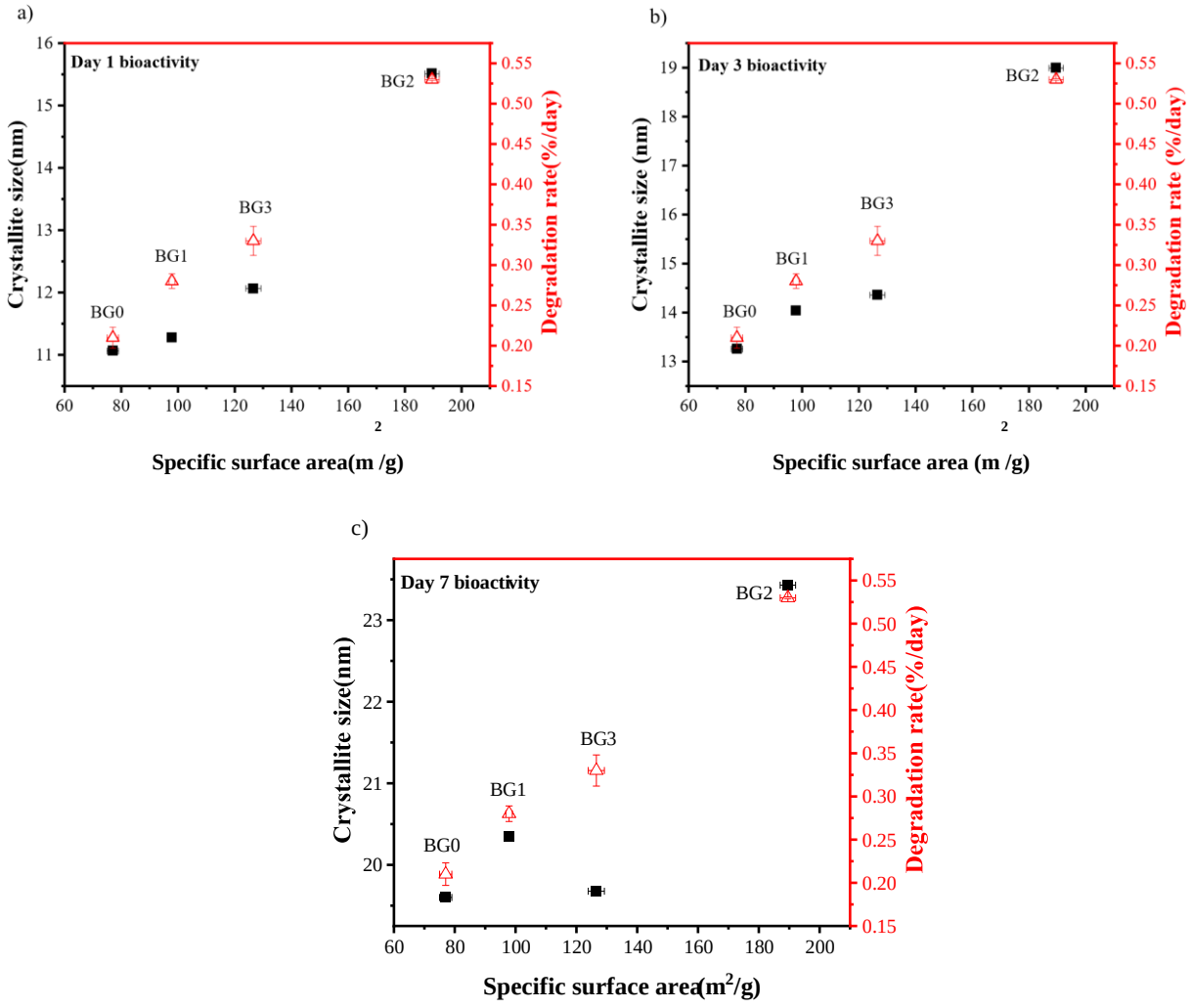

Figure 33. *Correlation between bioactivity (day 1 bioactivity (a), day 3 bioactivity (b), day 7 bioactivity(c)) and degradation rate as a function of specific surface area.*

5. CONCLUSIONS and RECOMMENDATIONS

5.1 Conclusions

In this study H_2O_2 untreated, 1M, 2M, and 3M H_2O_2 treated BG powders were successfully synthesized using sol-gel method. The results of this study generally indicate that utilizing H_2O_2 as a pore-forming agent in BG particles highly influence the specific surface area, bioactivity, and biodegradability properties. High solubility and decomposition property of H_2O_2 enables the formation of BG particles with high specific surface area, so that it can be used in place of conventional surfactant. It was also able to obtain BG particles with high purity and absence of residues like carbon based components and also silica BGs with a highly ordered porous structure have superior bioactivity properties were found. High specific surface area, pore volume and narrow pore size distribution can induce high invitro bioactivity of BG particles. According to the BET analysis, BG particles with high specific surface area were obtained for 2M H_2O_2 concentrations. The in vitro bioactivity test was done by SEM, XRD, EDS as well as FTIR analysis and reveals crystal HAp phase formation. In summary, the bioactivity and biodegradability tests indicated that the bioactivity was correlated well with the specific surface area; thus, the higher specific surfaces area of the BG particles contributed to the better bioactivity biodegradability of the BG.

5.2 Recommendations

Different pore forming agents have been used in order to synthesize BG particles with high SSA, better bioactivity, and biodegradability properties. Under this study, it was obtained that H_2O_2 enables to form pure BG with porous morphologies, and it is promising pore forming agent. Even though this work is constrained by time, working environment issue, and characterizations; some recommendations can be made based on the crucial findings. Analyzing other invitro tests like biocompatibility tests can lead to further analyze the BG particles property for further invivo tests and clinical applications. Furthermore, the application area of this BG particles can be widen by adding some therapeutic ions for cancer treatment, drug delivery, wound treatment and so on. These all suggestions will make the BGs to grow one step in the medical aspect.

6. REFERENCE

Abdullah, H. Z., Lee, T. C., Idris, M. I., & Selimin, M. A. (2020). Bio-ceramics for tissue engineering *Tissue Engineering Strategies for Organ Regeneration* (pp. 126-143): CRC Press.

Ahmadi, S., Behnamghader, A., & Asefnejaad, A. (2017). Sol-gel synthesis, characterization and in vitro evaluation of SiO2− CaO− P2O5 bioactive glass nanoparticles with various CaO/P2O5 ratios. *Digest Journal of Nanomaterials and Biostructures, 12*, 847-860.

Al-Bakhsh, B. A. J., Shafiei, F., Hashemian, A., Shekofteh, K., Bolhari, B., & Behroozibakhsh, M. (2019). In-vitro bioactivity evaluation and physical properties of an epoxy-based dental sealer reinforced with synthesized fluorine-substituted hydroxyapatite, hydroxyapatite and bioactive glass nanofillers. *Bioactive materials, 4*, 322-333.

Al-Harbi, N., Mohammed, H., Al-Hadeethi, Y., Bakry, A. S., Umar, A., Hussein, M. A., . . . Mkawi, E. M. (2021). Silica-based bioactive glasses and their applications in hard tissue regeneration: A review. *Pharmaceuticals, 14*(2), 75.

Almeida, R. M., & Gonçalves, M. C. (2021). Sol–gel process and products. *Encyclopedia of Glass Science, Technology, History, and Culture, 2*, 969-979.

Ana, I. D., Satria, G. A. P., Dewi, A. H., & Ardhani, R. (2018). Bioceramics for clinical application in regenerative dentistry. *Novel biomaterials for regenerative medicine*, 309-316.

Anand, A., Kundu, B., & Nandi, S. K. (2022). Mesoporous Bioactive Glass for Bone Tissue Regeneration and Drug Delivery. *Nanoengineering of Biomaterials*, 343-370.

Anand, A., Lalzawmliana, V., Kumar, V., Das, P., Devi, K. B., Maji, A. K., . . . Nandi, S. K. (2019).
Preparation and in vivo biocompatibility studies of different mesoporous bioactive glasses.
Journal of the Mechanical Behavior of Biomedical Materials, 89, 89-98.

Anil, A., Sadasivan, A., & Koshi, E. (2020). Physicochemical characterization of five different bone graft substitutes used in periodontal regeneration: an in vitro study. *Journal of International Society of Preventive & Community Dentistry, 10*(5), 634.

Baino, F., & Fiume, E. (2020). 3D printing of hierarchical scaffolds based on mesoporous bioactive glasses (MBGs)—Fundamentals and applications. *Materials, 13*(7), 1688.

Baino, F., Fiume, E., Miola, M., & Verné, E. (2018). Bioactive sol-gel glasses: processing, properties, and applications. *International Journal of Applied Ceramic Technology, 15*(4), 841-860.

Baino, F., Hamzehlou, S., & Kargozar, S. (2018). Bioactive glasses: where are we and where are we going? *Journal of functional biomaterials, 9*(1), 25.

Bakare, F. F., Chou, Y.-J., Huang, Y.-H., Tesfay, A. H., Moriga, T., & Shih, S.-J. (2019). Correlation of morphology and in-vitro degradation behavior of spray pyrolyzed bioactive glasses. *Materials, 12*(22), 3703.

Balamurugan, A., Sockalingum, G., Michel, J., Fauré, J., Banchet, V., Wortham, L., . . . Balossier, G. (2006). Synthesis and characterisation of sol gel derived bioactive glass for biomedical applications. *Materials Letters, 60*(29-30), 3752-3757.

Barrioni, B. R., de Laia, A. G. S., Valverde, T. M., da Mata Martins, T. M., Caliari, M. V., de Sa, M. A., . . .

de Magalhães Pereira, M. (2018). Evaluation of in vitro and in vivo biocompatibility and structure of cobalt-releasing sol-gel bioactive glass. *Ceramics International, 44*(16), 2033720347.

Bellucci, D., & Cannillo, V. (2018). A novel bioactive glass containing strontium and magnesium with ultra-high crystallization temperature. *Materials Letters, 213*, 67-70.

Ben-Arfa, B. A., Palamá, I. E., Salvado, I. M. M., Ferreira, J. M., & Pullar, R. C. (2020). The role of calcium (source & content) on the in vitro behaviour of sol–gel quaternary glass series.
Ceramics International, 46(1), 1065-1075.

Ben-Arfa, B. A., Fernandes, H. R., Miranda Salvado, I. M., Ferreira, J. M., & Pullar, R. C. (2018). Synthesis and bioactivity assessment of high silica content quaternary glasses with C a: P ratios of 1.5 and 1.67, made by a rapid sol-gel process. *Journal of Biomedical Materials Research Part A, 106*(2), 510-520.

Ben-Arfa, B. A., Fernandes, H. R., Salvado, I. M., Ferreira, J. M., & Pullar, R. C. (2018). Effects of catalysts on polymerization and microstructure of sol-gel derived bioglasses. *Journal of the American Ceramic Society, 101*(7), 2831-2839.

Brauer, D. S., & Jones, J. R. (2021). Bioactive Glasses. *Encyclopedia of Glass Science, Technology, History, and Culture, 2*, 991-1003.

Bueno, O. M. V. M., Herrera, C. L., Bertran, C. A., San-Miguel, M. A., & Lopes, J. H. (2021). An experimental and theoretical approach on stability towards hydrolysis of triethyl phosphate and its effects on the microstructure of sol-gel-derived bioactive silicate glass. *Materials Science and Engineering: C, 120*, 111759.

Bui, X. V., & Dang, T. H. (2019). Bioactive glass 58S prepared using an innovation sol-gel process. *Processing and application of ceramics, 13*(1), 98-103.

Cañas, E., Orts, M. J., Sánchez, E., Bellucci, D., & Cannillo, V. (2022). Deposition of bioactive glass coatings based on a novel composition containing strontium and magnesium. *Journal of the European Ceramic Society, 42*(13), 6213-6221.

Cao, X., Wang, G., Yang, Y., Cao, Y., & Cao, X. (2021). Biomolecules induce the synthesis of hollow hierarchical mesoporous structured hydroxyapatite microflowers: application in macromolecule drug delivery. *Journal of Materials Science, 56*, 7034-7049.

Catauro, M., & Ciprioti, S. V. (2021). Characterization of hybrid materials prepared by sol-gel method for biomedical implementations. A critical review. *Materials, 14*(7), 1788.

Chakraborty, P. K., Adhikari, J., & Saha, P. (2021). Variation of the properties of sol–gel synthesized bioactive glass 45S5 in organic and inorganic acid catalysts. *Materials Advances, 2*(1), 413425.

Chang, J., & Zhou, Y. (2018). Surface modification of bioactive glasses *Bioactive Glasses* (pp. 119-143): Elsevier.

Chaves, P., Garrido, M., Oliver, J., Pérez-Ruiz, E., Barragan, I., & Rueda-Domínguez, A. (2023). Preclinical models in head and neck squamous cell carcinoma. *British Journal of Cancer, 128*(10), 1819-1827.

Cheah, C. W., Al-Namnam, N. M., Lau, M. N., Lim, G. S., Raman, R., Fairbairn, P., & Ngeow, W. C. (2021). Synthetic material for bone, periodontal, and dental tissue regeneration: Where are we now, and where are we heading next? *Materials, 14*(20), 6123.

Chen, J., Zeng, L., Chen, X., Liao, T., & Zheng, J. (2018). Preparation and characterization of bioactive glass tablets and evaluation of bioactivity and cytotoxicity in vitro. *Bioactive materials, 3*(3), 315-321.

Chircov, C., Spoială, A., Păun, C., Crăciun, L., Ficai, D., Ficai, A., . . . Turculeț, Ș. C. (2020). Mesoporous silica platforms with potential applications in release and adsorption of active agents. *Molecules, 25*(17), 3814.

Chou, Y.-J., Hong, B.-J., Lin, Y.-C., Wang, C.-Y., & Shih, S.-J. (2017). The correlation of pore size and bioactivity of spray-pyrolyzed mesoporous bioactive glasses. *Materials, 10*(5), 488.

Chowdhury, S., Rakshit, A., Acharjee, A., & Saha, B. (2019). Novel amphiphiles and their applications for different purposes with special emphasis on polymeric surfactants. *ChemistrySelect, 4*(23), 6978-6995.

Chuni, T., Dachasa, K., Gochole, F., Hunde, T., & Bakare, F. F. (2023). Effect of Morphology on the In Vitro Bioactivity and Biocompatibility of Spray Pyrolyzed Bioactive Glass. *Advances in Materials Science and Engineering, 2023*.

Collins, M. N., Ren, G., Young, K., Pina, S., Reis, R. L., & Oliveira, J. M. (2021). Scaffold fabrication technologies and structure/function properties in bone tissue engineering. *Advanced Functional Materials, 31*(21), 2010609.

Dang, T. H., Bui, T. H., Guseva, E. V., Ta, A. T., Nguyen, A. T., Hoang, T. T. H., & Bui, X. V. (2020). Characterization of bioactive glass synthesized by sol-gel process in hot water. *Crystals, 10*(6), 529.

Deka, J. R., Song, Y., & Yang, Y.-C. (2018). The influence of isothermal aging, surfactant and inorganic precursors concentrations on pore size and structural order of mesoporous bioactive glass. *Solid State Sciences, 84*, 104-111.

Deshmukh, K., Kovářík, T., Křenek, T., Docheva, D., Stich, T., & Pola, J. (2020). Recent advances and future perspectives of sol–gel derived porous bioactive glasses: a review. *RSC Advances, 10*(56), 33782-33835.

Dhinasekaran, D., & Kumar, A. (2022). Fabrication of Bioactive Structures from Sol–Gel Derived Bioactive Glass. *Bioactive Glasses and Glass-Ceramics: Fundamentals and Applications*, 87117.

Du, M., Chen, J., Liu, K., Xing, H., & Song, C. (2021). Recent advances in biomedical engineering of nano-hydroxyapatite including dentistry, cancer treatment and bone repair. *Composites Part B: Engineering, 215*, 108790.

Durgalakshmi, D., Rakkesh, R. A., Aruna, P., Ganesan, S., & Balakumar, S. (2020). Bioactivity and hemocompatibility of sol–gel bioactive glass synthesized under different catalytic conditions. *New Journal of Chemistry, 44*(48), 21026-21037.

Durgalakshmi, D., Rakkesh, R. A., Kesavan, M., Ganapathy, S., Ajithkumar, T., Karthikeyan, S., & Balakumar, S. (2018). Highly reactive crystalline-phase-embedded strontium-bioactive nanorods for multimodal bioactive applications. *Biomaterials science, 6*(7), 1764-1776.

El-Fiqi, A., Buitrago, J. O., Yang, S. H., & Kim, H.-W. (2017). Biomimetically grown apatite spheres from aggregated bioglass nanoparticles with ultrahigh porosity and surface area imply potential drug delivery and cell engineering applications. *Acta biomaterialia, 60*, 38-49.

El-Fiqi, A., Kim, T.-H., Kim, M., Eltohamy, M., Won, J.-E., Lee, E.-J., & Kim, H.-W. (2012). Capacity of mesoporous bioactive glass nanoparticles to deliver therapeutic molecules. *Nanoscale, 4*(23), 7475-7488.

Ershad, M. (2018). *Physico-mechanical properties of rare-earth oxides substituted bioactive soda lime phosphosilicate glasses and glass ceramics.* IIT BHU (Varanasi).

Esposito, S. (2019). "Traditional" sol-gel chemistry as a powerful tool for the preparation of supported metal and metal oxide catalysts. *Materials, 12*(4), 668.

Faure, J., Drevet, R., Lemelle, A., Jaber, N. B., Tara, A., El Btaouri, H., & Benhayoune, H. (2015). A new sol–gel synthesis of 45S5 bioactive glass using an organic acid as catalyst. *Materials Science and Engineering: C, 47*, 407-412.

Fernandes, H. R., Gaddam, A., Rebelo, A., Brazete, D., Stan, G. E., & Ferreira, J. M. (2018). Bioactive glasses and glass-ceramics for healthcare applications in bone regeneration and tissue engineering. *Materials, 11*(12), 2530.

Ferraris, S., Yamaguchi, S., Barbani, N., Cazzola, M., Cristallini, C., Miola, M., . . . Spriano, S. (2020). Bioactive materials: In vitro investigation of different mechanisms of hydroxyapatite precipitation. *Acta biomaterialia, 102*, 468-480.

Fiume, E., Barberi, J., Verné, E., & Baino, F. (2018). Bioactive glasses: from parent 45S5 composition to scaffold-assisted tissue-healing therapies. *Journal of functional biomaterials, 9*(1), 24.

Fiume, E., Magnaterra, G., Rahdar, A., Verné, E., & Baino, F. (2021). Hydroxyapatite for biomedical applications: a short overview. *Ceramics, 4*(4), 542-563.

Fletcher, J., Alles, W., Keenan, T. J., & Wren, A. W. (2022). Bioactive Glass-Based Coatings: Concepts for Improving the Biocompatibility of Implantable Materials. *Bioactive Glasses and GlassCeramics: Fundamentals and Applications*, 293-310.

García, A., Cicuéndez, M., Izquierdo-Barba, I., Arcos, D., & Vallet-Regí, M. (2009). Essential role of calcium phosphate heterogeneities in 2D-hexagonal and 3D-cubic SiO2− CaO− P2O5 mesoporous bioactive glasses. *Chemistry of Materials, 21*(22), 5474-5484.

García, A., Izquierdo-Barba, I., Colilla, M., De Laorden, C. L., & Vallet-Regí, M. (2011). Preparation of 3D scaffolds in the SiO2–P2O5 system with tailored hierarchical meso-macroporosity. *Acta biomaterialia, 7*(3), 1265-1273.

Gautam, G., Kumar, S., & Kumar, K. (2022). Processing of biomaterials for bone tissue engineering: state of the art. *Materials Today: Proceedings, 50*, 2206-2217.

Gharbi, A., Kallel, A. Y., Kanoun, O., Cheikhrouhou-Koubaa, W., Contag, C. H., Antoniac, I., . . . Ashammakhi, N. (2023). A Biodegradable Bioactive Glass-Based Hydration Sensor for Biomedical Applications. *Micromachines, 14*(1), 226.

Ghorbanzade Zaferani, S. P., Nabian, N., Delavar, M., & Rabiee, S. M. (2021). Direct impregnation of MgO nanoparticles in 58S bioactive glass: bioactivity evaluation and antibacterial activity.
Iranian Journal of Science and Technology, Transactions A: Science, 45, 885-898.

Ghosh, S., Ray, A., & Pramanik, N. (2020). Self-assembly of surfactants: An overview on general aspects of amphiphiles. *Biophysical Chemistry, 265*, 106429.

Gupta, N., & Santhiya, D. (2018). Mesoporous bioactive glass and its applications *Bioactive Glasses* (pp. 63-85): Elsevier.

Hench, L. L. (2006). The story of Bioglass®. *Journal of Materials Science: Materials in Medicine, 17*(11), 967-978.

Hench, L. L., & Jones, J. R. (2015). Bioactive glasses: frontiers and challenges. *Frontiers in bioengineering and biotechnology, 3*, 194.

Hong, B.-J., Hsiao, C.-W., Bakare, F. F., Sun, J.-T., & Shih, S.-J. (2018). Effect of acetic acid concentration on pore structure for mesoporous bioactive glass during spray pyrolysis. *Materials, 11*(6), 963.

Hong, B.-J., & Shih, S.-J. (2017). Novel pore-forming agent to prepare of mesoporous bioactive glass using one-step spray pyrolysis. *Ceramics International, 43*, S771-S775.

Hu, Q., Chen, X., Zhao, N., & Li, Y. (2013). Facile synthesis and in vitro bioactivity of monodispersed mesoporous bioactive glass sub-micron spheres. *Materials Letters, 106*, 452-455.

Hu, Q., Chen, X., Zhao, N., Li, Y., & Mao, C. (2014). Fabrication and characterization of dodecylamine derived monodispersed mesoporous bioactive glass sub-micron spheres. *Journal of sol-gel science and technology, 69*(1), 9-16.

Hu, Q., Li, Y., Miao, G., Zhao, N., & Chen, X. (2014). Size control and biological properties of monodispersed mesoporous bioactive glass sub-micron spheres. *RSC Advances, 4*(43), 2267822687.

Huang, C., Yu, M., Li, H., Wan, X., Ding, Z., Zeng, W., & Zhou, Z. (2021). Research progress of bioactive glass and its application in orthopedics. *Advanced Materials Interfaces, 8*(22), 2100606.

Hupa, L. (2018). Composition-property relations of bioactive silicate glasses *Bioactive glasses* (pp. 135): Elsevier.

Ijaz, A., Yagci, M. B., Ow-Yang, C. W., Demirel, A. L., & Miko, A. (2020). Formation of mesoporous silica particles with hierarchical morphology. *Microporous and mesoporous materials, 303*, 110240.

Ingole, V., Sathe, B., & Ghule, A. (2018). Bioactive ceramic composite material stability, characterization. *Fundamental biomaterials: ceramics*, 273-296.

Issa, A. A., & Luyt, A. S. (2019). Kinetics of alkoxysilanes and organoalkoxysilanes polymerization: a review. *Polymers, 11*(3), 537.

Jang, J.-H., Lee, M. G., Ferracane, J. L., Davis, H., Bae, H. E., Choi, D., & Kim, D.-S. (2018). Effect of bioactive glass-containing resin composite on dentin remineralization. *Journal of dentistry, 75*, 58-64.

Kabtamu, D. M., Wu, Y.-n., & Li, F. (2020). Hierarchically porous metal–organic frameworks: Synthesis strategies, structure (s), and emerging applications in decontamination. *Journal of hazardous materials, 397*, 122765.

Kalpana, M., & Nagalakshmi, R. (2022). Nano hydroxyapatite for biomedical applications derived from chemical and natural sources by simple precipitation method. *Applied Biochemistry and Biotechnology*, 1-17.

Kargozar, S., Hooshmand, S., Hosseini, S. A., Gorgani, S., Kermani, F., & Baino, F. (2022). Antioxidant Effects of Bioactive Glasses (BGs) and Their Significance in Tissue Engineering Strategies. *Molecules, 27*(19), 6642.

Kargozar, S., Kermani, F., Mollazadeh Beidokhti, S., Hamzehlou, S., Verné, E., Ferraris, S., & Baino, F. (2019). Functionalization and surface modifications of bioactive glasses (BGs): tailoring of the biological response working on the outermost surface layer. *Materials, 12*(22), 3696.

Kargozar, S., Montazerian, M., Hamzehlou, S., Kim, H.-W., & Baino, F. (2018). Mesoporous bioactive glasses: Promising platforms for antibacterial strategies. *Acta biomaterialia, 81*, 1-19.

Kaur, G., Pickrell, G., Sriranganathan, N., Kumar, V., & Homa, D. (2016). Review and the state of the art: sol–gel and melt quenched bioactive glasses for tissue engineering. *Journal of Biomedical Materials Research Part B: Applied Biomaterials, 104*(6), 1248-1275.

Kaya, S., Cresswell, M., & Boccaccini, A. R. (2018). Mesoporous silica-based bioactive glasses for antibiotic-free antibacterial applications. *Materials Science and Engineering: C, 83*, 99-107. Kesse, X., Vichery, C., Jacobs, A., Descamps, S., & Nedelec, J.-M. (2020). Unravelling the Impact of Calcium Content on the Bioactivity of Sol–Gel-Derived Bioactive Glass Nanoparticles. *ACS Applied Bio Materials, 3*(2), 1312-1320.

Khalid, M. D., Zafar, M. S., Farooq, I., Khan, R. S., & Najmi, A. (2017). Bioactive glasses and their applications in dentistry. *JPDA, 26*(01), 33.

Khurshid, Z., Husain, S., Alotaibi, H., Rehman, R., Zafar, M. S., Farooq, I., & Khan, A. S. (2019). Novel techniques of scaffold fabrication for bioactive glasses *Biomedical, Therapeutic and Clinical Applications of Bioactive Glasses* (pp. 497-519): Elsevier.

Kokubo, T., & Yamaguchi, S. (2019). Simulated body fluid and the novel bioactive materials derived from it. *Journal of Biomedical Materials Research Part A, 107*(5), 968-977.

Kong, C. H., Steffi, C., Shi, Z., & Wang, W. (2018). Development of mesoporous bioactive glass nanoparticles and its use in bone tissue engineering. *Journal of Biomedical Materials Research Part B: Applied Biomaterials, 106*(8), 2878-2887.

Koons, G. L., Diba, M., & Mikos, A. G. (2020). Materials design for bone-tissue engineering. *Nature Reviews Materials, 5*(8), 584-603.

Koumba Ibinga, S. K., Fabre, J.-F., Bikanga, R., & Mouloungui, Z. (2019). Atypical reaction media and organized systems for the synthesis of low-substitution sugar esters. *Frontiers in Chemistry, 7*, 587.

Kumar, A., Aditya, A., & Murugavel, S. (2019). Effect of surfactant concentration on textural characteristics and biomineralization behavior of mesoporous bioactive glasses. *Materials Science and Engineering: C, 96*, 20-29.

Kumar, A., Murugavel, S., Aditya, A., & Boccaccini, A. R. (2017). Mesoporous 45S5 bioactive glass: Synthesis, in vitro dissolution and biomineralization behavior. *Journal of materials chemistry B, 5*(44), 8786-8798.

Kumawat, V. S., Bandyopadhyay-Ghosh, S., & Ghosh, S. B. (2022). An overview of translational research in bone graft biomaterials. *Journal of Biomaterials Science, Polymer Edition*, 1-44.

Kuo, C.-K., Chen, L.-G., Tseng, C.-F., & Chou, Y.-J. (2021). Influences of acid catalysts on the microstructure, bioactivity and cytotoxicity of bioactive glass nanoparticles prepared by spray pyrolysis. *Journal of Non-Crystalline Solids, 560*, 120710.

Lalzawmliana, V., Anand, A., Roy, M., Kundu, B., & Nandi, S. K. (2020). Mesoporous bioactive glasses for bone healing and biomolecules delivery. *Materials Science and Engineering: C, 106*, 110180.

Lei, B., Chen, X., & Koh, Y.-H. (2011a). Effects of acidic catalysts on the microstructure and biological property of sol–gel bioactive glass microspheres. *Journal of sol-gel science and technology, 58*, 656-663.

Lei, B., Chen, X., & Koh, Y.-H. (2011b). Effects of acidic catalysts on the microstructure and biological property of sol–gel bioactive glass microspheres. *Journal of sol-gel science and technology, 58*(3), 656-663.

Lei, B., Chen, X., Wang, Y., & Zhao, N. (2009). Synthesis and in vitro bioactivity of novel mesoporous hollow bioactive glass microspheres. *Materials Letters, 63*(20), 1719-1721.

Lei, B., Chen, X., Wang, Y., Zhao, N., Du, C., & Fang, L. (2010). Fabrication, structure and biological properties of organic acid-derived sol–gel bioactive glasses. *Biomedical Materials, 5*(5), 054103.

Lei, Q., Guo, J., Noureddine, A., Wang, A., Wuttke, S., Brinker, C. J., & Zhu, W. (2020). Sol–gel-based advanced porous silica materials for biomedical applications. *Advanced Functional Materials, 30*(41), 1909539.

Leite, Á. J., & Mano, J. (2017). Biomedical applications of natural-based polymers combined with bioactive glass nanoparticles. *Journal of materials chemistry B, 5*(24), 4555-4568.

Li, X., Wang, X., Chen, H., Jiang, P., Dong, X., & Shi, J. (2007). Hierarchically porous bioactive glass scaffolds synthesized with a PUF and P123 cotemplated approach. *Chemistry of Materials, 19*(17), 4322-4326.

Liang, Q., Liu, X., Zeng, G., Liu, Z., Tang, L., Shao, B., . . . Cheng, M. (2019). Surfactant-assisted synthesis of photocatalysts: Mechanism, synthesis, recent advances and environmental application. *Chemical engineering journal, 372*, 429-451.

Liu, X., Rahaman, M. N., & Fu, Q. (2011). Oriented bioactive glass (13-93) scaffolds with controllable pore size by unidirectional freezing of camphene-based suspensions: Microstructure and mechanical response. *Acta biomaterialia, 7*(1), 406-416.

Lopes, J. H., Bueno, O. M. V. M., Mazali, I. O., & Bertran, C. A. (2019). Investigation of citric acidassisted sol-gel synthesis coupled to the self-propagating combustion method for preparing bioactive glass with high structural homogeneity. *Materials Science and Engineering: C, 97*, 669-678.

Lopes, J. H., Magalhães, A., & Bertran, C. A. (2022). Morphological, structural, and in vitro bioactivity of core-shell-structured bioactive glass by multitechnical spectroscopic approach. *Ceramics International, 48*(6), 8039-8050.

Łukowicz, K., Zagrajczuk, B., Nowak, A., Niedźwiedzki, Ł., Laczka, M., Cholewa-Kowalska, K., & Osyczka, A. M. (2020). The role of CaO/SiO2 ratio and P2O5 content in gel-derived bioactive glass-polymer composites in the modulation of their bioactivity and osteoinductivity in human BMSCs. *Materials Science and Engineering: C, 109*, 110535.

Ma, Y., Zhang, C., Hou, C., Zhang, H., Zhang, H., Zhang, Q., & Guo, Z. (2017). Cetyl trimethyl ammonium bromide (CTAB) micellar templates directed synthesis of water-dispersible polyaniline rhombic plates with excellent processability and flow-induced color variation. *Polymer, 117*, 30-36.

Malik, S., Sundarrajan, S., Hussain, T., Nazir, A., Ayyoob, M., Berto, F., & Ramakrishna, S. (2021). Sustainable nanofibers in tissue engineering and biomedical applications. *Material Design & Processing Communications, 3*(6), e202.

Mehmood, Y., Khan, I. U., Shahzad, Y., Khalid, S. H., Asghar, S., Irfan, M., . . . Hussain, T. (2019). Facile synthesis of mesoporous silica nanoparticles using modified sol-gel

method: Optimization and in vitro cytotoxicity studies. *Pak. J. Pharm. Sci, 32*(4), 1805-1812.

Mehrabi, T., Mesgar, A. S., & Mohammadi, Z. (2020). Bioactive glasses: a promising therapeutic ion release strategy for enhancing wound healing. *ACS Biomaterials Science & Engineering, 6*(10), 5399-5430.

Migneco, C., Fiume, E., Verné, E., & Baino, F. (2020). A guided walk through the world of mesoporous bioactive glasses (MBGs): Fundamentals, processing, and applications. *Nanomaterials, 10*(12), 2571.

Moghanian, A., Firoozi, S., & Tahriri, M. (2017). Characterization, in vitro bioactivity and biological studies of sol-gel synthesized SrO substituted 58S bioactive glass. *Ceramics International, 43*(17), 14880-14890.

Moghanian, A., Tajer, M. H. M., Zohourfazeli, M., Miri, Z., & Yazdi, M. (2021). Sol-gel derived silicatebased bioactive glass: Studies of synergetic effect of zirconium and magnesium on structural and biological characteristics. *Journal of Non-Crystalline Solids, 554*, 120613.

Mohamed, M. G., Atayde Jr, E. C., Matsagar, B. M., Na, J., Yamauchi, Y., Wu, K. C.-W., & Kuo, S.-W. (2020). Construction hierarchically mesoporous/microporous materials based on block copolymer and covalent organic framework. *Journal of the Taiwan Institute of Chemical Engineers, 112*, 180-192.

Monajem-Isfahani, S. (2018). Sol-gel bioactive glasses for oral care applications.

Montazerian, M., & Zanotto, E. D. (2021). The Glassy State. *Encyclopedia of Materials: Technical Ceramics and Glasses, 2*, 448-461.

Mosaad, K. E., Shoueir, K. R., Saied, A. H., & Dewidar, M. M. (2021). New prospects in nano phased cosubstituted hydroxyapatite enrolled in polymeric nanofiber mats for bone tissue engineering applications. *Annals of Biomedical Engineering, 49*(9), 2006-2029.

Mouriño, V., Vidotto, R., Cattalini, J., & Boccaccini, A. (2019). Enhancing biological activity of bioactive glass scaffolds by inorganic ion delivery for bone tissue engineering. *Current Opinion in Biomedical Engineering, 10*, 23-34.

Mulchandani, N., & Katiyar, V. (2019). Bioactive Glasses: Prospects in Bone Tissue Engineering.

Advances in Sustainable Polymers: Processing and Applications, 67-83.

Neščáková, Z., Zheng, K., Liverani, L., Nawaz, Q., Galusková, D., Kaňková, H., . . . Boccaccini, A. R. (2019). Multifunctional zinc ion doped sol–gel derived mesoporous bioactive glass nanoparticles for biomedical applications. *Bioactive materials, 4*, 312-321.

Neto, A. S., & Ferreira, J. M. (2018). Synthetic and marine-derived porous scaffolds for bone tissue engineering. *Materials, 11*(9), 1702.

Nommeots-Nomm, A., Hupa, L., Rohanová, D., & Brauer, D. S. (2020). A review of acellular immersion tests on bioactive glasses—influence of medium on ion release and apatite formation.

International Journal of Applied Glass Science, 11(3), 537-551.

Oluwatosin, D. A., El Mabrouk, K., & Bricha, M. (2023). A review on Borate Bioactive glasses (BBG): effect of doping elements, degradation, and applications. *Journal of materials chemistry B*.

Oudadesse, H., Najem, S., Mosbahi, S., Rocton, N., Refifi, J., El Feki, H., & Lefeuvre, B. (2021). Development of hybrid scaffold: Bioactive glass nanoparticles/chitosan for tissue engineering applications. *Journal of Biomedical Materials Research Part A, 109*(5), 590-599.

ÖZEL, C., KIZIL, P., EMİR, C., & YÜCEL, S. THE USAGE OF BIOACTIVE GLASSES IN BONE TISSUE ENGINEERING.

Pahlevanzadeh, F., Emadi, R., Valiani, A., Kharaziha, M., Poursamar, S. A., Bakhsheshi-Rad, H. R., . . . Berto, F. (2020). Three-dimensional printing constructs based on the chitosan for tissue regeneration: State of the art, developing directions and prospect trends. *Materials, 13*(11), 2663.

Pajares-Chamorro, N., & Chatzistavrou, X. (2020). Bioactive glass nanoparticles for tissue regeneration. *Acs Omega, 5*(22), 12716-12726.

Pal, N., Lee, J.-H., & Cho, E.-B. (2020). Recent trends in morphology-controlled synthesis and application of mesoporous silica nanoparticles. *Nanomaterials, 10*(11), 2122.

Park, H., Rezabeigi, E., & Nazhat, S. N. (2021). Inorganic–Organic Hybrids: Mimicking Native Bone. *The Chemistry of Inorganic Biomaterials, 7*, 134.

Pedanaboyina, K. (2019). *Synthesis, Characterisation and Hydroxy Carbonated Apatite (Hca) Formation Studies on Sol-Gel Derived SiO2-CaO-P2O5, SiO2-CaO-Na2O-P2O5, SiO2-CaO-BaONa2OP2O5 Glass Systems.* National Institute of Technology Karnataka, Surathkal.

Punj, S., Singh, J., & Singh, K. (2021). Ceramic biomaterials: Properties, state of the art and future prospectives. *Ceramics International, 47*(20), 28059-28074.

Rahaman, M. N., Day, D. E., Bal, B. S., Fu, Q., Jung, S. B., Bonewald, L. F., & Tomsia, A. P. (2011).
Bioactive glass in tissue engineering. *Acta biomaterialia, 7*(6), 2355-2373.

Ramli, N., Sazali, E., Mahraz, Z. A., Ghoshal, S., Zain, S. M., Hisam, R., . . . Noor, F. (2023). Hard tissue repairing potency of mesoporous borosilicate bioactive glass: An in vitro assessment. *Journal of Non-Crystalline Solids, 609*, 122289.

Rastegari, E., Hsiao, Y., Lai, W., Lai, Y., Yang, T., Chen, S., . . . Chien, Y. (2021). An Update on
Mesoporous Silica Nanoparticle Applications in Nanomedicines. Pharmaceutics 2021, 13, 1067: s Note: MDPI stays neutral with regard to jurisdictional claims in published ….

Rezaei, Y., Moztarzadeh, F., Shahabi, S., & Tahriri, M. (2014). Synthesis, characterization, and in vitro bioactivity of sol-gel-derived SiO2–CaO–P2O5–MgO-SrO bioactive glass. *Synthesis and Reactivity in Inorganic, Metal-Organic, and Nano-Metal Chemistry, 44*(5), 692-701.

Salinas, A., Vallet-Regi, M., & Heikkilä, J. (2018). Use of bioactive glasses as bone substitutes in orthopedics and traumatology *Bioactive glasses* (pp. 337-364): Elsevier.

Salinas, A. J., & Esbrit, P. (2022). Mesoporous bioglasses enriched with bioactive agents for bone repair, with a special highlight of María Vallet-Regí's contribution. *Pharmaceutics, 14*(1), 202.

Sanders, L. M. (2018). *The Synthesis & Characterization of an Antibacterial Bioactive Glass Suitable as a Bone Void Substitute*: The University of Toledo.

Santos, S. C., Barreto, L. S., & dos Santos, E. A. (2016). Nanocrystalline apatite formation on bioactive glass in a sol–gel synthesis. *Journal of Non-Crystalline Solids, 439*, 30-37.

Sathiskumar, S., Vanaraj, S., Sabarinathan, D., Bharath, S., Sivarasan, G., Arulmani, S., . . . Ponnusamy, V. K. (2019). Green synthesis of biocompatible nanostructured hydroxyapatite from Cirrhinus mrigala fish scale–A biowaste to biomaterial. *Ceramics International, 45*(6), 7804-7810.

Schuhladen, K., & Boccaccini, A. R. (2021). Bioactive glass variants for tissue engineering: From the macro-to the nanoscale *Bioceramics* (pp. 353-373): Elsevier.

Schumacher, M., Habibovic, P., & van Rijt, S. (2021). Mesoporous bioactive glass composition effects on degradation and bioactivity. *Bioactive materials, 6*(7), 1921-1931.

Sergi, R., Bellucci, D., & Cannillo, V. (2020). A review of bioactive glass/natural polymer composites: State of the art. *Materials, 13*(23), 5560.

Shah, A. T., Ain, Q., Chaudhry, A. A., Ahmad, S., Zarif, F., Siddiqi, S. A., . . . ur Rehman, I. (2018). Acid catalysed synthesis of bioactive glass by evaporation induced self assembly method. *Journal of Non-Crystalline Solids, 479*, 1-8.

Shanmugam, K., & Sahadevan, R. (2018). Bioceramics—An introductory overview. *Fundamental biomaterials: ceramics*, 1-46.

Sharifi, E., Bigham, A., Yousefiasl, S., Trovato, M., Ghomi, M., Esmaeili, Y., . . . Sharifi, S. (2022). Mesoporous bioactive glasses in cancer diagnosis and therapy: stimuli-responsive, toxicity, immunogenicity, and clinical translation. *Advanced Science, 9*(2), 2102678.

Shearer, A., Montazerian, M., & Mauro, J. C. (2023). Modern definition of bioactive glasses and glassceramics. *Journal of Non-Crystalline Solids, 608*, 122228.

Shih, S.-J., Chou, Y.-J., & Panjaitan, L. V. P. (2013). Synthesis and characterization of spray pyrolyzed mesoporous bioactive glass. *Ceramics International, 39*(8), 8773-8779.

Shih, S.-J., Lin, Y.-C., Valentino Posma Panjaitan, L., & Rahayu Meyla Sari, D. (2016). The correlation of surfactant concentrations on the properties of mesoporous bioactive glass. *Materials, 9*(1), 58.

Siekkinen, M., Karlström, O., & Hupa, L. (2022). Effect of local ion concentrations on the in vitro reactions of bioactive glass 45S5 particles. *International Journal of Applied Glass Science, 13*(4), 695-707.

Singh, A. V. S. S. (2013). Basics of bone grafting and graft materials. *Clinical Implantology*, 283.

Skallevold, H. E., Rokaya, D., Khurshid, Z., & Zafar, M. S. (2019). Bioactive glass applications in dentistry. *International Journal of Molecular Sciences, 20*(23), 5960.

Soni, R., Kumar, N. V., Chameettachal, S., Pati, F., & Rath, S. N. (2019). Synthesis and optimization of PCL-bioactive glass composite scaffold for bone tissue engineering. *Materials Today: Proceedings, 15*, 294-299.

Spirandeli, B. R., Campos, T. M. B., Ribas, R. G., Thim, G. P., & de Sousa Trichês, E. (2020). Evaluation of colloidal and polymeric routes in sol-gel synthesis of a bioactive glass-ceramic derived from 45S5 bioglass. *Ceramics International, 46*(12), 20264-20271.

Tiskaya, M., Shahid, S., Gillam, D., & Hill, R. (2021). The use of bioactive glass (BAG) in dental composites: A critical review. *Dental Materials, 37*(2), 296-310.

Tite, T., Popa, A., Stuart, B., Fernandes, H., Chirica, I., Lungu, G., . . . Tanase, C. (2022). Independent and complementary bio-functional effects of cuo and ga2o3 incorporated

as therapeutic agents in silica-and phosphate-based bioactive glasses. *Journal of Materiomics, 8*(4), 893-905.

Todros, S., Todesco, M., & Bagno, A. (2021). Biomaterials and their biomedical applications: From replacement to regeneration. *Processes, 9*(11), 1949.

Vafa, E., Bazargan-Lari, R., & Bahrololoom, M. E. (2021). Synthesis of 45S5 bioactive glass-ceramic using the sol-gel method, catalyzed by low concentration acetic acid extracted from homemade vinegar. *Journal of Materials Research and Technology, 10*, 1427-1436.

Vafa, E., Tayebi, L., Abbasi, M., Azizli, M. J., Bazargan-Lari, R., Talaiekhozani, A., . . . Kamyab, H. (2022). A better roadmap for designing novel bioactive glasses: effective approaches for the development of innovative revolutionary bioglasses for future biomedical applications. *Environmental Science and Pollution Research*, 1-24.

Vallet-Regí, M. (2019). Bioceramics: from bone substitutes to nanoparticles for drug delivery. *Pure and Applied Chemistry, 91*(4), 687-706.

Vallet-Regi, M., & Salinas, A. J. (2021). Mesoporous bioactive glasses for regenerative medicine. *Materials Today Bio, 11*, 100121.

Vizureanu, P., Bălțatu, M. S., Sandu, A. V., Achitei, D. C., Nergis, D. D. B., & Perju, M. C. (2021). New Trends in Bioactive Glasses for Bone Tissue: A Review. *Current Concepts in Dental Implantology-From Science to Clinical Research*.

Wang, X., & Li, W. (2016). Biodegradable mesoporous bioactive glass nanospheres for drug delivery and bone tissue regeneration. *Nanotechnology, 27*(22), 225102.

Wang, X., Zhang, Y., Lin, C., & Zhong, W. (2017). Sol-gel derived terbium-containing mesoporous bioactive glasses nanospheres: In vitro hydroxyapatite formation and drug delivery. *Colloids and Surfaces B: Biointerfaces, 160*, 406-415.

Wang, Y., & Chen, X. (2017). Facile synthesis of hollow mesoporous bioactive glasses with tunable shell thickness and good monodispersity by micro-emulsion method. *Materials Letters, 189*, 325-328.

Wei, S., Ma, J.-X., Xu, L., Gu, X.-S., & Ma, X.-L. (2020). Biodegradable materials for bone defect repair. *Military medical research, 7*, 1-25.

Wen, C., Bai, N., Luo, L., Ye, J., Zhan, X., Zhang, Y., & Sa, B. (2021). Structural behavior and in vitro bioactivity evaluation of hydroxyapatite-like bioactive glass based on the SiO2-CaO-P2O5 system. *Ceramics International, 47*(13), 18094-18104.

Westhauser, F., Widholz, B., Nawaz, Q., Tsitlakidis, S., Hagmann, S., Moghaddam, A., & Boccaccini, A. (2019). Favorable angiogenic properties of the borosilicate bioactive glass 0106-B1 result in enhanced in vivo osteoid formation compared to 45S5 Bioglass. *Biomaterials science, 7*(12), 5161-5176.

Wisanuyotin, T., Paholpak, P., Sirichativapee, W., & Kosuwon, W. (2022). Allograft versus autograft for reconstruction after resection of primary bone tumors: a comparative study of long-term clinical outcomes and risk factors for failure of reconstruction. *Scientific reports, 12*(1), 14346.

Wu, C., Chang, J., & Xiao, Y. (2011). Mesoporous bioactive glasses as drug delivery and bone tissue regeneration platforms. *Therapeutic Delivery, 2*(9), 1189-1198.

Wu, C., Fan, W., & Chang, J. (2013). Functional mesoporous bioactive glass nanospheres: synthesis, high loading efficiency, controllable delivery of doxorubicin and inhibitory effect on bone cancer cells. *Journal of materials chemistry B, 1*(21), 2710-2718.

Wu, C., Miron, R., Sculean, A., Kaskel, S., Doert, T., Schulze, R., & Zhang, Y. (2011). Proliferation, differentiation and gene expression of osteoblasts in boron-containing associated with dexamethasone deliver from mesoporous bioactive glass scaffolds. *Biomaterials, 32*(29), 7068-7078.

Wu, X., Wei, J., Lu, X., Lv, Y., Chen, F., Zhang, Y., & Liu, C. (2010). Chemical characteristics and hemostatic performances of ordered mesoporous calcium-doped silica xerogels. *Biomedical Materials, 5*(3), 035006.

Wu, Z., Zhou, X., Zhang, Y., Luan, J., Yang, X., Wu, Z., & Wang, B. (2019). Synthesis and characterization of mesoporous bioactive glasses with highly ordered structures and high surface areas by a self-assembly process. *Journal of Non-Crystalline Solids, 517*, 1-8.

Xia, W., & Chang, J. (2006). Well-ordered mesoporous bioactive glasses (MBG): a promising bioactive drug delivery system. *Journal of Controlled Release, 110*(3), 522-530.

Xie, W., Chen, X., Li, Y., Miao, G., Wang, G., Tian, T., . . . Chen, X. (2020). Facile synthesis and in vitro bioactivity of radial mesoporous bioactive glass with high phosphorus and calcium content. *Advanced Powder Technology, 31*(8), 3307-3317.

Xun, Z., Li, S., Sun, Y., Jiang, S., Guo, M., Liu, H.-X., & Guan, Y. (2022). Morphology manipulation of silica nanoparticles via the catalytic templates reaction system. *Ceramics International, 48*(17), 24925-24934.

Yan, P., Wang, J., Liu, S., Ou, J., Lei, Z., & Yang, S. (2010). "Green" synthesis of highly ordered mesoporous bioactive glass using acetic anhydride as the catalyst. *Journal of Non-Crystalline Solids, 356*(28-30), 1514-1518.

Yan, X., Deng, H., Huang, X., Lu, G., Qiao, S., Zhao, D., & Yu, C. (2005). Mesoporous bioactive glasses. I. Synthesis and structural characterization. *Journal of Non-Crystalline Solids, 351*(40-42), 32093217.

Yan, X., Wei, G., Zhao, L., Yi, J., Deng, H., Wang, L., . . . Yu, C. (2010). Synthesis and in vitro bioactivity of ordered mesostructured bioactive glasses with adjustable pore sizes. *Microporous and mesoporous materials, 132*(1-2), 282-289.

Yan, X., Yu, C., Zhou, X., Tang, J., & Zhao, D. (2004). Highly ordered mesoporous bioactive glasses with superior in vitro bone-forming bioactivities. *Angewandte Chemie International Edition, 43*(44), 5980-5984.

Yao, H., Zou, X., Zheng, S., Hu, Y., Zhang, S., Liang, C., . . . Yang, L. (2021). Femtosecond laser-induced nanoporous layer for enhanced osteogenesis of titanium implants. *Materials Science and Engineering: C, 127*, 112247.

Yilmaz, B., Pazarceviren, A. E., Tezcaner, A., & Evis, Z. (2020). Historical development of simulated body fluids used in biomedical applications: A review. *Microchemical Journal, 155*, 104713.

Yun, H.-s., Kim, S.-e., & Hyun, Y.-t. (2008). Preparation of 3D cubic ordered mesoporous bioactive glasses. *Solid State Sciences, 10*(8), 1083-1092.

Yun, H.-s., Kim, S.-e., & Hyun, Y.-t. (2009). Preparation of bioactive glass ceramic beads with hierarchical pore structure using polymer self-assembly technique. *Materials Chemistry and Physics, 115*(2-3), 670-676.

Yun, H.-s., Kim, S.-h., Lee, S., & Song, I.-h. (2010). Synthesis of high surface area mesoporous bioactive glass nanospheres. *Materials Letters, 64*(16), 1850-1853.

Zambanini, T., Borges, R., Kai, K. C., & Marchi, J. (2019). Bioactive glasses for treatment of bone infections *Biomedical, therapeutic and clinical applications of bioactive glasses* (pp. 383-415): Elsevier.

Zhao, S., Li, Y., & Li, D. (2010). Synthesis and in vitro bioactivity of CaO–SiO2–P2O5 mesoporous microspheres. *Microporous and mesoporous materials, 135*(1-3), 67-73.

Zhao, Y., Zhang, Z., Pan, Z., & Liu, Y. (2021). *Advanced bioactive nanomaterials for biomedical applications.* Paper presented at the Exploration.

Zheng, K., & Boccaccini, A. R. (2017). Sol-gel processing of bioactive glass nanoparticles: A review. *Advances in Colloid and Interface Science, 249*, 363-373.

Zheng, K., Kapp, M., & Boccaccini, A. R. (2019). Protein interactions with bioactive glass surfaces: a review. *Applied Materials Today, 15*, 350-371.

Zheng, K., Niu, W., Lei, B., & Boccaccini, A. R. (2021). Immunomodulatory bioactive glasses for tissue regeneration. *Acta biomaterialia, 133*, 168-186.

Zheng, K., Sui, B., Ilyas, K., & Boccaccini, A. R. (2021). Porous bioactive glass micro-and nanospheres with controlled morphology: Developments, properties and emerging biomedical applications. *Materials Horizons, 8*(2), 300-335.

Zhu, Y., Wu, C., Ramaswamy, Y., Kockrick, E., Simon, P., Kaskel, S., & Zreiqat, H. (2008). Preparation, characterization and in vitro bioactivity of mesoporous bioactive glasses (MBGs) scaffolds for bone tissue engineering. *Microporous and mesoporous materials, 112*(1-3), 494-503.

Research Fund Acknowledgement

This research thesis was funded by Adama Science and Technology University under the grant number of, ASTU/SM-R/821/23 Adama, Ethiopia.